12-2007

A Finite Element Study of the Contact Stiffness of Homogenous Materials and Thin Films

Haitao Xu
University of Tennessee - Knoxville

To the Graduate Council:

I am submitting herewith a dissertation written by Haitao Xu entitled "A Finite Element Study of the Contact Stiffness of Homogenous Materials and Thin Films." I have examined the final electronic copy of this dissertation for form and content and recommend that it be accepted in partial fulfillment of the requirements for the degree of Doctor of Philosophy, with a major in Materials Science and Engineering.

George M. Pharr, Major Professor

We have read this dissertation and recommend its acceptance:

Hahn Choo, Easo P. George, Dayakar Penumadu, Yanfei Gao

Accepted for the Council:
Carolyn R. Hodges

Vice Provost and Dean of the Graduate School

(Original signatures are on file with official student records.)

To the Graduate Council:

I am submitting herewith a dissertation written by Haitao Xu entitled "A finite element study of the contact stiffness of homogenous materials and thin films." I have examined the final electronic copy of this dissertation for form and content and recommend that it be accepted in partial fulfillment of the requirements for the degree of Doctor of Philosophy, with a major in Materials Science and Engineering.

George M. Pharr, Major Professor

We have read this dissertation
and recommend its acceptance:

Hahn Choo

Easo P. George

Dayakar Penumadu

Yanfei Gao

Accepted for the Council:

Carolyn R. Hodges

Vice Provost and Dean of the
Graduate School

(Original signatures are on file with official student records.)

A FINITE ELEMENT STUDY OF THE CONTACT STIFFNESS OF HOMOGENOUS MATERIALS AND THIN FILMS

A Dissertation

Presented for the

Doctor of Philosophy Degree

The University of Tennessee, Knoxville

Haitao Xu

December 2007

DEDICATION

To my parents, Keru Xu and Xiuyun Xing for their unconditional love and support.

ACKNOWLEDGMENT

I would like to thank my advisor Prof. George M. Pharr, who I am so grateful to be able to study under his guidance, for giving me this precious opportunity with financial support and his patience over the years. I would like to thank my committee (Prof. Hahn Choo, Prof. Easo P.George, Prof. Dayakar Penumadu and Prof.Yanfei,Gao). I would also like to thank Dr. Warren Oliver at MTS Nano Instrument Inc. I am grateful to the faculty and staff in the Materials Science and Engineering Department at the University of Tennessee and my lab-mates for their help and friendship. I would also thank Tony Broeker for support my dissertation preparation during work. Special gratitude goes to my best friends at the University of Tennessee, Jun Xu, Caijun Su, Hongbin Bei, Gang Zuo, Songqing Wen and her husband Jun Xu, whose friendship made my studying life filled with joy. Finally, I would like to thank my sister Jiangling Xu, and wife Liang Ma, for their love and support over the years.

ABSTRACT

The applicability of the stiffness equation $S=2E_ra$ to elastic and elastic-plastic homogeneous materials and thin films on substrates is studied by finite element techniques. It is found that the stiffness equation works well in all these materials provided that a correction factor β is included. For elastic homogenous materials, the correction factor is examined for different friction conditions, Poisson's ratios, and indenter cone angles. In the case of elastic-plastic indentation with a 70.3° cone, the correction factor is very close to that for elastic indentation of a matching conical hole, which provides a convenient way to model the effects of plasticity.

Nanoindentation measurements using the stiffness equation for film/substrate systems may be affected by the substrate properties. To address this issue, a new equation describing the relationship between the effective compliance and the elastic properties of the film and the substrate for flat cylindrical punch indentation is derived. To apply this to conical indentation, it is shown that an effective film thickness should be used in the new relation to account for the geometry difference between a conical indenter and a flat punch. Finite element analysis (FEA) is used to obtain a simple equation which can be used to determine the effective film thickness, which is independent of the elastic properties of the films and substrates for compliant films on stiff substrates. The applicability of the new relation is examined by comparing it to FEA of elastic-plastic indentation by a cone. The new relation is also compared to Yu's approximate analytical solution to determine which is more accurate for obtaining the true contact radius from the measured stiffness. Although Yu's solution applies to a

broader range of materials, the new relation has distinct advantages in that it can be written in a simple algebraic form.

TABLE OF CONTENTS

LIST OF TABLES

LIST OF TABLES

1. Introduction

1.1 The contact stiffness of homogenous materials

Nanoindentation has been widely used to determine the elastic moduli and the hardness of materials at small scales [1]. The fundamental equation used to determine the elastic modulus, E, from the load-displacement curve was derived by Love and Sneddon [2-5] for a cone and was later shown by Pharr, Oliver and Brotzen [6] to be valid for any indenter which can be described as a solid of revolution of a smooth function. This relation is:

$$S = \frac{dP}{dh} = \frac{2}{\sqrt{\pi}} \frac{E}{1-\nu^2} \sqrt{A} = 2 \frac{E}{1-\nu^2} a \qquad (1.1)$$

where S is the stiffness of the initial part of the unloading curve, E is Young's modulus , ν is Poisson's ratio, $A=\pi a^2$ is the projected contact area, and a is the contact radius. How well Eq.(1.1) models real material properties affects the accuracy of measurements in nanoindentation tests. Much research was performed to examine the applicability of Eq.(1.1), either by numerical methods (including finite element simulation) or experiments.

King [7] first employed numerical methods and found that Eq.(1.1) should be modified by a correction factor, β, to account for the influence of the indenter geometry. He calculated β values for flat punches with circular, square and triangular cross sections and found that β is 1.034 for a flat-ended triangular punch. Vlassak and Nix [8] obtained β=1.058 for this punch by adopting an independent numerical method.

Bolshakov and Pharr [9] performed FEA of elastic-plastic indentation by a rigid

cone with a half included angle of 70.3° and found that the elastic moduli estimated from Eq.(1.1) are 5%-15% larger than actual values (equivalent to a larger β). Cheng and Cheng gave β=1.05 for materials without work hardening [10] and β=1.085 for both materials with and without work hardening [11] using FEA of elastic-plastic indentation by a 68° cone. Dao et al.[12] used FEA of elastic-plastic materials to get β=1.06 for a 70.3° cone and β=1.096 for a Berkovich indenter.

Efforts have also been made to use nanoindentation experiments with a Berkovich indenter to determine the appropriate value of β. Martin and Troyon [13] conducted nanoindentation experiments on fused quartz and obtained β=1.063. Strader et al.[14] developed a new method to accurately measure the projected contact area using SEM (scanning electron microscope) and found β =1.06.

An important study of the correction factor for the contact between a rigid conical indenter and an elastic half space was performed by Hay& Pharr [15]. After investigating Sneddon's derivation procedure of Eq. (1.1), they found that β>1 is caused by the fact that radial displacement of the contact surface is allowed in Sneddon's equation while the rigid indenter assumption of FEA and the diamond indenter used in experiments prevent this. An approximate solution that accounts for this was derived using an indenter which was modified from a perfect rigid cone by increasing its radius at each point to compensate for the inwardly directed radial displacement. After applying Sneddon's procedure to derive the load-displacement relation for this modified indenter shape, β was approximated as:

$$\beta = \pi \frac{\pi/4 + 0.15483073 \cot\theta \dfrac{(1-2\nu)}{4(1-\nu)}}{\left(\pi/2 - 0.83119312 \cot\theta \dfrac{(1-2\nu)}{4(1-\nu)}\right)^2} \tag{1.2}$$

where ν is Poisson's ratio, and θ is the half included angle of the cone.

Hay and Pharr also proposed another approach to account for the radial displacement by applying Eq.(1.1) to an indenter with slightly larger effective cone angle to make the final contact radius after radial displacement match exactly with that of indentation by a rigid cone. By using a simple geometric analysis, β is then given by:

$$\beta = 1 + \frac{(1-2\nu)}{4(1-\nu)\tan\theta} \tag{1.3}$$

The values of β from these approximate equations proved to provide a good estimation when compared to FEA results.

The findings of Hay and Pharr provide an important reference for β values for indentation experiments in materials with known ν and θ. However, there are several unresolved issues about the correction factor that need to be addressed. One is that how friction affects β, since the approximate analyses provided by Hay and Pharr assume frictionless conditions. Another is the origin of the correction factor for elastic-plastic indentation with a cone.

1.2 The contact stiffness in thin films on substrates

The stiffness equation corrected with β can be used to determine the elastic moduli of homogenous materials. However, this approach can be applied to film/substrate systems only when the indentation depth is a small fraction of film

thickness. This is possible for thicker films, but when the film thickness is very small, the displacement resolution of nanoindentation forces one to make indentations at depths comparable to the film thickness to obtain meaningful data. In this case, the measured stiffness is affected by the elastic properties of both the film and the substrate [16, 17]. To extract the true elastic moduli of the film, good analytical solutions that describe the relationship between the measured stiffness and the elastic properties of the film and the substrate are needed.

Doerner and Nix [18] suggested an empirical equation that relates the effective contact modulus to the elastic properties of the film and the substrate based on experimental data. King [7] modified the formula proposed by Doerner and Nix and used numerical methods to determine the unknown fitting parameter for a rigid flat cylindrical punch. Yu et al.[19] provided a numerical solution for conical indentation of film/substrate systems by solving Fredholm integral equations. Gao et al.[20] used a perturbation method to obtain an approximate analytical solution for indentation of elastic film/substrates systems by a rigid flat cylindrical punch, which proved to work well provided the film and substrate moduli differed by no more than a factor of 2. Bec et al. [21] provided a simple model to extract the film modulus from the stiffness measurements if the thickness of the film and the substrate modulus are known. Saha and Nix [22] modified King's solution to include a reduced film thickness that accounts for the geometry difference between a flat punch and a conical indenter. Han and Nix [23] modified Yu's solution to give a relationship between the measured stiffness and the projected contact radius when the elastic properties of films and substrate are known.

Among these solutions, those involving no adjustable parameters are generally most valuable since there is usually no convenient experimental way to determine the adjustable parameters without knowing the film properties *a priori*. In this regard, the approximate analytical solutions for flat cylindrical punch indentation of elastic film/substrate systems proposed by King, Gao et al., and Bec et al. have received considerable attention. These solutions play an important role in this dissertation and will now be discussed in detail.

The frictionless indentation of an elastic film/substrate system by a flat cylindrical punch is shown in Fig.1.1. A flat punch indenter with radius, a, is driven into the film/substrate system by applying a load P. The film and the substrate have elastic moduli, E_f and E_s, and Poisson's ratio, ν_f and ν_s, respectively. The penetration depth and the film thickness are represented by h and t, respectively.

For frictionless indentation of a half space of the homogenous substrate material by a circular flat punch, the exact solution is given by [4]:

$$S_0 = \frac{dP}{dh} = \frac{2}{\sqrt{\pi}} E_r \sqrt{A} = 2 \frac{E_s}{1-\nu_s^2} a \,. \qquad (1.4)$$

Here, S_0 represents the contact stiffness of the substrate material alone. The elastic modulus of the substrate can then be determined from a measurement of S_0 if Poisson's ratio is known or can be approximated.

For a film/substrate system, the reduced composite modulus E_r is affected by the elastic properties of the film and substrate, the film thickness, t, and the contact radius, a. Doerner and Nix first suggested an equation describing this relationship of the form:

$$\frac{1}{E_r} = \frac{1}{(1-\nu_f^2)/E_f(1-e^{-\alpha t\sqrt{A}})+(1-\nu_s^2)/E_s(1-e^{-\alpha t\sqrt{A}})} \tag{1.5}$$

where α is a fitting parameter that depends on the contact area and the film thickness and A is the contact area.

King employed numerical techniques to analyze indentation of film/substrate systems with flat-ended circular, square and triangular punches and suggested that Eq.(1.5) be modified to:

$$\frac{S}{S_0} = \frac{(1-\nu_s^2)/E_s}{(1-\nu_f^2)/E_f(1-e^{-\alpha t\sqrt{A}})+(1-\nu_s^2)/E_s e^{-\alpha t\sqrt{A}}} \tag{1.6}$$

Here, S is the contact stiffness for indentation of the film/substrate system and S_0 is the contact stiffness for a pure substrate material at the same contact area. Based on King's numerical analysis, graphs showing the dependence of the parameter α on $\sqrt{A/t}$ were

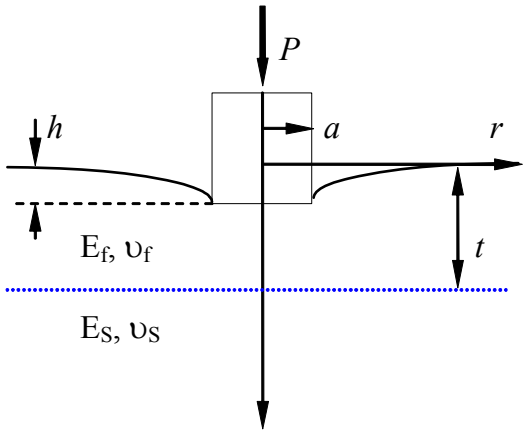

Figure 1.1 Geometry of a cylindrical punch indenting a film/substrate system

constructed for circular, square and triangular punches. Fig.1.2 shows the corresponding α values for different normalized punch sizes for indentation of a film/substrate system with a flat circular punch. We have extrapolated the curve to a wider range of normalized punch sizes by applying curve fitting with the corresponding equation shown in the figure. It is noted that the extrapolation curve yields negative α values when the normalized punch size is small. This is not realistic, and we replace negative α values with zero for small a/t ratios.

Gao et al. used a first order perturbation method for cylindrical punch indentation of film/substrate systems to derive an approximate analytical solution that relates the effective compliance $[(1- \nu)/\mu]_{eff}$ to the elastic properties of the film and substrate, the film thickness and the contact radius. The analysis gives:

$$C_{eff} = \left(\frac{1-\nu}{\mu}\right)_{eff} = \frac{1-[\nu_f I_1 + \nu_s (1-I_1)]}{\mu_f I_0 + \mu_s (1-I_0)} \tag{1.7}$$

Here, $C_{eff}= [(1- \nu)/\mu]_{eff}$ is the effective compliance, μ_f and μ_s are the shear moduli of the film and substrate, respectively, and I_1 and I_0 are weighting functions that can be calculated from:

$$I_0 = \frac{2}{\pi}\arctan(t/a) + \frac{1}{2\pi(1-\nu)}\left[(1-2\nu)(t/a)\ln\frac{1+(t/a)^2}{(t/a)^2} - \frac{(t/a)}{1+(t/a)^2}\right]$$
$$I_1 = \frac{2}{\pi}\arctan(t/a) + \frac{(t/a)}{\pi}\ln\frac{1+(t/a)^2}{(t/a)^2} \tag{1.8}$$

The effective compliance C_{eff} is important because it is experimentally measurable from the measured contact stiffness using the relation:

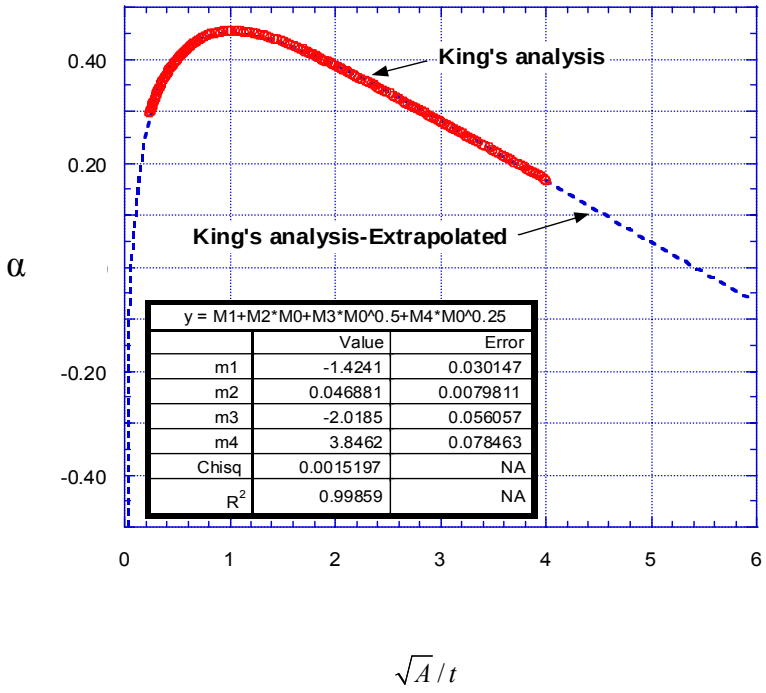

Figure 1.2 α values for different normalized punch sizes (flat circular punch indentation of film/substrate systems)

$$C_{eff}=\left(\frac{1-\nu}{\mu}\right)_{eff}=\frac{4a}{S} \tag{1.9}$$

It is often useful to express the stiffness as a normalized parameter S/S_0, where S_0 is the stiffness of the substrate material alone. In this context, Gao's solution may be written as:

$$\frac{S}{S_0}=\left(\frac{1-\nu_S}{\mu_S}\right)/\left\{\frac{1-[\nu_f I_1+\nu_S(1-I_1)]}{\mu_f I_0+\mu_S(1-I_0)}\right\} \tag{1.10}$$

Bec et al. proposed a simple model that includes the influence of the substrate's elasticity on the contact stiffness which may be written in form:

$$\frac{S}{S_0}=\frac{(1-\nu_S^2)/2E_S a}{\left(t/\left[(1+2t/\pi a)\pi a^2 E_f/(1-\nu_f^2)\right]+1/\left[(1+2t/\pi a)2aE_S/(1-\nu_S^2)\right]\right)} \tag{1.11}$$

This equation follows by simply assuming that flat cylindrical punch indentation is equivalent to compression of a cylinder of the film materials of radius a, length t, and modulus E_f sitting on an elastic substrate with modulus E_s. Under this assumption, the measured stiffness is the reciprocal sum of the cylinder stiffness $\pi a^2 E_f/[(1-\nu_f^2)t]$ and the substrate stiffness $2E_s a/(1-\nu_s^2)$. A polynomial function (1+2t/πa) is used to weight the stiffness expression to ensure that the composite stiffness has the correct limits when the contact radius is very small compared to the film thickness and the film has the same elastic properties as the substrate.

Among these solutions, Gao's solution and the Bec-Loubet solution have received a great deal of attention since they are closed formed without fitting parameters. Mencik et al [24] conducted nanoindentation experiments of 26 different film-on-substrate systems and compared the measurements with the prediction of Gao's solution and

Doerner and Nix functions, showing that Gao's solution describes the indentation response of the 26 film/substrate systems reasonably well.

In this dissertation, we will develop a new approximate analytical solution based on the perturbation method used by Gao et al. Based on comparison to finite element analysis (FEA), this solution generally works better than the others.

Since no closed-form solutions are available for nanoindentation of film/substrate systems with conical or Berkovich indenters, it is usual to approximate conical indentation by flat cylindrical punch indentation with the same contact area. However, in doing so, an important unresolved issue is how to correct for the fact that the conical and Berkovich indenters penetrate the film in a manner that effectively reduces the film thickness .This issue is directly addressed in this dissertation.

1.3 Objectives of this study

The first objective in this dissertation is to provide a thorough study of the factors that affect the correction factor β in the stiffness equation. It was shown in Hay et al's work that β for frictionless indentation depends on the half included angle of the cone and Poisson's ratio. For a flat cylindrical punch, Spence [25] and Storakers et al. [26] showed that β is affected by the friction and Poisson's ratio. The first part of this dissertation assesses all of these influences using FEA as the primary tool. From the FEA observations, simple physical explanations for the observed dependencies are derived.

A second objective is to determine β for elastic-perfectly-plastic materials indented by a cone. Here, we also employ FEA to show the equivalence between the stiffness for elastic-plastic indentation and that of conical indentation of an elastic surface

with a matching conical hole at the same contact radius. This concept is shown to be very useful in understanding the effects of plasticity on the correction factor β.

A third objective is to derive a new relation between the effective compliance and the elastic properties of films/substrate systems based on the perturbation method proposed by Gao et al. The new relation avoids a problem in Gao's solution in one important limit. FEA shows that the new relation is a significant improvement for the case of compliant films on stiff substrates.

A fourth objective is to assess the applicability of the King's solution, the Bec-Loubet solution, Gao's solution and the new relation and develop a method based on them that allows the approximate analytical solutions for the flat cylindrical punch to be used in the modeling of conical indentation of elastic film/substrate systems. Using a matching conical hole in the film to approximate the hardness impression caused by plasticity is shown to be a very useful concept.

A fifth objective is to study if our method for extracting film properties works for indentation of elastic-plastic films, and how β affects the accuracy of the method. We also investigate the critical ratio of the indentation depth to the film thickness which can be used to measure the true hardness of the film independent of the substrate.

Finally, we compare the stiffness measured from indentation of elastic-plastic film/substrate systems with that of elastic systems at the same contact radius to determine if β's are the same for both cases. In addition, Yu's solution and our new solution are compared with FEA results to determine which of them better describe the relationship between contact stiffness and contact radius.

The results in this dissertation pave the way for more accurate measurements of elastic modulus and hardness in monolithic materials and film/substrate systems.

2. Indentation of homogenous materials: A critical evaluation of the dependence of the correction factor in the stiffness equation on friction coefficient, Poisson's ratio and indenter angle

In this chapter, a comprehensive parametric study of the effects of indenter angle θ, Poisson's ratio ν, and friction coefficient μ on the correction factor β is undertaken.

We begin by examining the contact between a flat cylindrical punch and an elastic half space. Then, based on the effects of μ and ν on β from the FEA results for a flat cylindrical punch, we include θ effects to do a thorough study of β values for different combinations of μ, ν and θ for conical indenters. After establishing the β values for elastic indentation under different conditions, in a later chapter we will perform a similar study for the more realistic case of elastic-plastic indentation by conical indenters. We will show that using conical indentation into holes in the surface that match the indenter profile provides a good approximation of elastic plastic behavior, thus allowing us to avoid the complex simulation of elastic-plastic indentation.

The primary tool we use in this chapter is finite element analysis (FEA) for indentation of elastic homogenous materials with a flat cylindrical punch, cones with different half included angles, θ, and conical indentation of surfaces with matching conical holes. Based on the observations, physical explanations for the effects of friction, half-included angle θ and Poisson's ratio ν on the correction factor β are given.

2.1 β for indentation of an elastic half space with a flat cylindrical punch

A schematic illustration of indentation of an elastic half space by a rigid, flat cylindrical punch is shown in Fig.2.1. In this figure, a is the contact radius, which is

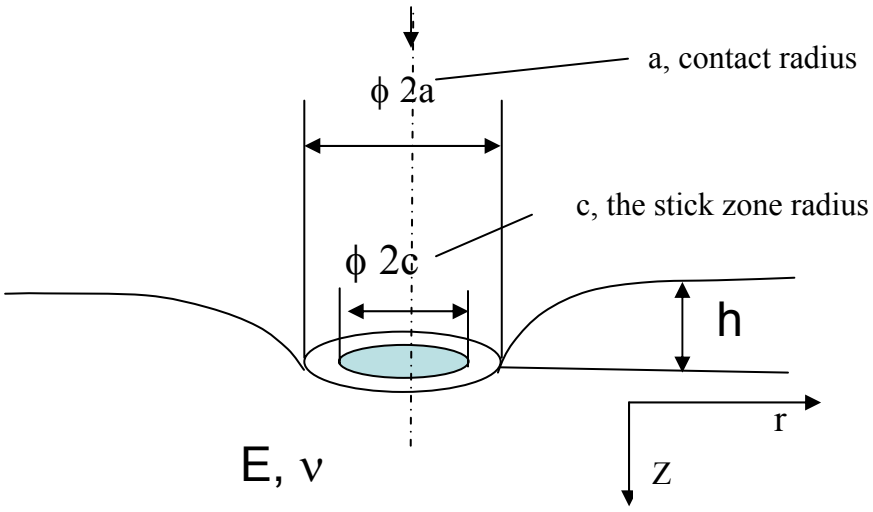

Figure 2.1 A schematic illustration of indentation of an elastic half space with a flat cylindrical punch

also the radius of the punch. P is the indentation load, h is the indentation depth, E is Young's modulus and ν is Poisson's ratio. If Coulomb friction with a friction coefficient μ is assumed at the indenter-specimen interface, then there will be a "stick zone" of radius c in which no slip occurs.

For frictionless contact, there is no stick region under the punch. Since Eq.(1.1) was derived based on frictionless contact, β should then be 1 independent of Poisson's ratio. It should be noted, however, that points in the contact region under the punch move toward the punch center. The equation to calculate the radial displacement of the contact surface points is [27]:

$$\bar{u}_r(r) = -\frac{(1-2\nu)(1+\nu)}{\pi E}\sin^{-1}(\frac{r}{a}) \tag{2.1}$$

In the case of fully adhesive contact between the flat punch and the elastic half space, the stick radius c is equal to the contact radius a. As shown by Shield and Anderson [28] from energy considerations, a perfectly rough punch (fully adhered) penetrates less than a rough punch, and the latter penetrates less than a frictionless punch for a given load. This indicates that β for the fully adhesive case should be larger than frictionless or finite friction indentation. The correction factor for this case has been given by Spence [25] as:

$$\beta\left(\mu=\infty,\nu\right)=\frac{1-\nu}{1-2\nu}\ln\left(3-4\nu\right) \tag{2.2}$$

However, realistic friction conditions in experiments are finite and the contact region is composed of a stick-slip region. In the stick zone $-c \le r \le c$

$$\sigma_{rz} < \left|\mu\sigma_{zz}\right|, \tag{2.3}$$

while in the slip zone $c \le |r| \le a$

$$\sigma_{rz} = |\mu \sigma_{zz}| \ . \tag{2.4}$$

Spence showed that the ratio of stick zone radius to contact radius, c/a, is independent of the indentation depth h in the case of flat punch contact and monotonically increases with load due to the self similarity of the stress field. Storaker [25] further proved that the c/a ratios are independent of contact profiles using finite element simulation. Both of these studies focused mainly on the derivation of the unique relationship between the stick zone size c and the friction coefficient μ. Although Spence plots the correction factors against the stick zone size c for ν=0 and 0.25, it is not convenient to use his results to obtain the corresponding β values. A comprehensive plot of correction factor values for different combinations of μ and ν will thus be very useful.

In this regard, we will use finite element simulation of indentation of an elastic half space by a rigid flat cylindrical punch with varying μ and ν to construct this plot. A simple physical explanation of the dependence of β on the stick-zone size (and μ and ν) is given.

2.1.1. Finite element analysis

The commercial software ABAQUS was employed. Due to the symmetry of a flat cylindrical punch, we can simplify the indentation as an axisymmetric problem to avoid the complexity of three dimensional modeling and reduce the computation time. The flat punch was modeled as analytical rigid body with fixed radius of 1μm. The elastic half space was modeled as a block in 400μm width and 400μm height, which proved to be large enough to avoid boundary effects on the results. The elastic modulus E was fixed at

100GPa. Due to the infinite stress under the edge of the flat punch, a fine mesh with a small element size 10^{-3} compared to punch radius was adopted in that region. The mesh details are shown in Fig.2.2. The indentation procedure was implemented by applying a small downward displacement of 10^{-2} compared to a, the flat punch radius. Axisymmetric boundary conditions were applied to the centerline of the specimen, and roller boundary conditions were applied to the bottom of the specimen. To model the effects of friction coefficient μ and Poisson's ratio ν on the correction factor β, we increased μ from 0 to ∞ and varied ν from 0 to 0.5 for each friction coefficient.

It is noted that how to model the flat punch is vital for the accurate results. We can model the flat punch as a rigid block with a vertical edge which makes a sharp angle or a flat punch without a vertical edge. For the first case, the point at the sharp edge should not be placed on a node because the normal of the two edges of the punch are perpendicular to each other at that intersection and the direction of movement of the node is not well defined, producing errors in the calculations. The latter model avoids this problem and was used in all results presented here.

It is also noted that friction needs to be modeled correctly to obtain accurate stick and slip zone sizes. In ABAQUS, the penalty method or Lagrange method can be used to model friction. However, the default elastic slip value for the penalty method is too large compared to the contact radius to obtain accurate stick zone sizes. Therefore in our simulations, Lagrange method was mostly used. However, this method does not work under some situations, and when this occurred, the penalty method was employed with a small value, 10^{-8}, chosen as the allowable elastic slip.

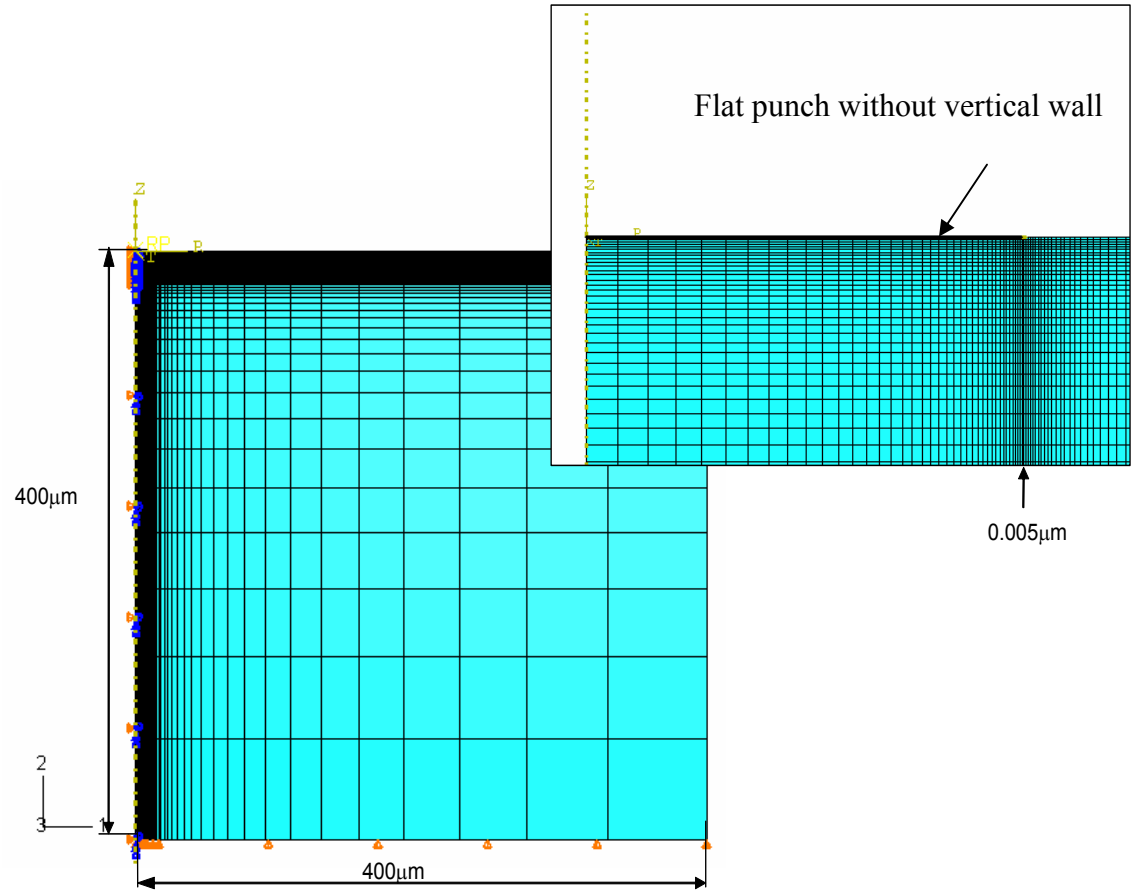

Figure 2.2 The finite element mesh for the elastic indentation with a flat cylindrical punch and the details of contact region

2.1.2. Results and discussions

In order to illustrate the importance of a correct FEA model, we first show the correction factors for different μ and ν when the inappropriate model of indentation with the vertical edge of a flat punch right on a node is used. As shown in Fig.2.3, the correction factors are essentially independent of friction coefficient and significantly different from the predictions from Spence. Moreover, even for no friction, there is an influence of Poisson's ratio on β.

Fig.2.4 plots the correction factors β determined with the correct model (no vertical wall) against ν for different friction coefficients. It is apparent that β is independent of Poisson's ratio for frictionless contact, agreeing well with the predictions of Eq (1.1). By comparing the correction factors from FEA for a fully adhesive contact or the cases of $\mu \geq 0.8$ with the predictions from Spence in Eq (2.2), we also observe good agreement. For finite μ, the correction factors increase with increasing μ, and the lower limit and upper limit are bounded by values for frictionless and full adhesive contact. Fig.2.4 provides a convenient and accurate method to determine β for the indentation of an elastic half space by a rigid flat cylindrical punch for a given μ and ν.

The physical origin of the effects of the friction coefficients and Poisson's ratios on the correction factors can be understood as follows. In the case of frictionless contact, β is always 1 independent of ν. The reason is that all the surface points are able to slip freely in the tangential direction in a manner consistent with Sneddon's analysis. The normal load applied to the punch, P, can then be predicted accurately from Eq.(1.1) for a give Poisson's ratio without being influenced by the tangential stress and $\beta=1$. For a fully

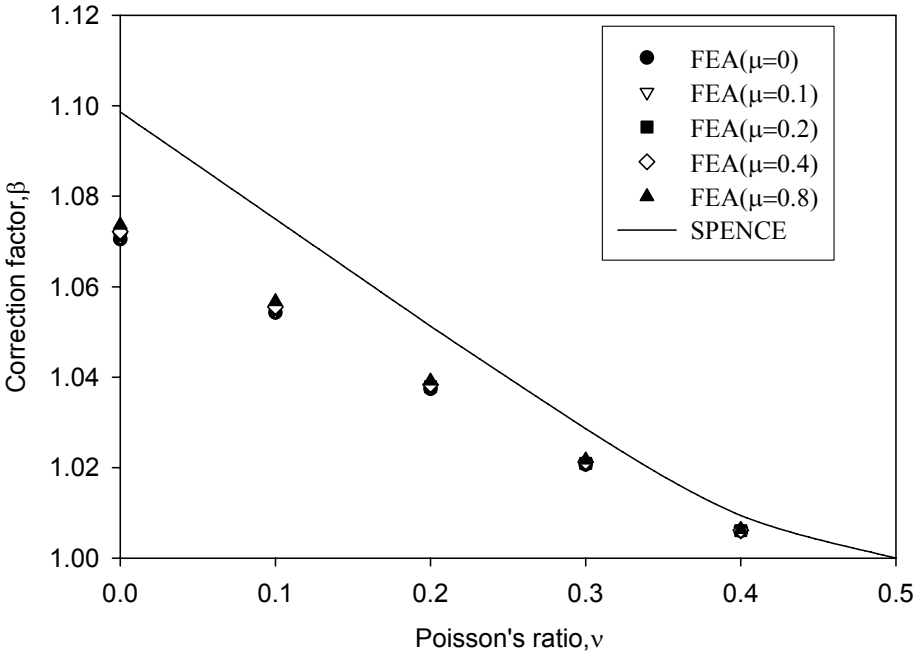

Figure 2.3 Dependence of the correction factor β on friction coefficient when the wrong FEA model is used.

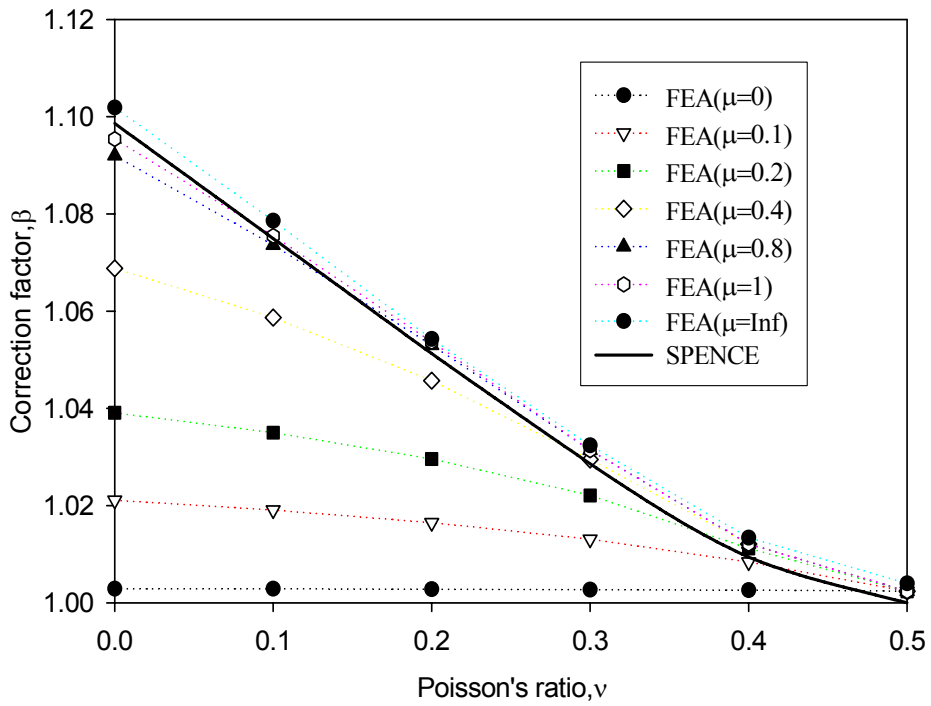

Figure 2.4 Dependence of the correction factor β on Poisson's ratio as determined by finite element simulation for flat punch

adhesive contact, β only depends on ν. In this case, the stick zone radius c is equal to the contact radius a due to the infinite friction, and each point in the contact region is prohibited from sliding toward the punch center along the tangential direction. According to Eq.(2.1), we know that sliding of the surface points should be larger for smaller ν in the frictionless case. To prevent the sliding of these points in fully adhesive contact, a tangential force with direction opposite to the sliding must be applied. In addition, the magnitude of the required tangential force will increase with decreasing Poisson's ratios for the same stick zone size c. Since the normal force is coupled with the tangential force, the required normal force is larger for a smaller Poisson's ratio for the same indentation depth h. This explains why the correction factor values will increase with decreasing Poisson's ratios for the fully adhesive contact.

For a finite μ, β will increase with increasing μ for a given ν (excluding ν=0.5). In this case, there exists a stick zone with radius c surrounded by an annulus of slip in the contact region. It was shown by Spence that c/a only depends on μ and ν. For a given ν, increasing μ will increase c, and in turn increase the normal load needed to give a tangential force large enough to prevent slip of the surface points in the stick zone. Therefore, a larger μ corresponds to a larger β.

In the case of $\nu = 0.5$ and a finite μ, friction does not have effect on the correction factors because the surface points under the indenter do not move tangentially for this incompressible material under all friction conditions including the frictionless case.

2.2 β for indentation of an elastic half space with conical indenters

In Hay and Pharr's paper, the predictions of Eqs. (1.2) and (1.3) match the results of FEA for frictionless indentation of an elastic half space by conical indenters with half-included angles of 42.28°, 60°, 70.32° and 80°. However, the correction factors from FEA in their study were limited to ν=0, 0.2 and 0.4. A complete comparison between the correction factors determined by FEA and the Hay-Pharr solution, including more Poisson's ratios and different friction conditions, are included in this section.

2.2.1. Finite element analysis

Similar to the flat punch simulations, conical indentation is modeled as an axisymmetric problem. The indenter is modeled as a rigid body. The specimen is modeled as a rectangular block 200μm in width and 200μm in height. These dimensions proved to be large enough to avoid boundary effects on the results. The mesh near the indenter tip and along the contact region were refined to provide convergent results. Details of the mesh are shown in Fig.2.5. In general, results fluctuated due to mesh discretization effects for the shallow indentation depth less than 50nm, Therefore, a minimum indentation depth, 50nm, was used by applying a downward displacement on the reference point attached to the indenter. β was determined from the ratio of the load from FEA to that calculated from Sneddon's solution at the same indentation depth which was at least 50nm. This method is based on the assumption that $a = 2h\tan\theta/\pi$, which was validated by Hay et al. The other boundary conditions were the same as those used in flat punch indentation. The elastic modulus of the material was fixed at 100GPa and

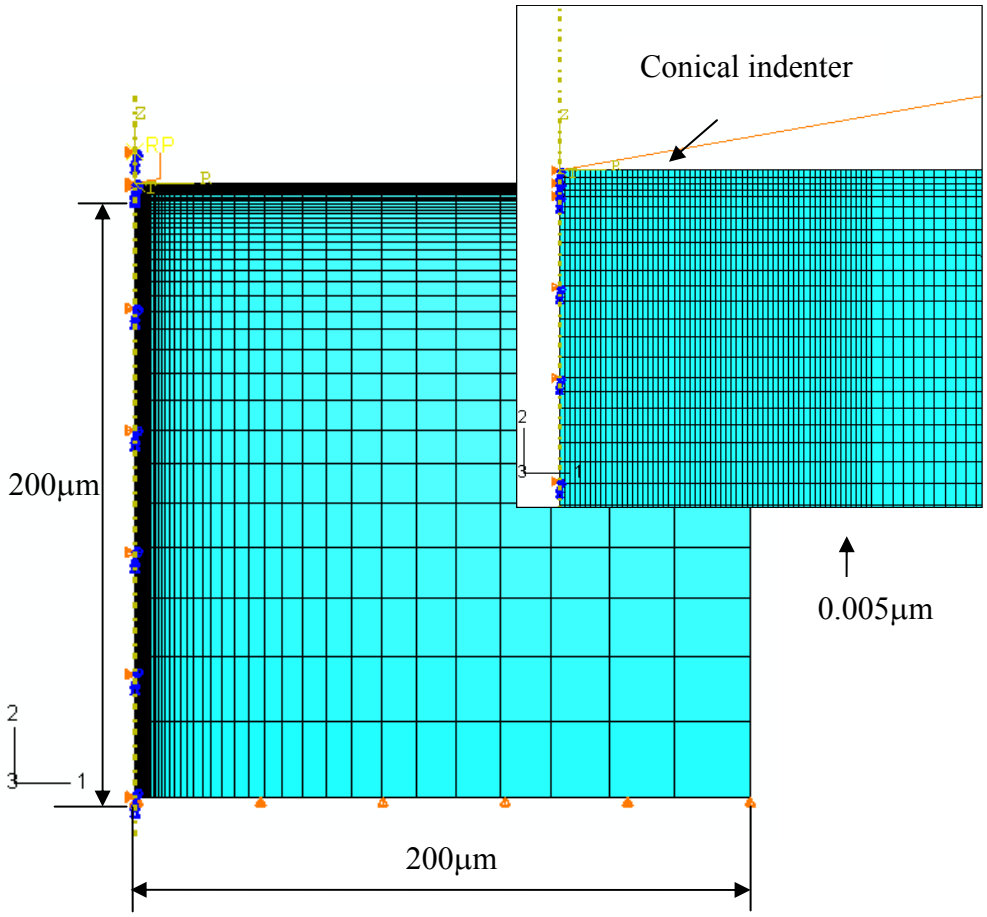

Figure 2.5 The finite element mesh for elastic indentation with a conical indenter and details of contact region.

Poisson's ratios ranging from 0 to 0.5 were examined. In addition, three sets of friction conditions including the frictionless case, μ=0.2 and 1 were modeled.

2.2.2. Results and discussions

To assess the accuracy of Eq.(1.2) and Eq.(1.3), their predictions of the dependencies of β on ν and θ for frictionless conical indentation are presented for comparison to the finite element results in Fig.2.6. It is apparent that Eq.(1.3), which has a much simpler form, gives better accuracy than Eq. (1.2). The estimation matches well with finite element results over the entire range of indenter angles examined. Note that for the conical indenter with a very sharp angle of 40°, only several elements were in contact, and the FEA results may not be reliable.

Fig.2.6 also provides strong evidence supporting the physical origin of β for conical indentation of elastic homogenous materials as proposed by Hay and Pharr. Specifically, β results from the constraint of the radial displacement of contact surface points by the rigid indenter since the radial displacements will disappear for all θ when ν=0.5 or θ=90° (for all ν values). β should be 1 in these cases, as is the case in Fig.2.6.

The effects of friction on β values for cones with half-included angles from 40° to 90° for ν=0, 0.3 and 0.5 are shown in Fig.2.7. It is noted that the results for the 40° cone may not be reliable due to small number of elements in contact. From a practical sense are very important observations that friction has little effect on β values for θ in the range from 50° to 70° for all Poisson's ratios, and that for ν=0.3 or larger, friction effects can be neglected for $50° \le \theta \le 80°$. Based on this finding, it appears that Eq.(1.3) may be

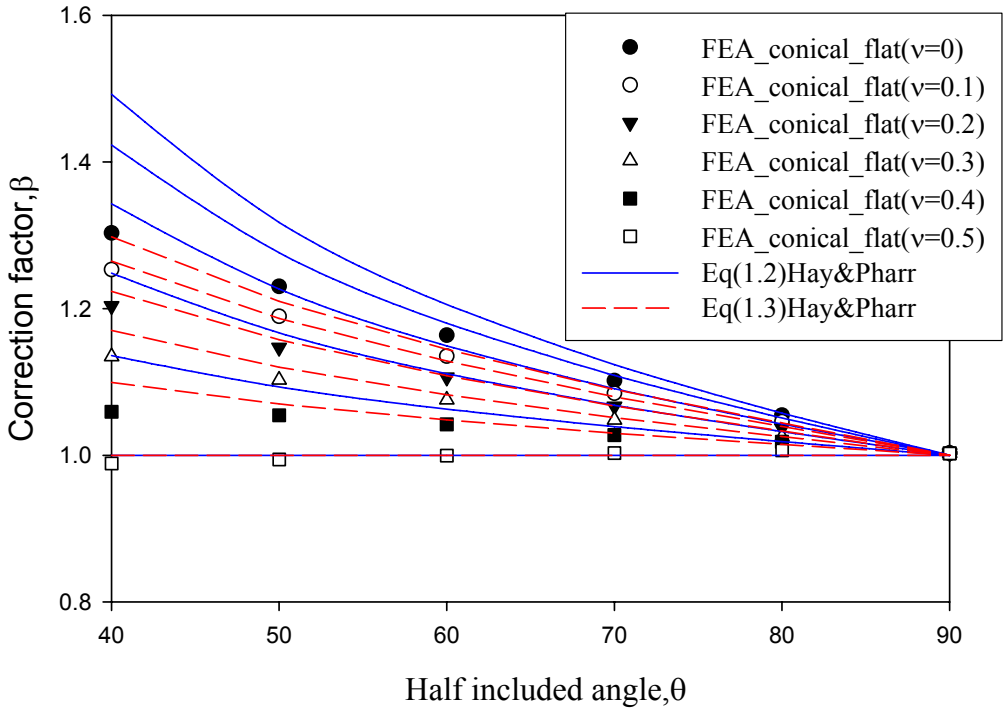

Figure 2.6 The dependence of β on μ and ν from FEA results for a frictionless conical indenter and comparison with Hay&Pharrs' equations.

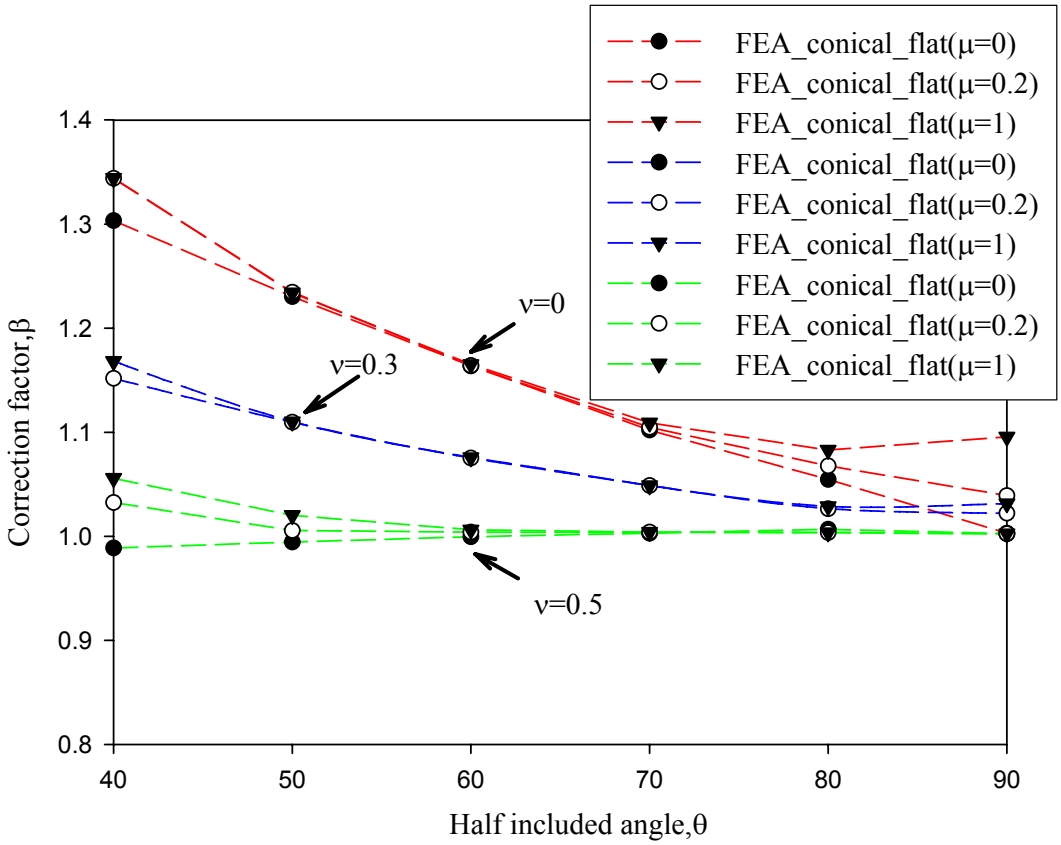

Figure 2.7 The effects of μon β values for conical indentation of elastic materials with ν=0, 0.3 and 0.5 by conical indenters of different θ

used to provide a good approximation of β in many practical situations. For $\theta \geq 80°$, there is some effect of friction on the behavior which is consistent with the observations in the flat punch.

Based on these observations, a partial physical explanation for the effects of μ, θ and ν on β for a rigid conical indenter can be developed. β values for elastic indentation with a rigid conical indenter under different friction conditions are controlled by two constraints. The first is the prohibition of radial displacement caused by the rigid conical indenter. This constraint affects β in most cases except θ=90° or ν=0.5. This is why the β values for frictional cases are larger than or at least equal to those without friction. The other constraint is caused by the tangential friction force, which prevents the contact surface points from sliding toward the indenter tip. We have shown that β for a flat punch under different friction conditions is affected by μ and ν through the slip-stick zone sizes; the smaller ν and the larger μ, the larger the β. A similar relationship exists for conical indenters when θ is large and Poisson's ratios are small. It is noted that the half included angle at which the dependence of β on friction begins to be important will be lower for a smaller ν. However, it is unclear why the second constraint does not affect β when θ is in the range from 50° to 70°. The FEA results suggest that the projected tangential force is only significant for large cone angles and small Poisson's ratios.

2.3 β for indentation of a conical indenter into a surface with a matching conical hole

A real indentation experiment with a conical or pyramidal indenter involves complex elastic and plastic deformation. One important difference for elastic-plastic

indentation is that the half space does not remain flat, and the unloading process is complicated by the "hole" in the surface created by plasticity. To study how β may be affected by a hole in the surface of the half space, we performed finite element simulation for indentation of a conical indenter into a surface with a matching conical hole. The equivalence to elastic-plastic indentation is shown in the next chapter. In this section, we focus on the effects of μ and ν on β for the indentation of surfaces with elastic holes by cones with different θ.

2.3.1 Finite element analysis

The indented material was modeled as a block with 400μmx400μm, which is large enough to avoid the far field boundary effects. A hole in the elastic material was used to model the hardness impression. To simplify, the hole had the same geometry as the conical indenter. For comparison among cases of different θ, all the surface radii of the holes were fixed at 1μm. The same elastic moduli as in previous simulations were used. A mesh convergence study showed that convergence was achieved when the element under the contact edge was 0.01a. Mesh details are shown in Fig.2.8, and the same boundary conditions were used as in previous sections. To study the effects of μ,ν, and θ on β, ν's were selected as 0, 0.3 and 0.5 for θ ranging from 30° to 90° at an interval 5° under different friction conditions including μ=0, 0.2 and ∞. The value of β was determined by comparing the load from FEA with that predicted from Eq.(1.1) at the same contact radius.

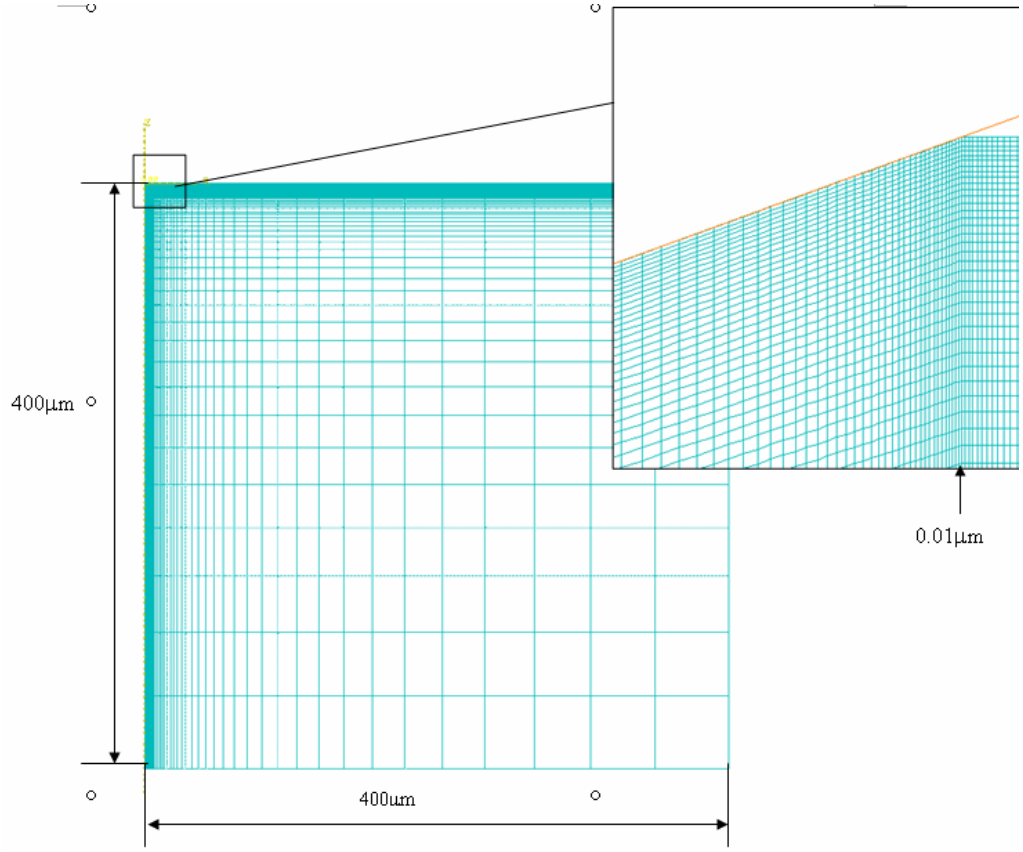

Figure 2.8 The finite element mesh for indentation of a surface with a conical hole by a conical indenter, and the details of contact region.

2.3.2. Results and discussions

Fig.2.9 plots β from FEA for frictionless indentation for ν=0, 0.3 and 0.5. To compare the flat surface case with the matching conical hole case, we include the prediction of Eq.(1.3), which matches well with the FEA results for the flat surface (shown in Section 2.2.2). It is seen that β increases first with decreasing θ and then decreases while β increases continuously for a flat surface when ν<0.5. For indentation with the hole with ν=0.5, β decreases with decreasing θ, while β for the flat surface is always 1 independent of θ. A partial explanation for this is given later.

One important observation in Fig.2.9 is that for ν=0.3, the estimation of Eq.(1.3) agrees well with FEA results when θ³ 60°. This indicates that Eq.(1.3) may be a good approximation of β in practical experiments since this equation applies to both conical indentation of flat surface and a matching conical hole. It is noted that Eq.(1.3) does not work so well for ν=0.

The effects of friction μ and indenter angle θ on β for matching conical holes for ν=0, 0.3 and 0.5 are shown in Fig.2.10 (a), (b), and (c), respectively. We observe that friction has little effect on β when θ is in the range from 60° to 80° for ν=0.3. Since many materials have a Poisson's ratio close to 0.3, this means that experiments performed with a 70.3° cone may be insensitive to friction. In the cases of ν=0.0 and ν=0.5, the range with little friction effect is 60° -70° and 75°- 90°.

Fig.2.10. (c) can be used to understand the physical origin of the influence of friction on β. It is shown in the figure that β increases continuously as θ decreases for μ=¥ but continuously decreases for μ=0.

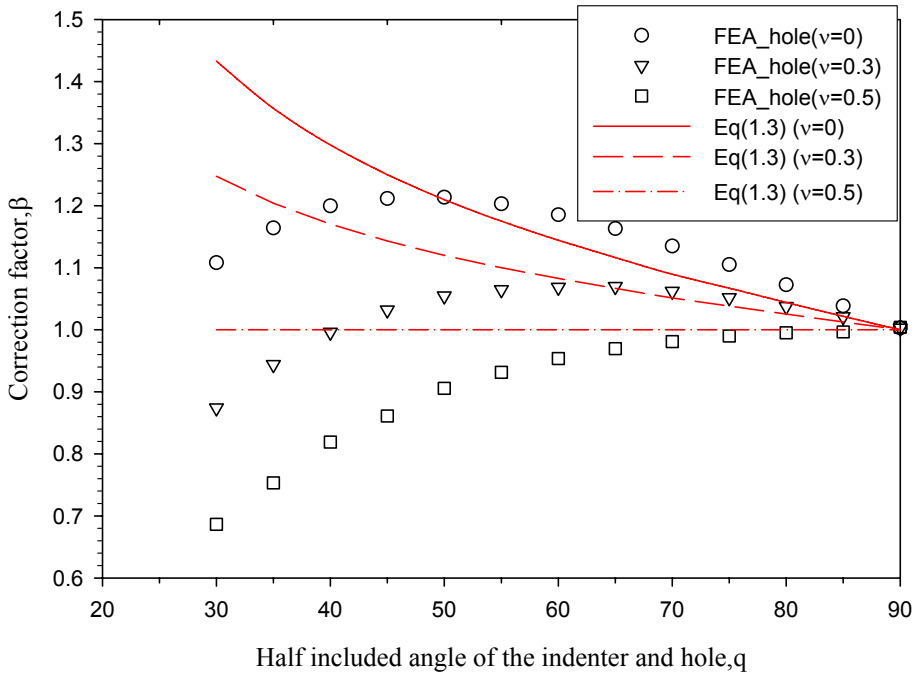

Figure 2.9 The dependence of β, ν and θ for conical indentation of matching conical holes and comparison with Eq.(1.3) (μ=0).

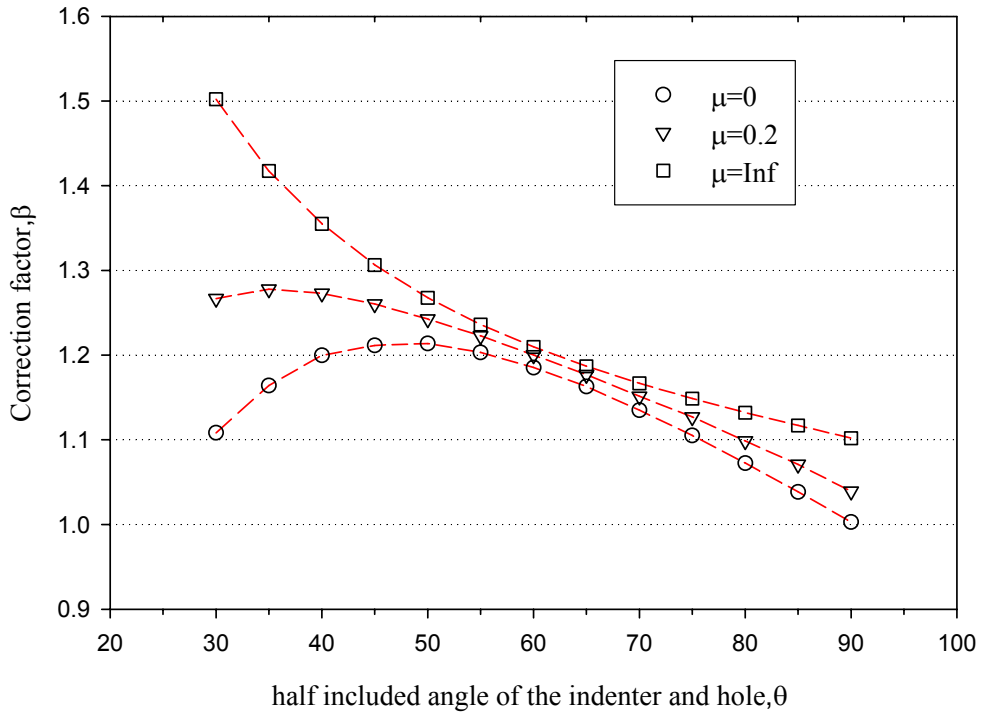

(a) ν=0

Figure 2.10 The influence of μ on β for indentation of elastic matching conical holes by conical indenters with different θ. (a) ν=0, (b) ν=0.3, (c) ν=0.5

Figure 2.10, cont.

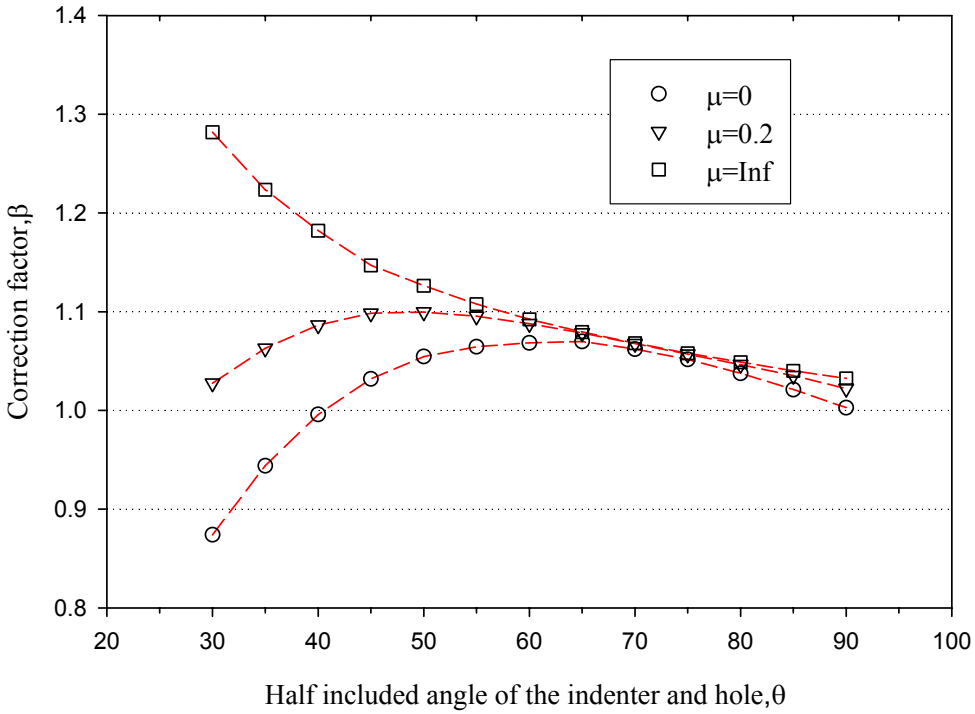

(b) ν=0.3

Figure 2.10, cont.

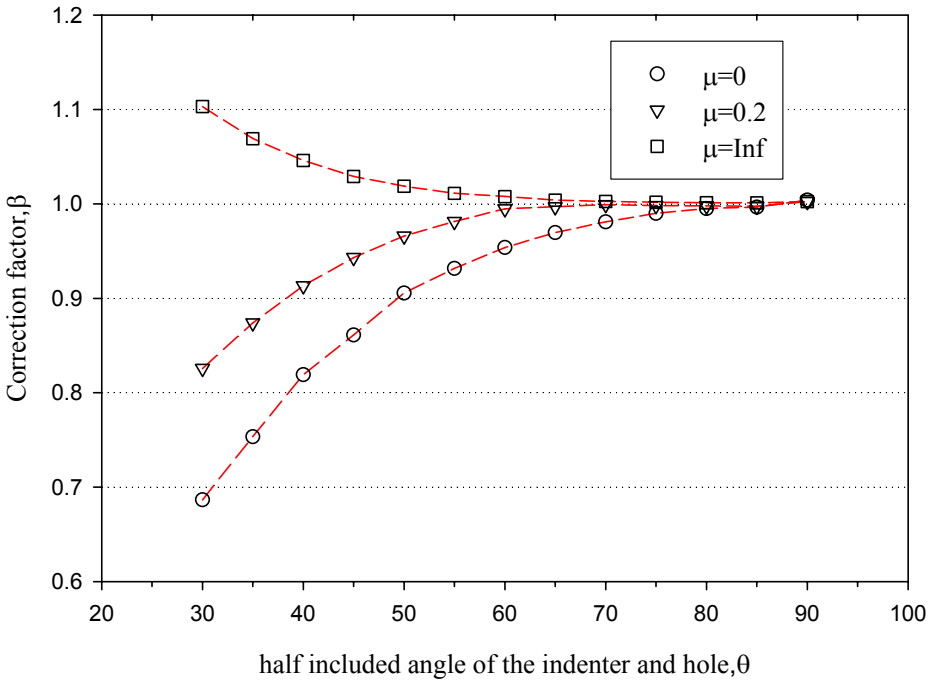

(c) ν=0.5

First, let us consider the case of $\mu=\infty$. In this case, the conical indenter is bonded perfectly to the matching conical hole, and the indentation load is transmitted to the specimen by a force normal to the indenter-specimen interface and a shear force along the interface. As shown in Fig.2.11, only the normal component of the indentation load is applied to the interface when $\theta=90°$, while only the shear component is transmitted to the interface when $\theta = 0°$. For the 90° cone, which is just the flat punch, the normal pressure is $p = P/(\pi a^2)$, and $\beta=1$ when $\nu=0.5$. As $\theta\rightarrow 0$, the shear stress τ also$\rightarrow 0$ because the interfacial area $\rightarrow\infty$. This means that contact stiffness$\rightarrow\infty$, or equivalently that $\beta\rightarrow\infty$, this explaining the increases in β with decreasing θ. We can also consider this from a geometric perspective. For a matching conical hole with a half-included angle θ and radius a, $\tau = P\sin\theta/(\pi a^2)$ if the normal load is transmitted to the interface entirely by shear. τ is 0 when $\theta = 0°$, and thus the stiffness is very high. Since β is 1 for $\theta=90°$ and reaches maximum at $\theta = 0°$, this explains why β increases with decreasing θ for a fully bonded indenter-specimen interface.

We now consider the case $\mu=0$. Since there is no friction at the indenter-specimen interface, the shear component along the interface must be zero. It is then necessary to determine the load normal to the interface in the hole. As shown in Fig.2.12, P is the indentation load, p is the contact pressure, and p_1 is the pressure on the indenter applied at the interface which must be normal to the indenter-hole interface. Since the vertical forces should balance, we have:

$$p_1' \; A_1 \sin\theta = p' \; \pi a^2 \qquad (2.5)$$

Here, A_1 is the area of the interface between the indenter and a matching conical hole

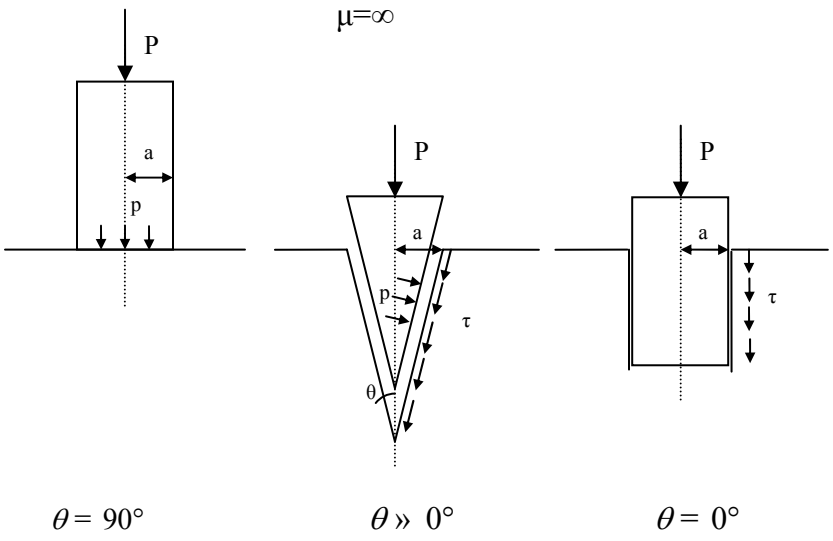

Figure 2.11 A schematic illustration of force transmission at the indenter-specimen interface for matching conical holes with different θ. (μ=)

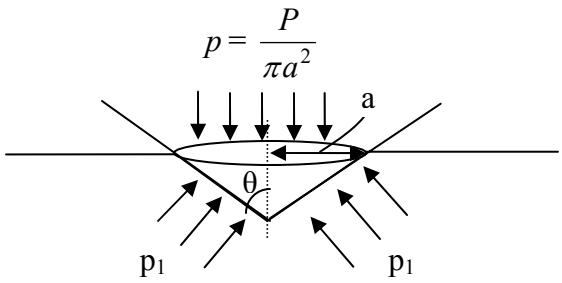

Figure 2.12 A schematic illustration of pressure transmission at the indenter-specimen interface for matching conical holes with different θ. (μ=0)

with a half included angle θ and base radius a, which may be calculated from:

$$A_1 = \frac{2\pi a}{2\pi a / \sin\theta} \times \pi\left(\frac{a}{\sin\theta}\right)^2 = \frac{\pi a^2}{\sin\theta} \tag{2.6}$$

The pressure normal to the interface,p_1, is then calculated by dividing the load by the area:

$$p_1 = \frac{p \times \pi a^2}{A_1 \times \sin\theta} = \frac{p \times \pi a^2}{\frac{\pi a^2}{\sin\theta}\sin\theta} = p\,. \tag{2.7}$$

This shows that the pressure normal to the interface in the specimen is the same as the contact pressure, irrespective of θ, indicating that for a given indentation pressure, the total force normal to the interface will be larger for a smaller θ due to the larger interface area. This is illustrated by using Fig.2.13. In all cases, the indentation pressure is the same due to the same contact radius and indentation load, but the wedging force $P_1=A_1xp_1=A_1xp$ is the largest in Case 3 because the interface area is larger. In addition, for smaller θ, a given horizontal displacement of the indenter-specimen interface will result in a larger vertical motion of the indenter for purely geometric reasons. Thus, the stiffnesses and β decrease with decreasing θ for μ=0.

For finite μ, the variation of β with θ is bounded by the limits of μ=0 and μ=∞. Lastly, we explain the influence of ν on β. For μ=0, the indentation of a matching conical hole can be simplified as a simple compression process like that shown in Fig.2.14. By analogy to flat punch indentation, the lateral displacement increases as ν decreases, so more material is pushed toward the region under the indenter tip for a smaller Poisson's ratio. This will increase the indentation load needed to drive the indenter to the same

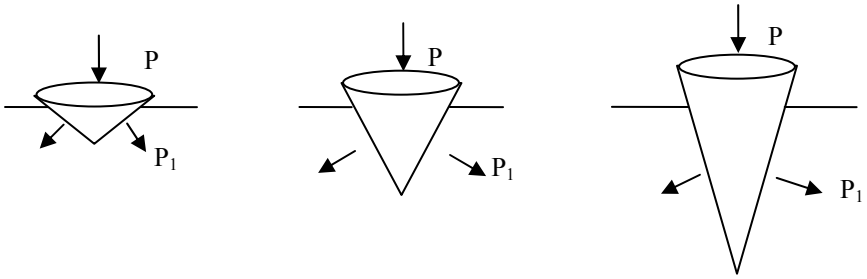

Figure 2.13 Influence of θ on the load normal to the indenter-specimen interface for conical indentation of a matching conical hole. (μ=0)

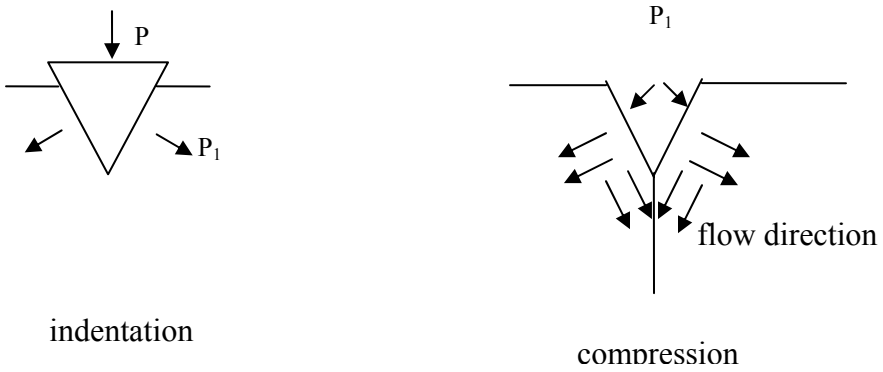

Figure 2.14 A schematic illustration of the influence of ν on β. (μ=0)

penetrate depth. Thus, the stiffness is larger for a small Poisson's ratio, and β increases with decreasing ν. Similar principles can be applied to the other frictional cases.

2.4 Conclusions

By employing FEA to indentation of elastic homogenous flat materials by a flat cylindrical punch and conical indenters and indentation of a matching conical hole with a conical indenter, we obtain the following important conclusions:

1. For frictionless contact between a flat cylindrical punch and an elastic half space, β values are always 1 for all ν. For fully adhesive contact, β can be estimated from Eq.(2.2). In the case of finite μ, Fig.1.4 can be used as the reference.

2. For frictionless indentation of flat elastic half spaces by conical indenters, Eq.(1.3) can be used to approximate the correction factors for a given ν and θ. The influences of friction on β are small when θ is in the range from 50° to 70° for all Poisson's ratios.

3. In the case of conical indentation of a matching conical hole, Eq.(1.3) can be used to predict β when θ is in the range from 60° to 90° for ν=0.3. The effects of friction are negligible for all Poisson's ratios when θ=70° and 80°. A partial explanation of the influences of μ,ν, and θ on β is given.

3. Influences of plasticity on the correction factor β

One important aspect of the stiffness equation and the correction factor β that has not yet been addressed is how they are influenced by plasticity. Real nanoindentation experiments involve complex elastic-plastic deformation, and the stiffness equation is often used without consideration of its applicability for elastic-plastic indentation processes. Previous finite element studies have shown that the stiffness equation works well for elastic-plastic indentation, but questions still remain about what β should be used in data analysis. Therefore, the main objective of this chapter is to study the origin of the correction factor in the stiffness equation for elastic-plastic indentation by a rigid cone.

Two major differences between elastic indentation and elastic-plastic indentation are as follows:

1. The unloading procedure for an elastic indentation starts from surface deformation caused entirely by elastic deformation that will disappear after full unloading. However, during elastic-plastic indentation, a permanent hardness impression is formed that remains after unloading.

2. The contact surface during elastic indentation always sinks in, while the surface in elastic-plastic indentation may have sink-in or pile-up depending on E_s/σ_y and n, where σ_y is the yield stress and n is the work hardening exponent given by $\sigma = K\varepsilon^n$. Fig.3.1 shows a schematic of sink-in and pile-up for elastic-plastic indentation. Two different contact areas, A_{max} and A_{nom} are defined. A_{max} is the projected contact area at maximum load, which is the true contact area, while A_{nom} is the nominal contact area which is calculated from the indentation depth, h, and the geometry of the indenter. For a conical

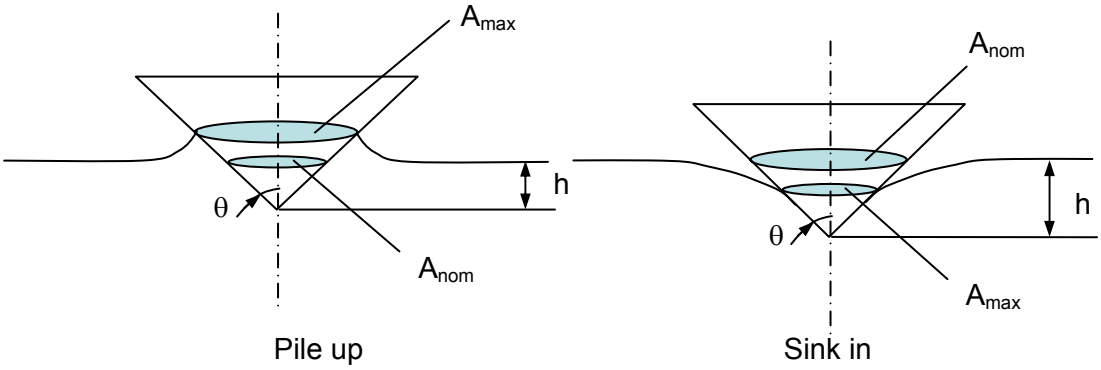

Figure 3.1 A schematic of pile-up and sink-in defining Anom and Amax

indenter, $A_{nom}=\pi a_{nom}^2=\pi h^2 \tan^2\theta$. In case of soft materials with pile-up, A_{max} is larger than A_{nom}, and the trend is opposite for hard materials that sink in.The influence of the formation of the permanent hardness impression needs to be considered mainly because the stiffness used in the stiffness equation is measured from the initial part of the unloading curve. It is reasonable to hypothesize that the unloading procedure from the plastic hardness impression for elastic-plastic indentation is different from a matching elastic hole for elastic indentation and the correction factor depends on the exact shape of the hardness impression. In Chapter 2, we showed that the elastic hole approximating the hardness impression in elastic-plastic indentation has a significant effect on β. If we can show that elastic-plastic indentation is equivalent or similar to the elastic indentation of a hole, the origin of the correction factor for elastic-plastic indentation can be understood and used in the practical analysis of indentation P-h data.

As shown in Fig.3.2, one important issue that must be addressed is which contact area, A_{max} or A_{nom}, is appropriate; that is, when materials piles up during elastic-plastic contact, is the appropriate area to be used in the stiffness equation, the maximum area which includes the influence of pile-up or the nominal area which ignores it?

In this chapter, we employ FEA to elastic-plastic indentation by a conical indenter with a half-included angle of 70.3°to show the applicability of the stiffness equation and determine the necessary correction factor β. By comparing the results to elastic indentation of a cone in a matching conical hole, we draw conclusions about the accuracy of approximating the influences of plasticity based on elastic calculations. A comparison between FEA results of elastic-plastic indentation and elastic indentation into a hole for

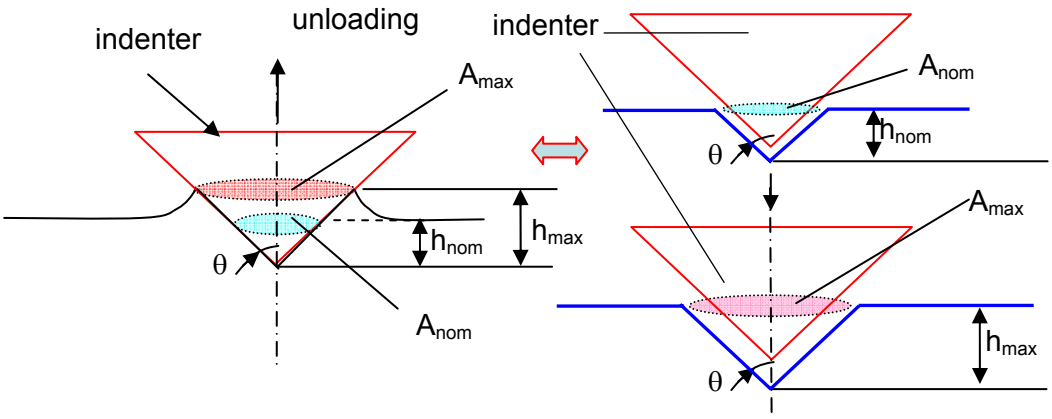

Figure 3.2 A schematic of the unloading process for indentation of elastic-plastic materials with pile up phenomenon and the loading into holes premade in elastic materials.

conical indenters with different half-included angles ranging from 40° to 80° shows that both cases give similar correction factors when $\theta \geq 60°$.

3.1 The correction factor for indentation of elastic-plastic materials by a rigid conical indenter with $\theta = 70.3°$

3.1.1 Finite element simulation procedure

The commercial finite element analysis software ABAQUS was used to simulate the indentation of elastic-plastic materials by a rigid conical indenter with half-included angle of 70.3°. The indented material was modeled as a cylinder 200μm high and 200μm in radius. Fixed boundary conditions and the axisymmetric boundary conditions were applied to the bottom surface and the centerline of the specimen, respectively. The indenter was driven into the sample to different indentation depths from 100nm to 800nm by applying displacements to the reference point of the rigid indenter. Frictionless contact between the indenter and the sample was assumed. To determine the contact area accurately, the mesh in the contact region between the indenter and the specimen was refined so that the minimum element size varied from 5nm to 20nm depending on the material properties and the indentation depth. Further away from the contact region, a coarser mesh was used. Details of the mesh are shown in Fig.3.3.

The specimen was modeled as an elastic-plastic isotropic material with elastic modulus E, Poisson's ratio, ν, and the yield stress, σ_y. To model soft and the hard materials, the elastic modulus and Poisson's ratio were fixed at E=100GPa and ν=0.3 respectively, and the yield stress values were selected as 0.1GPa and 10GPa, respectively. The Von Mises yield criterion was used in all simulations. To examine the effects of

Figure 3.3 The finite element mesh for the elastic-plastic indentation with a 70.3º conical indenter, and the details of contact region

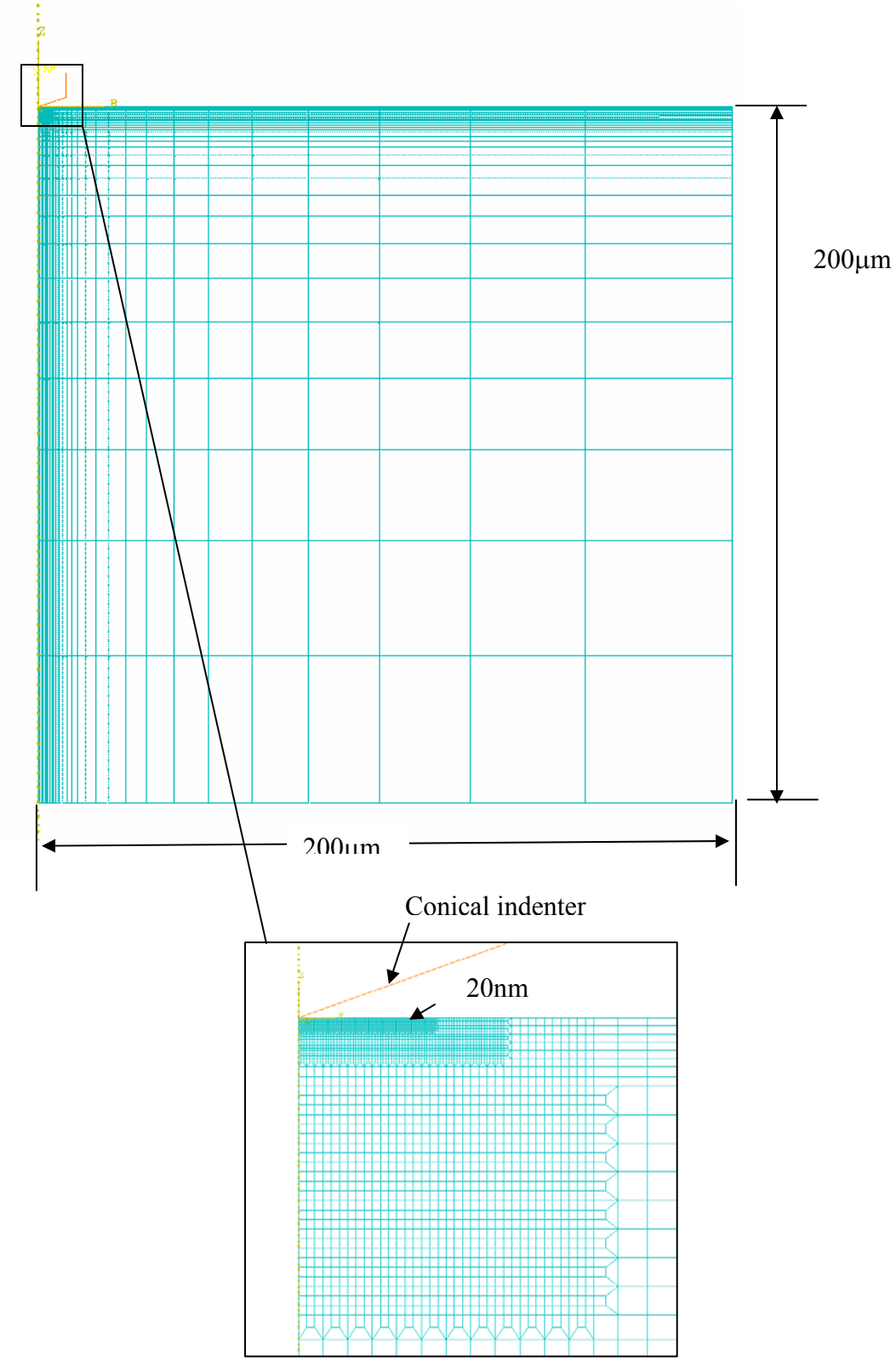
200µm
200µm
Conical indenter
20nm

work hardening, two different linear work hardening rates were examined. $\eta=0$ and $\eta=10\sigma_y$ where η is the linear work hardening rate $d\sigma/d\varepsilon$. The former is elastic-perfectly-plastic deformation while the latter represents a moderate rate of work hardening. In the post-processing stage, a_{max} was measured from the deformed mesh at maximum load, and the initial unloading stiffness was determined by employing a power law fit when the applied load decreased to 90% of P_{max}. The nominal contact radius a_{nom} was calculated from h and the indenter geometry.

3.1.2 Results of finite element analysis of elastic-plastic indentation

FEA results for conical indentation of elastic-plastic materials for different indentation depths h=0.1, 0.2, 0.4 and 0.8μm are summarized in Table 3.1. The pile-up /sink-in parameter $c = a_{\max} / a_{nom}$ is also included in the table to show that the materials chosen in our simulations represent both soft (pile-up) and hard (sink-in) materials. When c is larger than 1, pile up occurs. When c is less than 1, the materials sink in. As shown in Table 3.1, when there is no work hardening the c values are 1.25 for the soft material (σ_y =0.1GPa) and 0.68 for the hard one(σ_y =10GPa), indicating that we have materials representative of large pile up and sink in. Theoretically, c should be $2/\pi$=0.6366 for elastic contact in which sink-in occurs [3,5] and is 1.263 for rigid plastic materials according to the slip-line theory [29]. The calculations approach these two bounds very nicely. After applying moderate work hardening (η=10), c decreases for both types of materials, indicating that work hardening decreases the degree of pile up and promotes sink-in. The table also shows the ratio of the stiffness observed in the finite element

Table 3.1 Summary of the correction factor β for elastic-plastic indentation by a 70.3°cone using different area and work hardening parameters.

E=100GPa ν=0.3	h (μm)	$c=a_{max}/a_{nom}$ η=0	$c=a_{max}/a_{nom}$ $\eta=10\sigma_y$	$S_{fea}/S_{sned\_a_{max}}$ η =0	$S_{fea}/S_{sned\_a_{nom}}$ η =0	$S_{fea}/S_{sned\_a_{max}}$ $\eta=10\sigma_y$	$S_{fea}/S_{sned\_a_{nom}}$ $\eta=10\sigma_y$
σ_y=0.1GPa	0.1	1.2467	1.1018	1.0729	1.3143	1.0824	1.1930
	0.2	1.2489	1.1015	1.0733	1.3387	1.0857	1.1944
	0.4	1.2589	1.1022	1.0863	1.3662	1.0872	1.1869
	0.8	1.2600	1.1022	1.0872	1.3699	1.0892	1.2006
σ_y=10GPa	0.1	0.6815	0.6546	1.0517	0.7170	1.0493	0.6871
	0.2	0.6839	0.6546	1.0512	0.7152	1.0502	0.6866
	0.4	0.6875	0.6546	1.0461	0.7185	1.0530	0.6887
	0.8	0.6851	0.6545	1.0534	0.7218	1.0582	0.6927

analysis, S_{fea}, to that computed from Eq.(1.1),S_{sned}. In addition, S_{sned} is computed in two ways. In one, the maximum contact radius a_{max} is used to determine S_{sned} and in the other a_{nom} is used. Inspection of the results shows that the ratio S_{fea}/S_{snedon} deviates significantly from 1.0 when the nominal contact radius is used, while the ratio is much closer to 1.0 when a_{max} is used. This indicates that it is the maximum contact area rather than nominal contact area determines the stiffness, and we can conclude that the stiffness equation Eq.(1.1) works well in elastic-plastic indentation by a rigid 70.3° cone if the true contact radius, a_{max}, is used. However, the FEA results are higher than stiffness equation predictions by about 4.5% to 9% depending on the material properties. We suggest that the average overestimation value 1.06-1.07 can be used as an approximate correction factor β for elastic-plastic indentation by a cone with 70.3° half-included angle to determine the elastic modulus accurately using the corrected stiffness equation. However, it should be noted that the observations here are only for a 70.3° cone, and β may differ significantly from the Sneddon solution for sharp indenters. This will be shown later.

3.2 Comparison to elastic indentation of a conical indenter in a matching conical hole

The FEA results of elastic indentation into a hole are compared with the FEA results for elastic-plastic indentation in Fig.3.4 for ν=0.3 and θ=70.3°. The figure also includes a prediction from Sneddon's equation, Eq.(1.1). Since both a_{max} and a_{nom} are used in the case of elastic indentation into a hole and Eq.(1.1), the stiffness values are plotted against the indentation depth used in the finite element calculations for elastic-plastic indentation. The deformed mesh is included in the figure to show the influence of

pile-up and sink-in on the stiffness. It is seen that for piled-up materials (Fig.3.4 a), a_{max} is larger than a_{nom}, and using a_{max} as the hole radius gives a better approximation of the stiffness. It should be noted that the conical indentation of a matching conical hole will give larger stiffness than the Sneddon's equation at the same contact radius due to the correction factor.

As shown in Fig.3.4, elastic indentation into a hole with radius a_{max} gives stiffnesses that agree well with FEA results of elastic-plastic indentation and somewhat larger than the prediction from the stiffness equation, while using a_{nom} as the hole radius gives stiffnesses that deviate significantly. This indicates that elastic indentation into a hole is indeed equivalent to the unloading procedure in elastic-plastic indentation if the true contact radius, a_{max}, is used. Thus one contribution to the correction factor in elastic-plastic indentation is due to the existence of the hardness impression, that is, the change in geometry for a flat half-space used in the Sneddon solution to a non-flat surface. However, we can not separate the effects of the permanent impression from the effects of the prohibition of radial displacement in FEA of elastic indentation.

Values of β extracted from the data in Fig.3.4 are replotted in Fig.3.5 in order to compare the elastic-plastic results with elastic calculations for a cone in a matching hole with a contact radius equal to a_{max}. It is seen that FEA of the elastic-plastic indentation has a slightly larger normalized stiffness than that for FEA of elastic indentation into a hole for materials showing pile up, but has a lower one for materials that sink in. This dependence on materials properties might be partially caused by the inaccuracy of determining the contact radii from FEA. However, the correction factor values for elastic indentation into a hole are

Figure 3.4 Comparison of the stiffness values based on FEA of elastic-plastic indentation, FEA of elastic indentation into a matching hole and the prediction of Eq.(1.1) for ν=0.3 and θ=70.3°. (amax and anom were used in the latter two cases.)

(a) E=100GPa,σ_y=0.1GPa; (b)E=100GPa, ,σ_y=10GPa

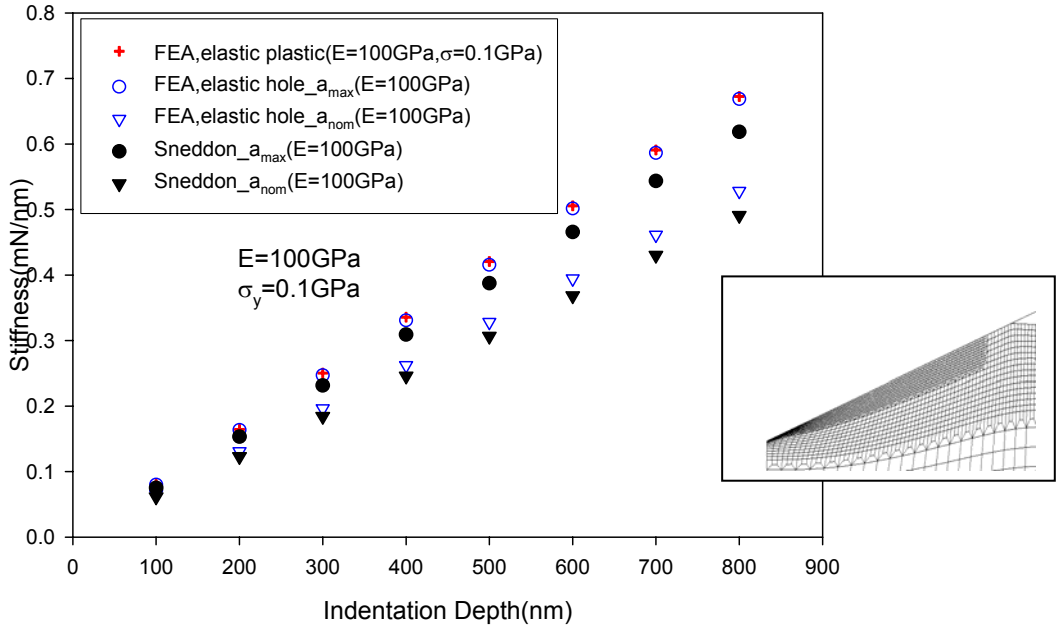
FEA,elastic plastic(E=100GPa,σ=0.1GPa)
FEA,elastic hole_a_max(E=100GPa)
FEA,elastic hole_a_nom(E=100GPa)
Sneddon_a_max(E=100GPa)
Sneddon_a_nom(E=100GPa)
E=100GPa
σ_y=0.1GPa
Stiffness(mN/nm)
Indentation Depth(nm)
0.0
0.1
0.2
0.3
0.4
0.5
0.6
0.7
0.8
0
100
200
300
400
500
600
700
800
900

(a)

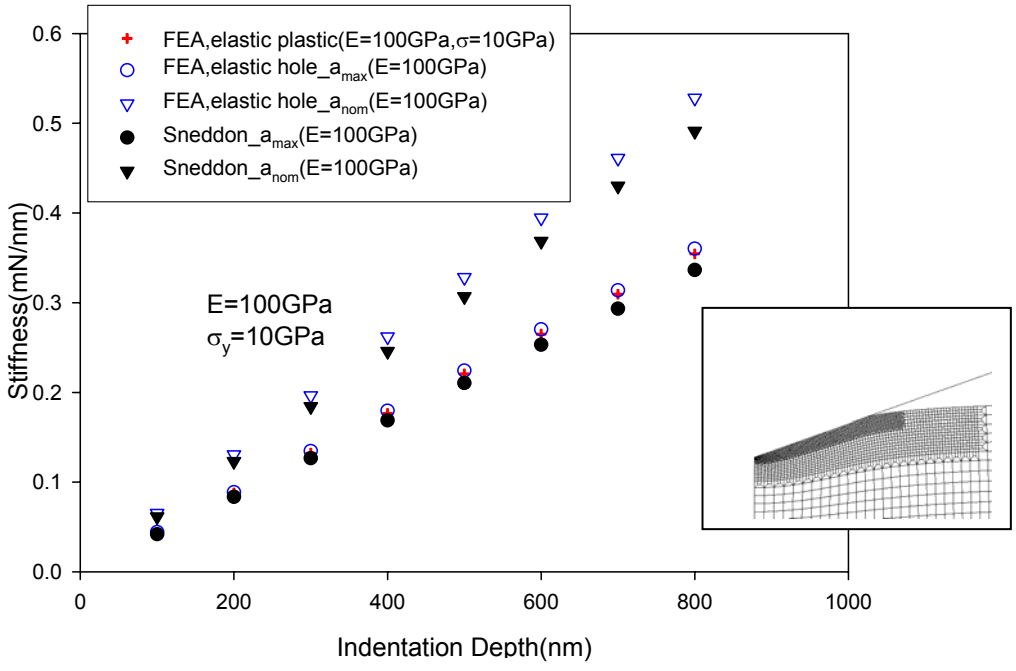
FEA,elastic plastic(E=100GPa,σ=10GPa)
FEA,elastic hole_a_max(E=100GPa)
FEA,elastic hole_a_nom(E=100GPa)
Sneddon_a_max(E=100GPa)
Sneddon_a_nom(E=100GPa)
E=100GPa
σ_y=10GPa
Stiffness(mN/nm)
Indentation Depth(nm)
0.0
0.1
0.2
0.3
0.4
0.5
0.6
0
200
400
600
800
1000

(b)

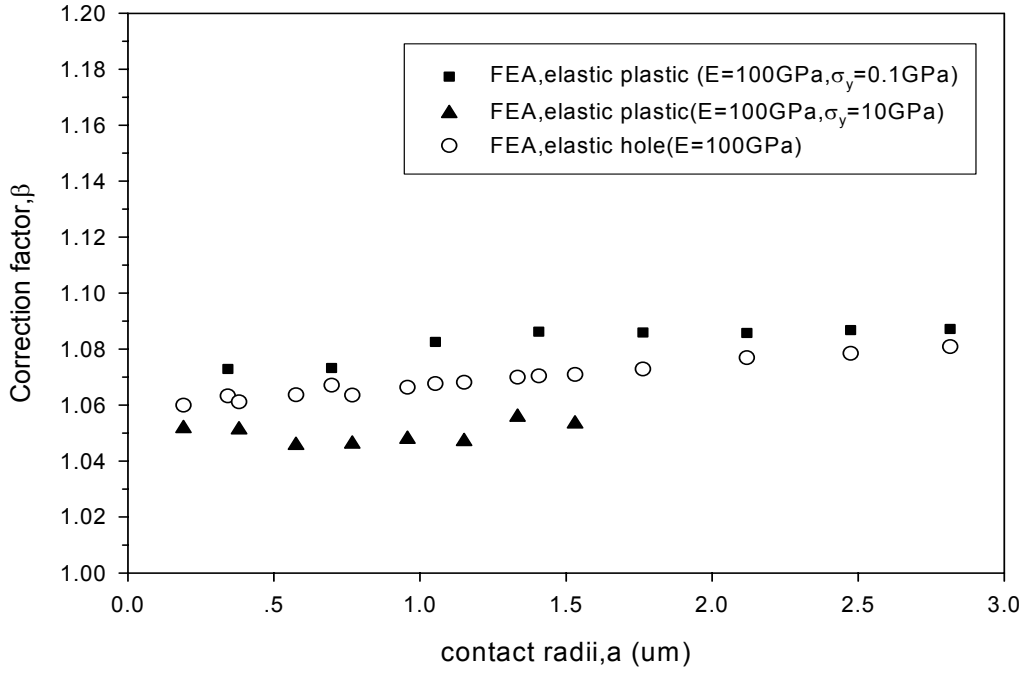

Figure 3.5 Variation of correction factor, β, with contact radii, a, for elastic-plastic indentation and elastic indentation into a hole by a 70.3° cone (frictionless contact)

in the range from 1.06 to 1.08 and the ones from FEA of elastic-plastic indentation are in the range from 1.04 to 1.09 from both hard and soft materials. Thus, they are all approximately in the same range. In addition, 1.06-1.07, the average value of the correction factor for elastic-plastic indentation falls in the stiffness range for elastic indentation into a hole. We thus propose that a value of β of 1.06-1.07 is appropriate for elastic-plastic indentation, and that this value can be understood from strictly elastic calculations of indentation of a conical indention into a matching conical hole. The possible errors in the stiffness are within $\pm$3% for extremely soft and hard materials.

3.3 The dependence of the correction factor on half-included angle

The dependence of β on the angle of the indenter was explored over the range θ=40°-80° for elastic-plastic materials in the case of no friction and ν=0.3. Fig.3.6 compares the correction factors from FEA of elastic-plastic indentation to those of elastic indentation into holes for the same contact radii a_{max}. It is seen that both cases give similar correction factors independent of the hardness of the elastic-plastic materials when the half included angle $\theta \geq 60°$, while the correction factors from FEA of elastic-plastic indentation for sharp cones are significantly different for soft materials and hard ones. The deviation for sharp cones in elastic-plastic indentation of soft materials is associated with a large pile up around the indenter. The FEA mesh is distorted heavily and only 2-4 elements are in contact for $\theta = 40°$. For hard materials, the sharp cone gives convergence problems. For these reasons, the small angles simulations may be subject to error.

Another point worth noting in Fig.3.6 is that the correction factors from elastic-

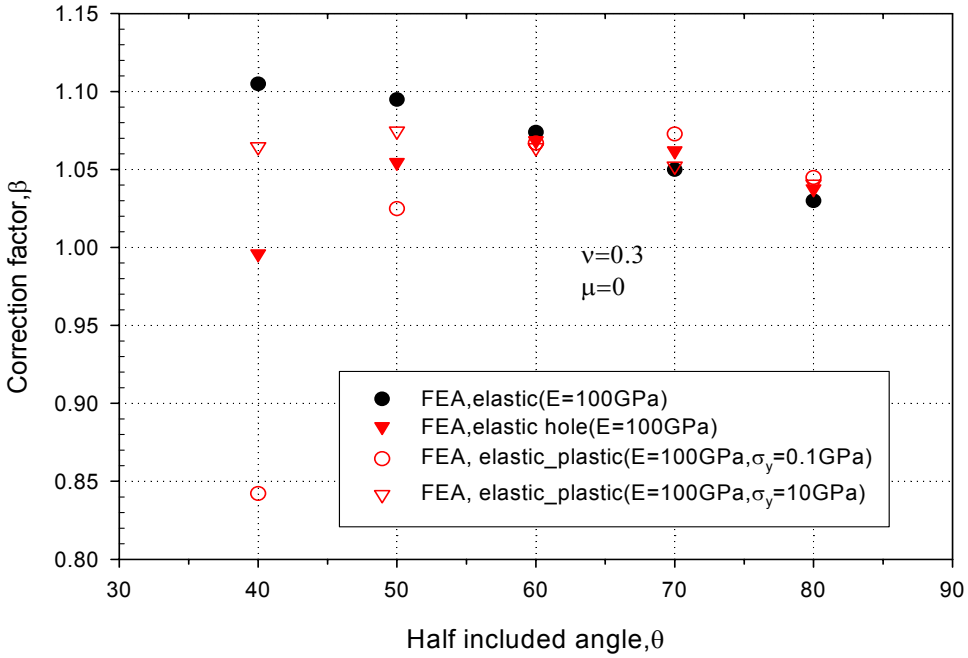

Figure 3.6 Comparison of correction factors, β, from FEA of indentation into elastic holes and FEA of indentation of elastic-plastic materials for different half included angles, θ (ν=0.3, frictionless).

plastic indentation, elastic indentation into a hole, and elastic indentation on flat surface are almost indistinguishable when the half-included angle $\theta \geq 60°$ .However, the correction factors from elastic indentation onto a flat surface continue to increase while those from elastic indentation into a hole and elastic plastic indentation decrease with decreasing the half included angle. This indicates that the correction factors in elastic-plastic indentation (equivalent to elastic indentation into a hole) are significantly influenced by the hardness impression while those from elastic indentation onto a flat surface are caused by prohibition of radial displacement.

To further explore this conclusion, Fig.3.7 compares the correction factors from FEA of elastic indentation into a hole with FEA of elastic indentation onto a flat surface for Poisson's ratio =0.499. For this value of ν, the radial displacement will disappear and thus can not contribute to changes in β. If the correction factors for elastic indentation into holes are caused by the plastic impression and not related to radial displacement, the correction factor will not be 1 even when Poison's ratio is 0.5 because the shape of the holes are different for different conical indenters. As shown in Fig.3.7, the correction factors from FEA of elastic indentation into a flat surface are close to 1, independent of the cone angles while the ones of elastic indentation into a hole decrease from 1 to 0.7 when the cone angle decreases from 90° to 30°. Thus, the decrease in β with decreasing angle is caused by the hardness impression.

3.4 Conclusions

In this chapter, finite element analysis was conducted for indentation of elastic-plastic materials, a matching conical hole premade in elastic materials, and a flat surface

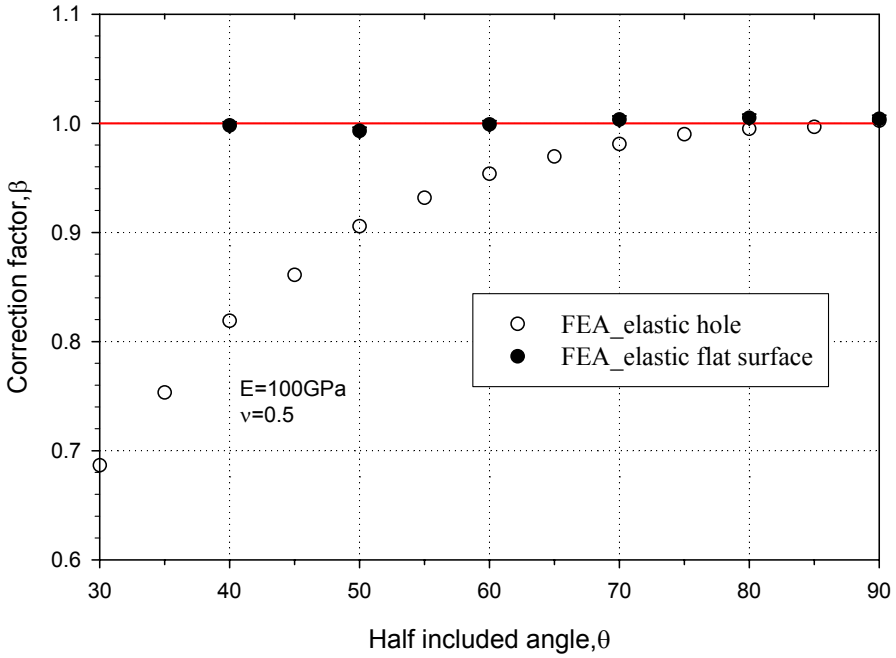

Figure 3.7 Variation of Correction factor, β, with half included angle, θ (ν=0.5,μ=0)

in elastic materials. The following conclusions were revealed:

1. The stiffness equation can be applied to elastic-plastic indentation by a rigid cone but a correction factor should be included to improve its accuracy. The effect of work hardening on the correction factor is not significant.
2. The unloading procedure during nanoindentation of elastic-plastic materials can be approximated by indentation of an elastic material in which the plastic hardness impression is modeled as a conical hole that matches the conical indenter.
3. Whether the material piles up or sinks in, a value of $\beta=1.065$ is a good approximation for a 70.3°conical indenter.
4. For $\nu=0.5$, the correction factor is caused only by the hole formed by the plasticity. For other Poisson's ratios, both the radial displacement and the presence of the hardness impression affect β.

4. An improved relation for the effective elastic compliance of a film/substrate system during indentation by a flat cylindrical punch

In previous chapters, FEA results showed that the stiffness equation, Eq.(1.1), modified with the correction factor β, can be used to determine elastic moduli from the load-displacement curves of conical indentation of elastically homogenous and elastic-plastic homogenous materials. However, due to substrate effects, this method is of questionable value for thin films on substrates when the film thickness is very small compared to the penetration depth. In this case, the elastic modulus measured from the stiffness equation is a composite quantity that is affected by the elastic properties of both the films and the substrates. To extract the film modulus from the measured composite modulus, a good analytical solution that describes the relation between the measured stiffness and the elastic properties of the film and substrate is needed. In this chapter, we will derive a new analytical solution based on the perturbation method used by Gao et al [20].

Gao's solution is based on a first-order elastic perturbation method in which a known exact solution for a homogeneous half space is modified to account for different elastic constants in a thin region near the surface representing the film. The formulation is given in terms of the shear modulus, μ, and Poisson's ratio, ν. As shown in Fig.4.1, the solution applies to the indentation of a thin film of thickness, t, on a semi-infinite substrate indented by frictionless, rigid, flat cylindrical punch of radius, a, loaded to a force, F, to produce a displacement, h. For a homogeneous material, the exact solution is given by [4]

$$\left(\frac{1-\upsilon}{\mu}\right) = 4a\frac{dh}{dF}, \tag{4.1}$$

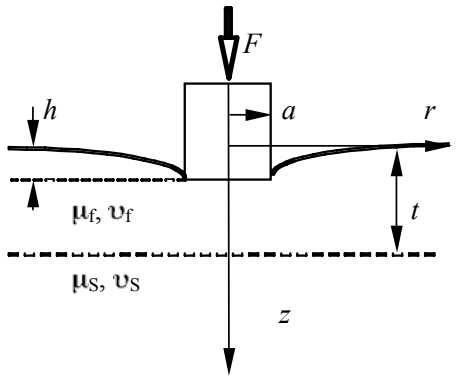

Figure 4.1 Geometry used to describe indentation of a film/substrate system by a flat cylindrical punch.

where the material parameter $(1-\nu)/\mu$ is called the effective compliance [16]. This quantity can be determined experimentally from the known radius of the punch, a, and the measured compliance dh/dF. In Gao's analysis, a perturbation to the half space to account for a difference in the film and substrate properties is accomplished in two separate ways, either: (1) the initially homogeneous material is taken to have the properties of the substrate with the surface layer perturbed to the properties of the film, or (2) the initially homogeneous material is given the properties of the film with the perturbation transforming the lower portion to the properties of the substrate. Letting μ_f and ν_f denote the properties of the film and μ_s and ν_s those of the substrate, the effective compliance when the perturbation occurs in the film is given by

$$\left[\frac{1-\nu}{\mu}\right]_{eff} = \frac{1-\nu_s}{\mu_s}\left[1-\frac{(\nu_f-\nu_s)}{(1-\nu_s)}I_1-\frac{(\mu_f-\mu_s)}{\mu_s}I_0\right] \tag{4.2}$$

where the weighting functions I_0 and I_1 are functions of the normalized film thickness $\xi = t/a$ given by Eq.(1.8). The mathematical form of Eq.(4.2) shows that the function I_0 accounts for differences in shear modulus, whereas I_1 accounts for Poisson's ratio effects. Both weighting functions have simple limits, approaching zero as $t/a \to 0$ and increasing to unity as $t/a \to \infty$. Although not given explicitly in Gao's paper, the equivalent expression when the perturbation takes place in the substrate is given by

$$\left[\frac{1-\nu}{\mu}\right]_{eff} = \frac{1-\nu_f}{\mu_f}\left[1-\frac{(\nu_s-\nu_f)}{(1-\nu_f)}(1-I_1)-\frac{(\mu_s-\mu_f)}{\mu_f}(1-I_0)\right] \tag{4.3}$$

Noting that Eqs.(4.2) and (4.3) must, to first order, give the same result, and that the solution must degenerate to the homogenous solution in the limiting cases $t/a \to 0$

(i.e., a homogeneous material with properties of the substrate) and $t/a \to \infty$ (i.e., a homogeneous material with properties of the film), Gao suggested that the expressions be combined to the simple form:

. $$\left[\frac{1-\upsilon}{\mu}\right]_{eff} = \frac{1-\upsilon_S-(\upsilon_f-\upsilon_S)I_1}{\mu_S+(\mu_f-\mu_S)I_0} \tag{4.4}$$

Comparison with finite element simulations showed that Eq.(4.4) is accurate to within 7% provided the film and substrate shear moduli vary by no more than a factor of 2 or 3. Larger variations were not considered, presumably due to the first order nature of the approximation.

Although the limits when $t/a \to 0$ and $t/a \to \infty$ are correctly described by Eq.(4.4), there are other physically important limits that must also be considered. One is the limit $\mu_f \to \infty$, for which Eq.(4.4) reduces to an effective compliance of zero, i.e., the film-substrate system is infinitely rigid. This is what is expected since the film as modeled is infinite in its lateral extent, implying that the force exerted by the indenter is distributed evenly through the rigid film over an infinite area, producing vanishingly small stresses in the substrate. Another important limit is $\mu_s \to \infty$, for which Eq.(4.4) reduces to

$$\left[\frac{1-\upsilon}{\mu}\right]_{eff} = \frac{1-\upsilon_S-(\upsilon_f-\upsilon_S)I_1}{\mu_S(1-I_0)} \tag{4.5}$$

This limit, corresponding to a compliant film on a rigid substrate, is clearly incorrect since the effective compliance in this case should depend primarily on the shear modulus of the film, not the substrate. This leads to important inaccuracies in Gao's solution

when $\mu_f < \mu_s$.

What we wish to show here is that the problem in Gao's solution when $\mu_f < \mu_s$ can largely be eliminated by a simple modification to the solution that maintains the spirit of the first order perturbation approximation. Finite element methods are used to show that the new relation is remarkably accurate, even when the substrate modulus is as much as 10 times greater than that of the film. On the other hand, the new relation does not give the correct limit when $\mu_f \to \infty$, but even so, its accuracy is still as good as or better than Eq.(4.4). In addition, it is shown that a simple weighted average of the two solutions can be used to further improve the accuracy.

4.1 Derivation of a new relation

The new relation is derived by simple substitutions into Eqs.(4.2) and (4.3) and combination of the resulting equations using a slightly different method than that used by Gao. Without loss of first order accuracy, the term μ_s appearing in the denominator of the last term on the right hand side of Eq.(4.2) can be replaced by μ_f giving

$$\left[\frac{1-\nu}{\mu}\right]_{eff} = \frac{1-\nu_s}{\mu_s}\left[1 - \frac{(\nu_f - \nu_s)}{(1-\nu_s)} I_1 - \frac{(\mu_f - \mu_s)}{\mu_f} I_0\right], \tag{4.6}$$

and the term μ_f appearing in the denominator of the last term on the right hand side of Eq.(4.3) can be replaced by μ_s to give:

$$\left[\frac{1-\nu}{\mu}\right]_{eff} = \frac{1-\nu_f}{\mu_f}\left[1 - \frac{(\nu_s - \nu_f)}{(1-\nu_f)}(1-I_1) - \frac{(\mu_s - \mu_f)}{\mu_s}(1-I_0)\right]. \tag{4.7}$$

Making the substitution into Eq.(4.2) assures that when $\mu_f < \mu_s$, the effective

compliance depends primarily on the modulus of the film rather than the substrate. The substitution into Eq.(4.3) is needed to assure that the two equations can be combined in a self-consistent manner.

To combine the relations, we propose a slightly different combination scheme. Gao combined Eqs.(4.2) and (4.3) to the form of Eq.(4.4) using the first order approximation $1-\alpha-\beta \cong (1-\alpha)/(1+\beta)$ (α<<1 and β<<1). Here, we use $1-\alpha-\beta \cong (1-\alpha)(1-\beta)$, which when combined with Eqs.(4.6) and (4.7) gives:

$$\left[\frac{1-\nu}{\mu}\right]_{eff} = \left[1-\nu_s+(\nu_s-\nu_f)I_1\right]\left[\frac{(1-I_0)}{\mu_s}+\frac{I_0}{\mu_f}\right]. \tag{4.8}$$

This new relation for the effective compliance has a particularly simple form since the first term in square brackets on the right hand side incorporates all the Poisson ratio effects while the second term accounts for the effects of the shear modulus. The equation maintains the correct limits when $t/a \to 0$ and $t/a \to \infty$, but more importantly, the rigid substrate limit $\mu_s \to \infty$ is given by

$$\left[\frac{1-\nu}{\mu}\right]_{eff} = \left[1-\nu_s+(\nu_s-\nu_f)I_1\right]\left(\frac{I_0}{\mu_f}\right), \tag{4.9}$$

which depends only on the shear modulus of the film and not the substrate. On the other hand, the rigid film limit $\mu_f \to \infty$ is given by

$$\left[\frac{1-\nu}{\mu}\right]_{eff} = \left[1-\nu_s+(\nu_s-\nu_f)I_1\right]\left(\frac{1-I_0}{\mu_s}\right), \tag{4.10}$$

is not correct since the effective compliance should be zero in this case. In this regard, Eq.(4.8) might be expected to work better when $\mu_f < \mu_s$ and Gao's relation (Eq.(4.4))

when $\mu_f > \mu_s$. How well these relations perform is now assessed by finite element simulation.

4.2 Finite element simulation procedures

Indentation with a cylindrical punch was simulated using the ABAQUS® finite element code. The punch was modeled as a rigid cylinder with a radius of 1μm and the film/substrate system as a cylinder 200 μm high and 200 μm in radius with the film bonded to the substrate. To determine the effects of different indenter radius to film thickness ratios *a/t*, the film thickness was varied from 0.1 μm to 10 μm. The punch and specimen were modeled as an axisymmetric body with a small element size of 0.040 μm in the contact area. Further away, a coarser mesh was employed with fixed boundary conditions at the bottom of the specimen and along its centerline. The sample was modeled as an elastically isotropic material with Young's modulus E and Poisson's ratio ν. The modulus of the substrate was fixed at E_s = 10 GPa while the film moduli were varied in the range E_f = 1 to 100 GPa. Poisson's ratio for the film and substrate were fixed at 0.3 in all calculations first. Then Poisson's ratio of the substrate was chosen at 0.1 and 0.4 to represent the limits respectively. ν_f was varied in the range from 0.0 to 0.5 at an interval 0.1 corresponding to each ν_s value. E_f and E_s were fixed at 10GPa to study the effects of Poisson's ratio only. The indenter was driven in to a depth of 0.050 μm, with the specimen compliance determined from the load-displacement data generated in the simulations.

To verify the mesh and simulation procedures, indentation of a homogeneous

material (i.e., film and substrate properties the same) was examined for comparison to the stiffness equation. The mesh and specimen size were refined until the differences in the simulated and theoretical compliances were less than 1%.

4.3 Results and Discussion

Results of the finite element simulations are compared to predictions of the new relation (Eq.(4.8)) in Fig. 4.2 and Gao's relation (Eq.(4.4)) in Fig. 4.3. In both figures, the range of film to substrate shear moduli is $0.1 \le \mu_f / \mu_s \le 10$, that is, the modulus ratios span a range much greater than the factor of 2 considered in Gao's work. Close inspection of the data shows that the new relation gives more accurate predictions over the entire range, but particularly so when $\mu_f < \mu_s$. In fact, for $\mu_f < \mu_s$, Eq.(4.8) is usually well within 10% of all the finite element results whereas Gao's solution may deviate by as much as a factor of 2. The new relation thus provides a much better approximation, especially when the film is more compliant than the substrate.

Further inspection of the results in Figs.4.2 and 4.3 reveals that the finite element results generally fall somewhere between the predictions of Eq.(4.4) and Eq.(4.8), suggesting that a weighted average of the two solutions might be used to further improve the accuracy. Letting α be the weighting factor ($0 \le \alpha \le 1$), the weighted effective compliance can be written as:

$$\left[\frac{1-\nu}{\mu}\right]_{eff} = \alpha\left[1-\nu_s+(\nu_s-\nu_f)I_1\right]\left[\frac{(1-I_0)}{\mu_s}+\frac{I_0}{\mu_f}\right]+(1-\alpha)\frac{1-\upsilon_S-(\upsilon_f-\upsilon_S)I_1}{\mu_S+(\mu_f-\mu_S)I_0}, \quad (4.11)$$

where $\alpha = 1$ corresponds to the compliance given by the new relation and $\alpha = 0$ to Gao's

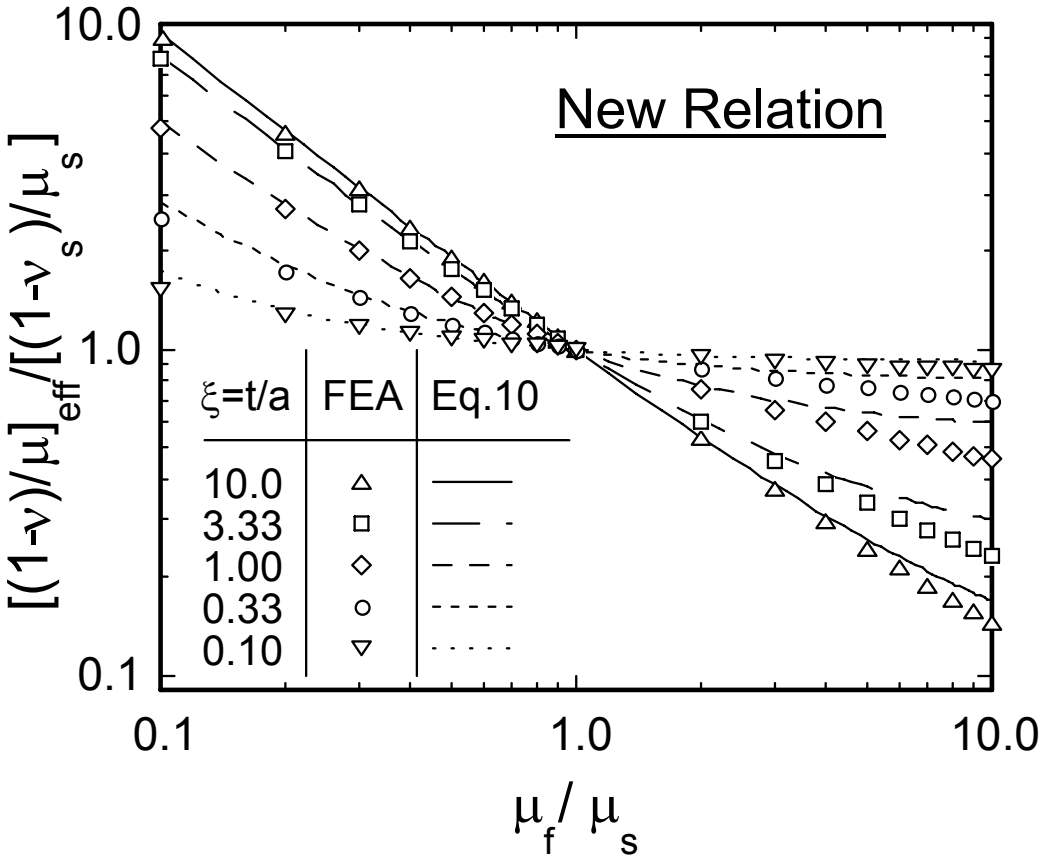

Figure 4.2 Comparison of finite element analysis results (FEA) to predictions of the new relation for the effective compliance, Eq.(4.8).

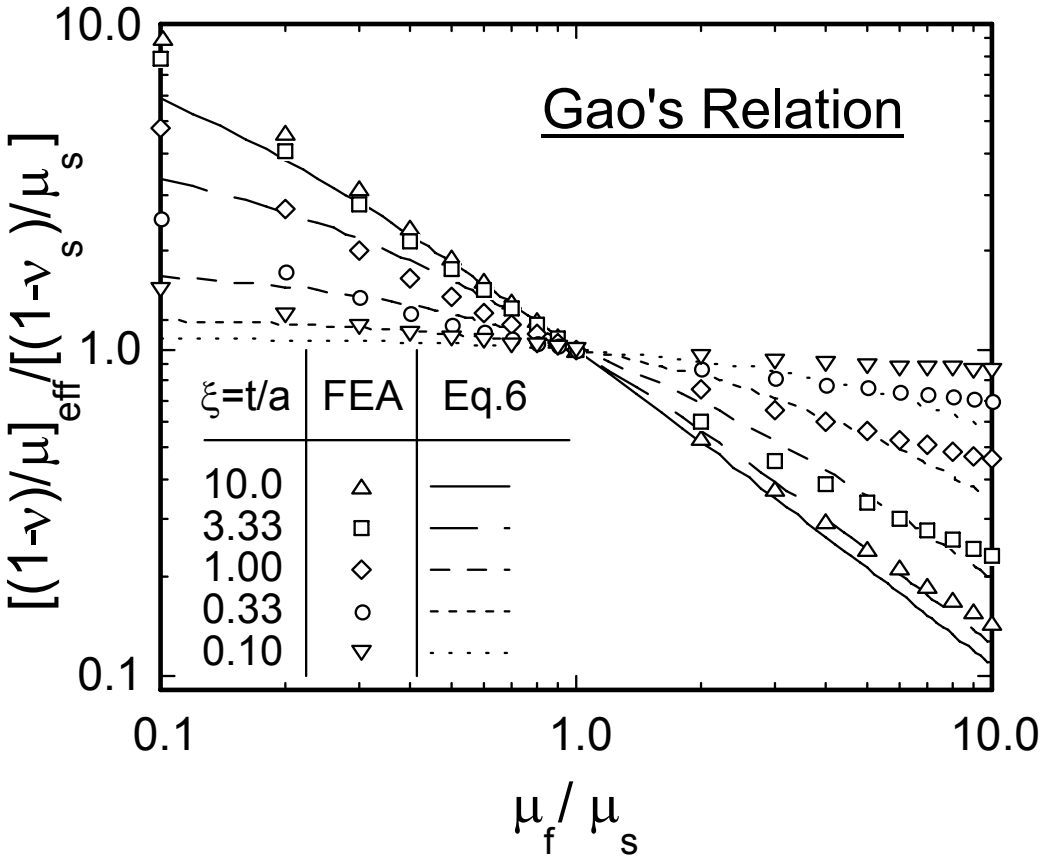

Figure 4.3 Comparison of finite element analysis results (FEA) to predictions of the Gao's relation for the effective compliance, Eq.(4.4).

relation. A numerical examination of the data revealed that the best value of □ depends on $\xi = t/a$ in the manner prescribed in Table 4.1. Thus, if one knows the contact radius and the film thickness, the appropriate weighting factor can be estimated. Unfortunately, there may often be instances in experimental work when the contact radius is not known well, due, for instance, to pile-up or sink-in. In this case, it would be useful to have a single value that can be used to provide a reasonable approximation. By examining the data we have found that $\alpha = 0.89$ works well for $\mu_f < \mu_s$ (accuracy of better than 9% over the entire range), and $\alpha = 0.69$ is a good choice for $\mu_f > \mu_s$ (accuracy of better than 6% over the entire range). It should be noted that the accuracies listed here are those for the extreme cases; for 95% of the finite element results, the accuracy is better than 5%.

Lastly, the effects of Poisson's ratio are shown in Fig.4.4 by comparing finite element results with the new relation and Gao's relation. Both relations give essentially the same good approximation in the case of ν_s=0.1. However, the new relation has a significant deviation when ν_f is less than 0.2 while Gao's relation works well for the whole range of ν_f for ν_s=0.4. Since 0.3 is the most commonly used Poisson's ratio in nanoindentation experiments and both relations work well independent of Poisson's ratio of the substrate materials, the new relation is preferred due to the better accuracy describing the relationship between the effective compliance and E_f.

4.3 Conclusions

A new relation describing the relationship between the effective compliance of thin films on substrates is derived based on the first order perturbation method used by

Table 4.1 Weighting factors α that minimize the maximum difference between finite element analysis results and Equation (4.11) for different values of ξ=t/a

□ =t/a	$\mu_f < \mu_s$		$\mu_f > \mu_s$	
	Weighting factor □	Maximum difference	Weighting factor □	Maximum difference
10.00	0.99	<1%	0.62	-1.19%
3.33	0.97	<1%	0.65	2.54%
1.00	0.93	-1.00%	0.67	1.97%
0.33	0.82	-1.16%	0.74	<1%
0.10	0.72	-1.46%	0.79	<1%

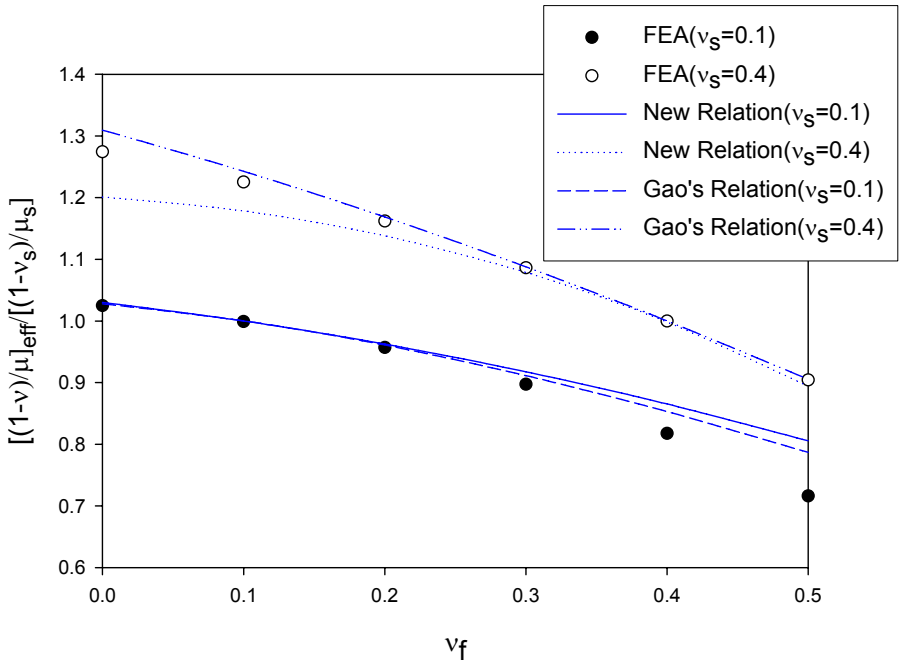

Figure 4.4 .Comparison of FEA results to predictions of the new relation (Eq.(4.8)) and Gao's relation(Eq.(4.4)) to study the effects of vf/vs(a/t=1, Ef=Es=10GPa).

Gao. The FEA results show that the new relation works better than the Gao's solution for compliant films on stiff substrates, with errors less than 10%. A weighted average of the two solutions with an appropriate weighting parameter can predict the film modulus with accuracies of 9% and 6% for $\mu_f < \mu_s$ and $\mu_f > \mu_s$, respectively. The new relation does not model the dependence on Poisson's ratio as well as Gao's relation when ν_f is less than 0.2, but both relations work well for $\nu_f = 0.3$ and different ν_s.

5. A new method for making substrate-independent measurements of thin film elastic moduli by nanoindentaion

In this chapter, we compare the approximate analytical solutions for flat cylindrical punch indentation of elastic film/substrate systems developed by King, Gao et al., Bec et al., and the new relation developed in the previous chapter with finite element simulation results to determine which works best. Then, finite element simulations of the conical indentation of elastic film/substrate systems with matching conical holes to account for the plastic hardness impression are performed to determine what effective film thickness that should be used in the flat punch analytical solutions to approximate the conical indentation. Based on these results, a new method to measure the elastic modulus of compliant thin films on stiff substrates is proposed. The applicability of the new method is tested by comparing its predictions to FEA.

5.1 Assessment of the approximate analytical solutions for a flat punch

Finite element simulations of indentation of elastic film/substrate systems with a flat cylindrical punch were implemented using the commercial finite element software ABAQUS. The punch was modeled as a rigid body and the specimen as a cylinder which has dimension 200μm in height and 200μm in radius. These were found to be large enough to satisfy the half space assumption. To simplify the simulation, the punch and specimen were modeled as axisymmetric bodies. An axisymmetric boundary condition was applied to the centerline and roller boundary conditions to the bottom of the specimen. The indentation procedure was implemented by applying a downward displacement of 20nm, to the reference point of the rigid flat cylindrical punch.

Different a/t ratios were examined to study their effects on the normalized stiffness, S/S_0. The specific values were 0.2793, 0.558, 0.8379, 1.117, 1.3965, 1.676, 2.234, 2.5136, and 2.7928. The reason for the choice of these values will be given later. In each simulation, the film thickness was fixed as 1μm and the flat punch radii were allowed to change. For each a/t ratio, different mesh densities were adopted to assure a sufficient number of contact elements under the punch; typically, forty elements were in contact. The sizes of the elements in the transition region from the film to the substrate were almost constant to reduce the discontinuities in the stress field caused by different mesh sizes.

Both the film and substrate materials were assumed to be isotropic elastic with two types of film/substrate systems modeled. One was composed of compliant films on stiff substrates. In this case, E_s was fixed to 10 GPa, while E_f was chosen as 1, 2, 4, and 8GPa. The other consisted of stiff films on compliant substrates. E_s was still 10GPa with E_f of 20, 40, 80, and 100 GPa. Both ν_f and ν_s were fixed at 0.3, .i.e., the effect of Poisson's ratio was not considered.

To verify the effectiveness of the mesh, indentations of homogenous substrate materials with flat punches of different contact radii were simulated. Fig.5.1 shows that the correction factor, β, which is obtained by comparing the stiffness of FEA with the prediction from Eq.(1.1) at the same contact radius, is almost 1 with errors less than 1% for frictionless contact, indicating the meshes used for different a/t ratios yield almost the same results, and mesh effects are negligible.

Fig.5.2 compares the normalized stiffnesses S/S_0 from finite element analysis to

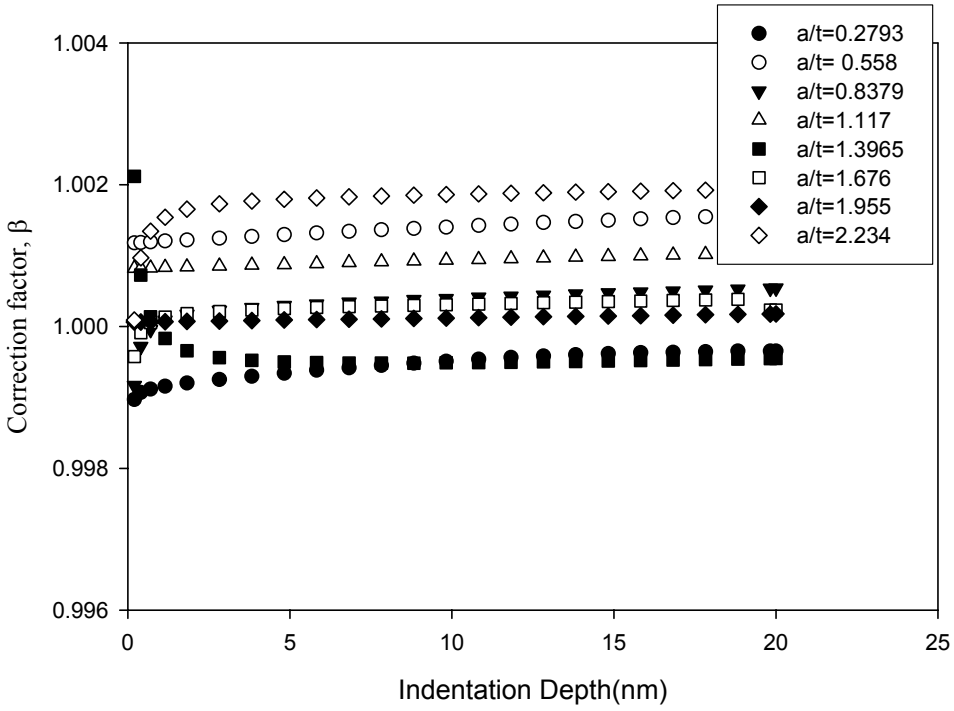

Figure 5.1 A plot of correction factors β for a homogenous substrate material demonstrating that β is close to 1 from all normalized contact sizes, a/t.

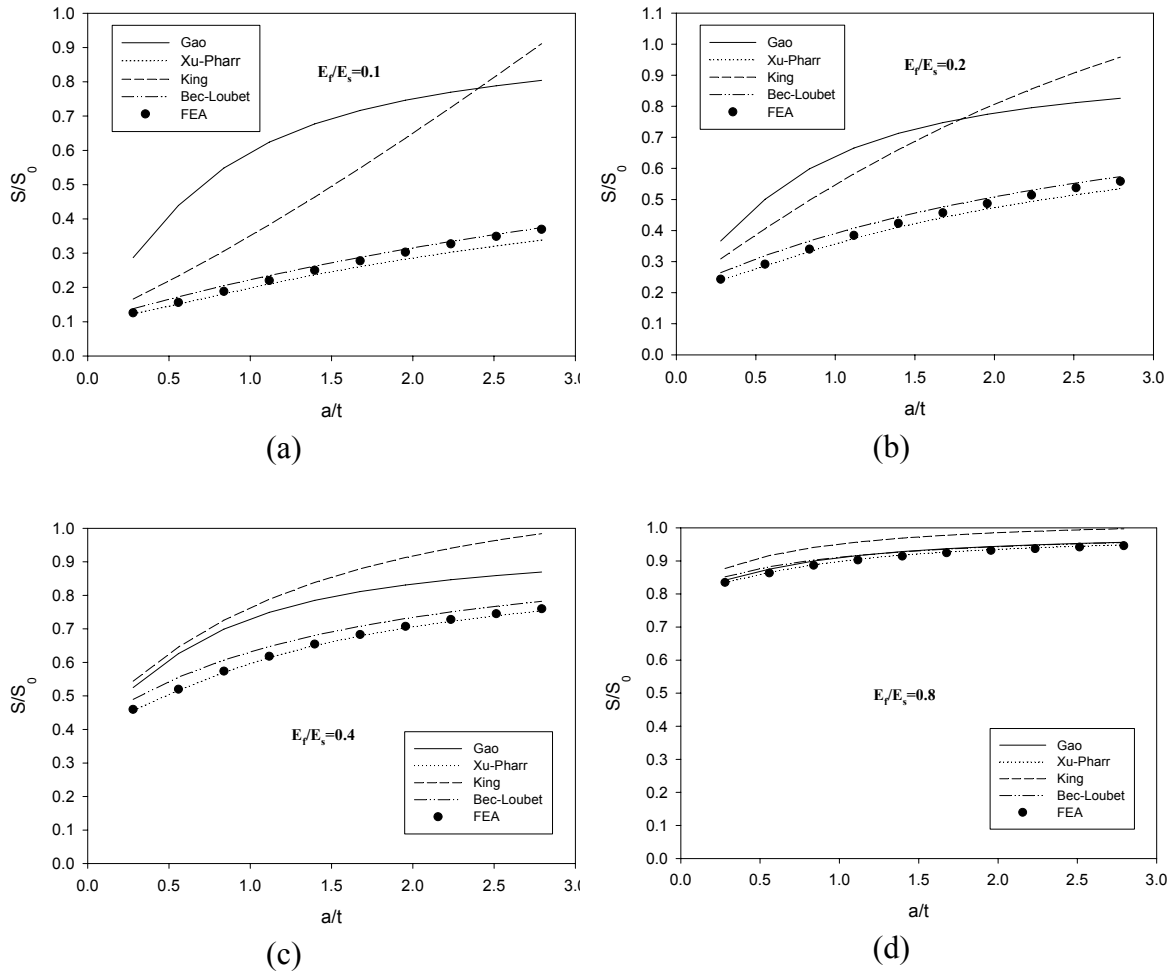

Figure 5.2 Comparison of finite element results with approximate analytical solutions for flat circular punch indentation of compliant films on stiff substrates:

(a) E_f/E_s=0.1, (b) E_f/E_s=0.2, (c) E_f/E_s=0.4, (d) E_f/E_s=0.8.

those predicted from the four approximate analytical solutions for the case of compliant films on stiff substrates. In each plot, the normalized stiffnesses are plotted as functions of the normalized contact radius a/t. E_f/E_s ratios are in the range from 0.1 to 0.8. As shown in the figure, the Bec-Loubet solution and the Xu-Pharr solution agree well with finite element results, even when E_f/E_s=0.1, while Gao's solution and King's solution deviate significantly except the case of E_f/E_s ratio =0.8. For E_f/E_s ratios of 0.1 and 0.2, the Bec-Loubet solution approaches the FEA results more closely than the Xu-Pharr solution for large a/t ratios and the opposite is observed for small a/t ratios.

Fig.5.3 shows results for stiff films on compliant substrates (E_f/E_s >1) and demonstrates that all the approximate solutions work well for a small elastic mismatch between the film and substrate such as E_f/E_s=2. However, for large mismatches, the deviations become large. Although the Xu-Pharr solution is generally more accurate than other solutions, the degree to which it underestimates the FEA results can not be ignored when E_f/E_s is larger than 4.

To test the accuracy of the finite element results, the simulations were reproduced using a different meshing procedure in which the radius of the flat circular punch was fixed as 1μm and the film thickness was varied to obtain the same a/t ratios as in the previous FEA simulations. Due to the change of the geometry, the mesh was significantly different. The results in Fig.5.4 show that essentially the same results are obtained indicating the adequacy of the mesh and the finite element procedures.

The finite element results show that the Xu-Pharr solution and the Bec-Loubet solution work much better than the other solutions for compliant films on stiff substrates.

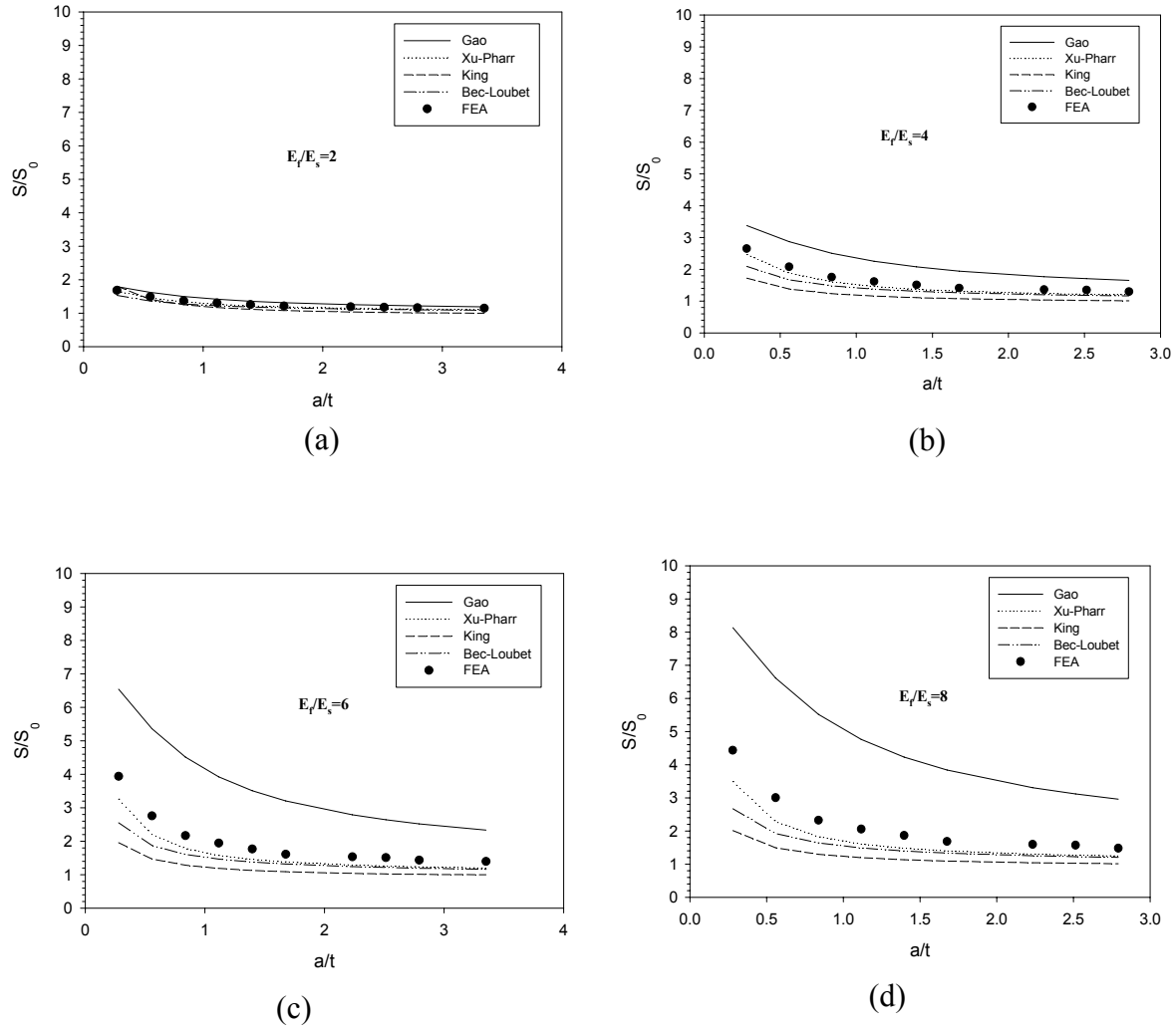

Figure 5.3 Comparison of finite element results with approximate analytical solutions for flat circular punch indentation of stiff films on compliant substrates:

(a) E_f/E_s=2, (b) E_f/E_s=4, (c) E_f/E_s=6, (d) E_f/E_s=8.

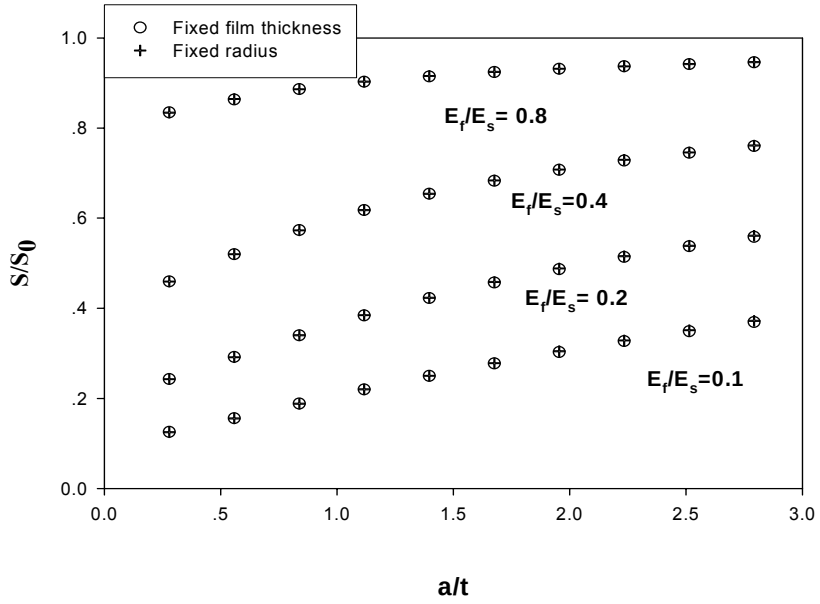

Figure 5.4 Test of the effectiveness of meshes by comparing two different sets of finite element simulations.

For stiff films on compliant substrates, no accurate solutions are yet available. As a result, we focus from here only on the case of compliant films on stiff substrates. Using the Xu-Pharr and Bec-Loubet solutions, it is possible to estimate the film moduli E_f that would be measured from the stiffnesses and contact area determined in the finite element calculations. Fig.5.5 compares the errors in E_f calculated from the Xu-Pharr solution with those computed from the Bec-Loubet solution. Two additional finite element simulations results with a/t ratios of 0.05 and 0.1 were performed to check if the two solutions yield the correct limit (zero error) as a/t approaches zero, corresponding to an infinitely thick film. In these cases, the flat punch radii are small compared to the film thickness and the measured elastic moduli should be close to the actual elastic moduli of film. It is found that both solutions have the correct limits. Note that the error in the Bec-Loubet solution reaches a maximum when a/t is 0.558 especially for E_f/E_s=0.1. The reason is that the term 2a/t in Eq.(1.11) forces the Bec-Loubet solution to have the correct limit as $a/t \rightarrow 0$. Without this term, the solution would give the wrong limit.

The graphs in Fig.5.5 show that the error in E_f estimated from the Bec-Loubet solution and the Xu-Pharr solution are less than 15% when E_f/E_s =0.1, 0.2, 0.4 and 0.8. The Bec-Loubet's solution always underestimates E_f, while the Xu-Pharr solution overestimates E_f except in the case of E_f/E_s =0.8. For E_f/E_s =0.1, the Xu-Pharr solution estimates E_f more accurately than the Bec-Loubet solution when the a/t ratio is less than 1.117, and the situation is the opposite when a/t ratio is larger than 1.117. For E_f/E_s =0.2, the Xu-Pharr solution has a smaller absolute error than the Bec-Loubet solution in the case of a/t ratio less than 1.955, and when the a/t ratio is larger than 1.955, the Bec-

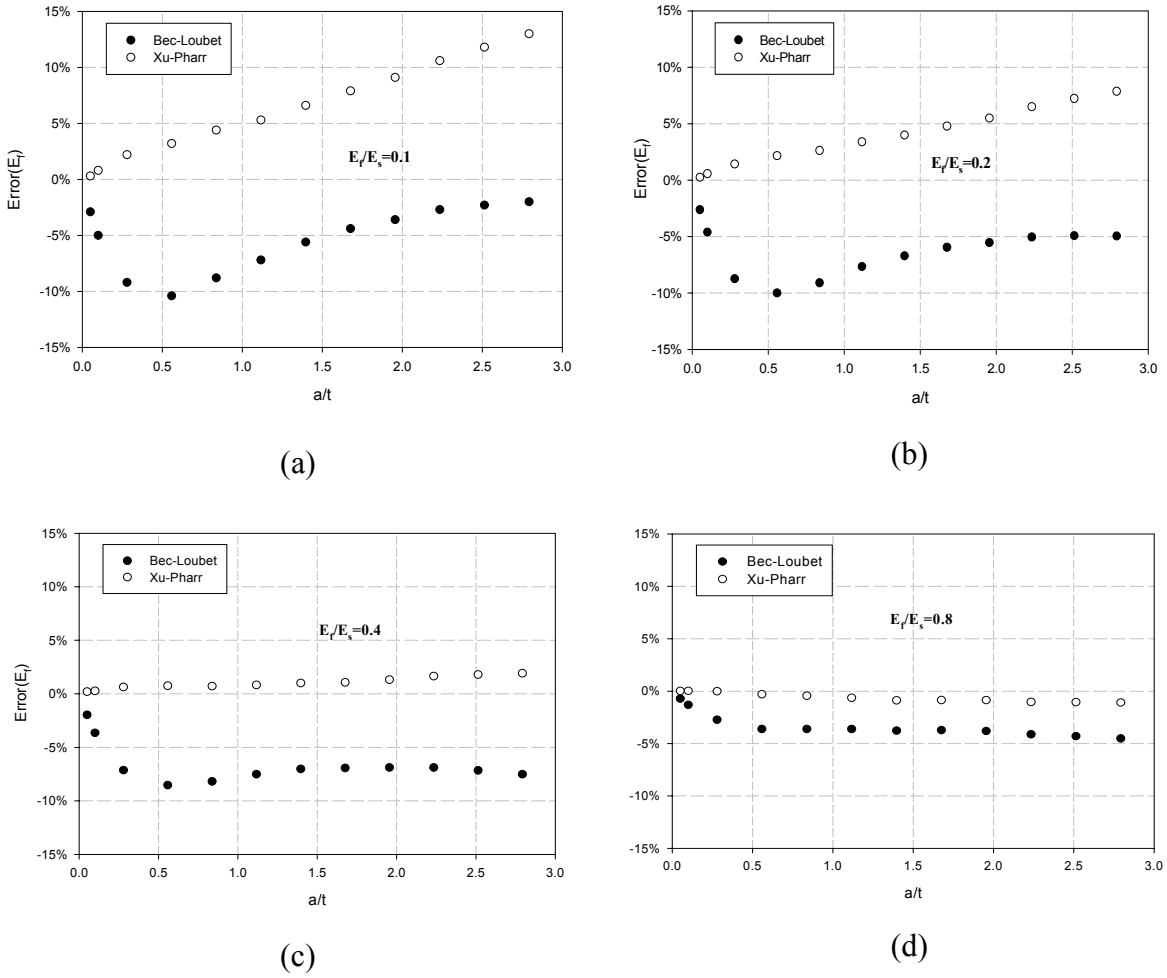

Figure 5.5 A comparison of errors in Ef for the Bec-Loubet and Xu-Pharr solutions. (a) E_f/E_s=0.1, (b) E_f/E_s=0.2, (c) E_f/E_s=0.4, (d) E_f/E_s=0.8.

Loubet solution is better. For E_f/E_s =0.4, the Xu-Pharr solution yields E_f errors less than 5% while using the Bec-Loubet solution results in errors larger than 5% if a/t is larger than 0.01. For E_f/E_s =0.8, both solutions give the error less than 5%, but the Xu-Pharr solution is more accurate.

Overall, the Xu-Pharr solution predicts the elastic modulus of the films more accurately than the Bec-Loubet solution for E_f/E_s ratios are in the range from 0.4 to 1. In addition, the Xu-Pharr solution works better if the a/t ratio is small ,even when E_f/E_s is 0.1. If E_f/E_s is less than 0.4 and the a/t ratio is large, the Bec-Loubet solution is preferred.

5.2 Application of the approximate analytical solutions to conical indentation

Since the Xu-Pharr solution and the Bec-Loubet solution are derived on the basis of contact by a flat cylindrical punch, a question naturally arises as to how well these solutions apply to indentation of film/substrate systems with a conical indenter. However, before applying them, two problems are needed to be addressed.

The first problem is what film thickness should be used in the approximate analytical solutions for the flat punch (the Xu-Pharr or Bec-Loubet solutions) to model the conical indentation. Fig.5.6 (a) shows a schematic of conical indentation of a film/substrate system. The indentation depth of the conical indenter is h, the film thickness is t, and the contact radius is a. King [7] suggested the total film thickness t should be used in the flat punch analytical solutions to approximate conical indentation. This assumes that conical indentation is equivalent to the flat punch indentation at a given contact radii for the same film/substrate system. This case usually underestimates the effect of the elastic properties of substrate because the penetration of the conical indenter

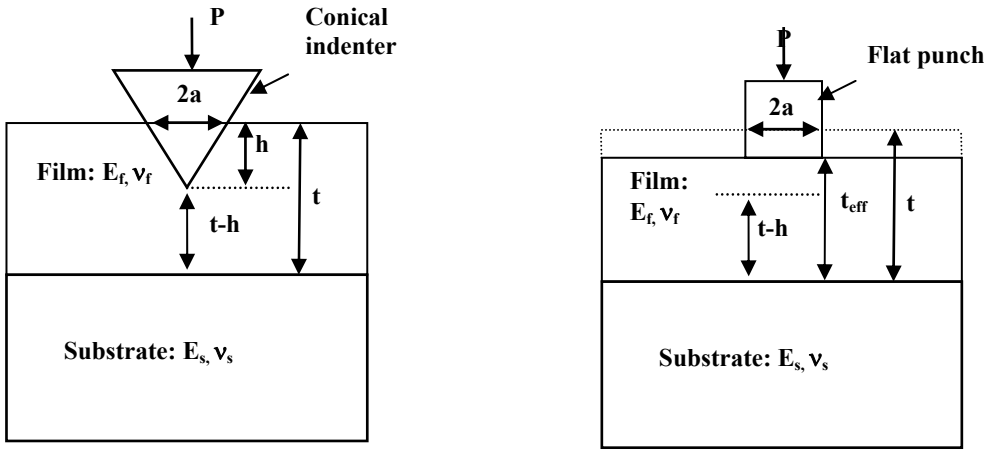

Figure 5.6 Schematic of conical indentation and flat punch indentation of film/substrate systems: (a) conical indentation, (b) flat punch indentation

into the film is neglected in the flat punch model, that is, the tip of the conical indenter is closer to the substrate than the flat punch. Saha and Nix [22] propose that the film thickness should be reduced by the penetration of conical indenter, and a reduced film thickness (t-h) should be used in the flat punch solution. This approximation usually overestimates the effect of substrate, since for conical indentation, only the tip of the indenter is close to the film/substrate interface and the sides of indenter are further from the interface than the tip. Hence, the film thickness used in flat punch model should probably be between the reduced film thickness and the total film thickness, as shown in Fig.5.6 (b). We define this film thickness as the effective film thickness. In the next part of this chapter we will use finite element simulation of conical indentation and flat punch indentation to determine the effective film thickness.

The other problem is how to account for the permanent hardness impression formed during the conical indentation of elastic-plastic materials, which we know to affect the stiffness of homogenous materials. For conical indentation of elastic-plastic film/substrate systems, a permanent impression is formed in the film due to the plasticity. To avoid the complexity of simulating elastic-plastic indentation, the elastic unloading from the plastic impression (shown in Fig.5.7(a)) can be modeled as the elastic reloading of the conical indenter into a hole in the film which has the same geometry as the impression (Fig.5.7(b)). To simplify the model, we make two assumptions: one is that no pile up and sink in occur during the conical indentation; the other is that the hardness impression matches the geometry of the conical indenter. To compare FEA of conical indentation of an elastic hole with flat punch indentation, the same contact radii are

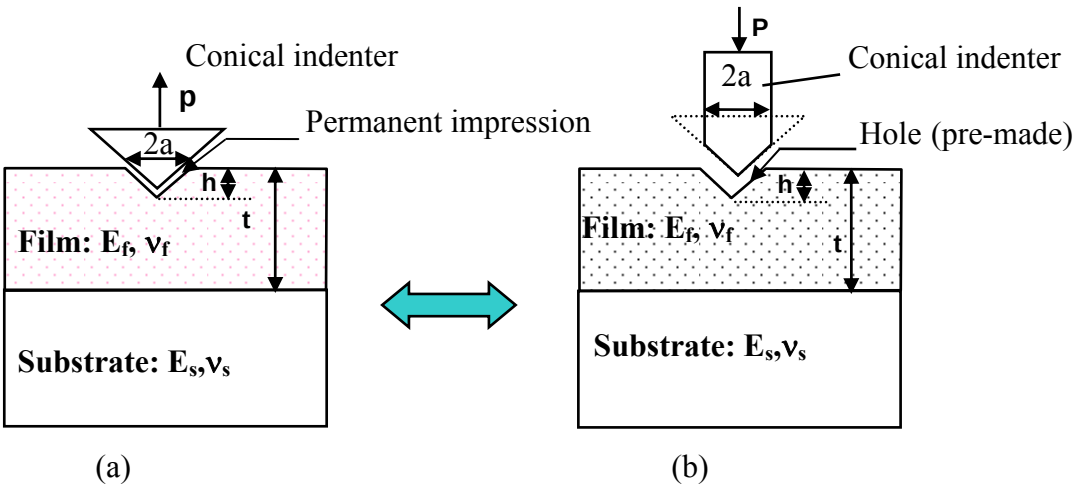

Figure 5.7 Schematic illustration of (a) elastic-plastic contact and (b) elastic contact of a conical indenter in a conical hole in the film.

selected for both cases, and the hole depth is determined from the geometry of the conical indenter. Choosing different contact areas allows us to study the effects of different indentation depths on the accuracy of the approximate solutions. In Chapter 3, we showed the equivalence of conical indentation of elastic holes and the unloading procedure of conical indentation of homogenous elastic-plastic materials.

5.3 Determination of the effective thickness by finite element simulation

The effective film thickness can be determined by finite element simulation of elastic contact of a conical indenter in a conical hole of depth h and comparing to flat punch indentation at the same contact area.

The conical indenter is modeled as a rigid body with a half included angle of 70.3°. The specimen is modeled as a cylinder with height and radius 400μm, which are large enough to satisfy the half space assumption. The boundary conditions are the same as for simulations of the flat punch indentation.

In order to facilitate comparison, the same a/t ratios as in the FEA of flat punch indentation are used. The a/t values are 0.2793, 0.558, 0.8379, 1.117, 1.3965, 1.676, 1.9550, 2.234, 2.5136, and 2.7928 respectively. Because a= h tan 70.3°, the corresponding h/t values are 0.1, 0.2, 0.3, 0.4, 0.5, 0.6, 0.7, 0.8, 0.9 and 1.0, and this is the reason we chose the irregular a/t ratios values for flat punch indentation. In conical indentation, h is the vertical depth of the hole pre-made in the film. For example, h/t=1 means that the depth of the hole is equal to the film thickness and the tip of hole is right at the interface between film and substrate. In our simulations, the film thickness was fixed as 1μm and the radius of the hole was allowed to vary. Due to the geometric

relationship between the radius of the hole and the depth of the hole, the depth is set when the radius is fixed. The elastic properties of the film and substrate used in conical indentation simulations are the same as those used in the simulations of flat punch indentations.

To verify the effectiveness of the different meshes, conical indentations of homogenous substrate materials with different contact radii were simulated. Fig.5.8 shows that β is in the range from 1.045 to 1.055 when the indentation depth is larger than 5nm. This indicates the meshes used for the different a/t ratios can yield consistent results with the previous FEA calculations for conical indentation of matching conical holes in homogenous materials. It is noted that β obtained here is slightly different from that in Chapter 2. The reason for that the mesh used in this chapter was an early version that is not as accurate as that in Chapter 2. Although the β values here are slightly less than the ones in Chapter 2, this will not affect the normalized stiffness since the same correction factor values are used to determine S and S_0 and the influence of β on S/S_0 cancels out. S_0 is the contact stiffness of homogenous substrate materials with a conical hole.

Similarly, we also did a set of simulations of conical indentations in which the hole radius was fixed and the film thickness was changed to keep the same a/t values to check the validity of the meshes. Fig.5.9 shows plots of S/S_0 against a/t for conical indentation simulations using the different meshes. It is seen that both cases give almost the same results, indicating that the simulation models for conical indentation are appropriate. In addition, results for flat punch indentations are plotted in Fig.5.9 to compare with the conical indentation at the same a/t ratios. In the case of $E_f<E_s$, the

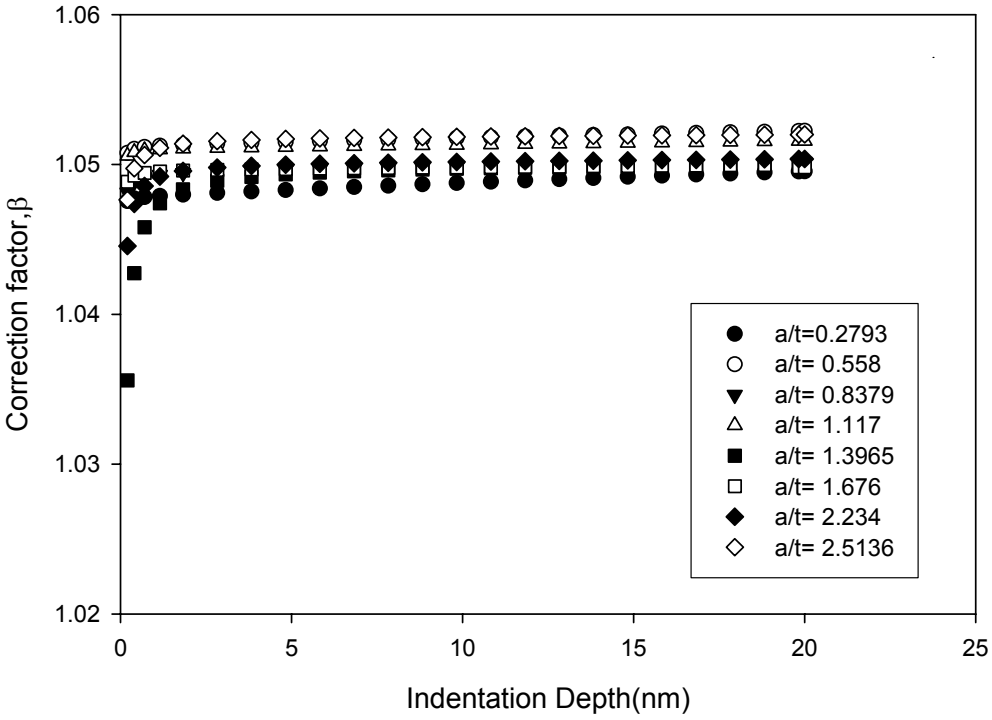

Figure 5.8 The correction factor β for conical indentation of a conical hole for a homogenous material demonstrating the adequacy of the mesh.

normalized stiffness of the conical indentation is similar to that for flat punch indentation for the same a/t ratio when the a/t ratio is small. With increasing a/t, conical indentation yields higher normalized stiffness than flat punch indentation due to the influence of the stiff substrate. It is noted that the difference between conical indentation and flat punch indentation decreases as the difference between E_f and E_s decreases for all a/t ratios. In the case of $E_f>E_s$, the normalized stiffness for conical indentation is almost the same as flat punch indentation for all a/t ratio values. Therefore, the total film thickness can be used with the approximate analytical solutions of flat punch indentation to model the conical indentation. However, recall that we do not have good analytical solutions for flat punch indentation when $E_f>E_s$.

In the case of compliant films on stiff substrates, the normalized stiffness of conical indentation is larger than flat punch indentation when a/t is large. This indicates the substrate effect is more significant in conical indention than in flat punch indentation at the same contact radii and film thickness. To obtain the same normalized stiffness, an effective film thickness must be used.

Here, we suggest a method to determine the effective film thickness based on a comparison between the normalized stiffness values from FEA results of conical indentation and flat punch indentation (shown in Fig.5.10). Curve fitting is used to connect the data points for flat punch indentation simulations smoothly. As shown in Fig.5.10, the effective film thickness is defined by finding the a/t value on the curve for the flat punch which yields the same normalized stiffness as the conical indentation. This a/t ratio for the equivalent flat punch indenter is a/t_{eff}, and the effective film thickness t_{eff}

Figure 5.9 Plots of S/S0 values from FEA for conical indentation and flat cylindrical punch indentation of elastic film/substrate systems as a function of a/t ratios. Open circles (o) represent the flat punch, Cross (x) and plus (+) signs represent conical indentation with fixed film thickness and with fixed contact radius, respectively.

(a) $E_f<E_s$ (b) $E_f>E_s$

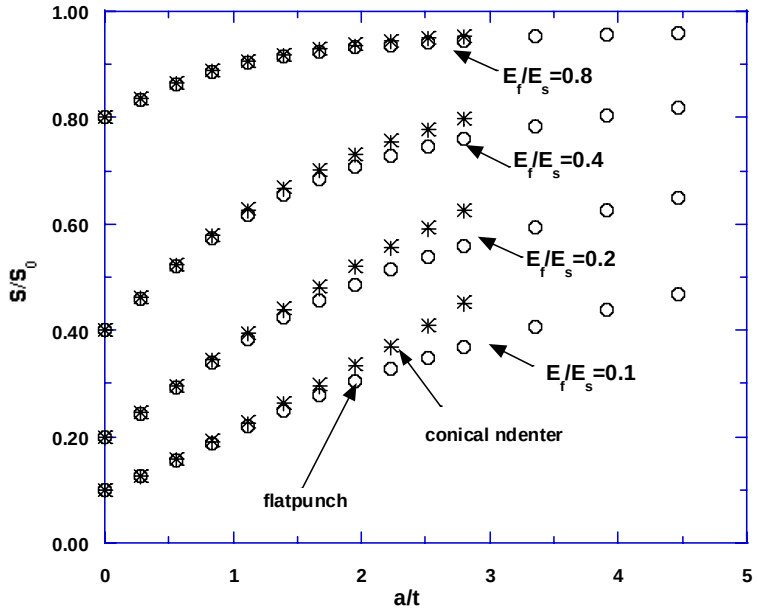
1.00
0.80
0.60
0.40
0.20
0.00
S/S0
0
1
2
3
4
5
a/t
Ef/Es=0.8
Ef/Es=0.4
Ef/Es=0.2
Ef/Es=0.1
conical ndenter
flatpunch

(a)

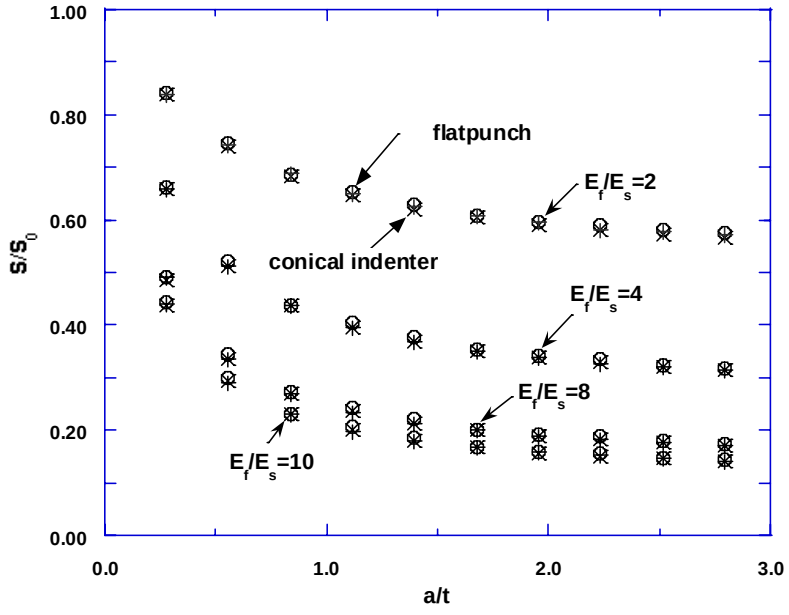
1.00
0.80
0.60
0.40
0.20
0.00
S/S0
0.0
1.0
2.0
3.0
a/t
flatpunch
Ef/Es=2
conical indenter
Ef/Es=4
Ef/Es=8
Ef/Es=10

(b)

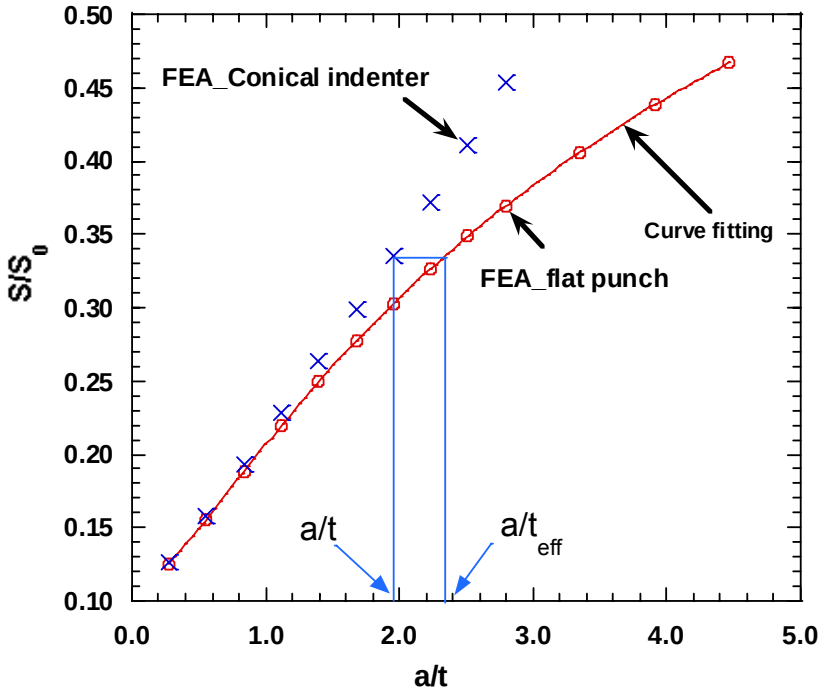

Figure 5.10 Schematic of the method used to determine the effective film thickness from the plots of S/S0 vs. a/t ratios for conical and flat punch indentation.

can be determined because the contact radius values are the same for the conical indentation and flat punch indentation. Additional simulations of flat punch indentation with a/t larger than 2.7928 were performed to determine the effective film thickness for conical indentation with a/t=2.7928(h/t =1), which is the case of conical indentation with a depth of penetration equal to the film thickness.

Using this method, the effective thickness values for different depth holes corresponding to different conical indentation depths were calculated. The variation of the effective thickness is plotted against hole depth in Fig.5.11 where both parameters are normalized with respect to the total film thickness. An important observation is that the effective film thickness is almost independent of E_f/E_s, even when the hole depth is 70% of the film thickness. This allows us to use curve fitting to obtain a single equation to describe the relationship between t_{eff}/t and h/t for compliant films on stiff substrates. The scatter in the computed effective film thickness for h/t=0.1 is probably due to calculation inaccuracies for the small contacts. After deleting this outlier, a second order polynomial fitting of the mean t_{eff}/t values gives:

$$\frac{t_{eff}}{t}=1.00-0.09\left(\frac{h}{t}\right)-0.19\left(\frac{h}{t}\right)^2 \qquad (5.1)$$

Eq.(5.1) is very important because of its independence of E_f/E_s. It can be used to determine the effective film thickness from the measured indentation depth and the film thickness in indentation experiments.

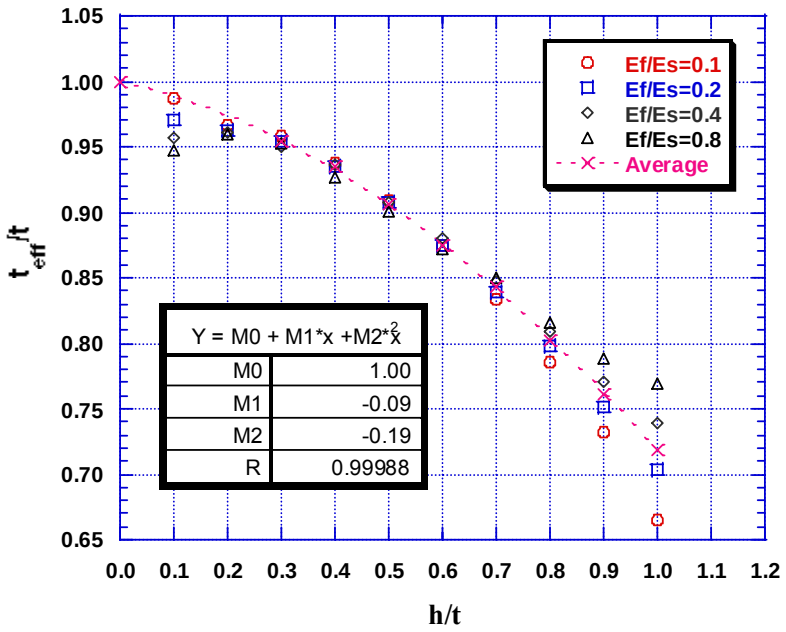

Figure 5.11 The effective film thickness for different h/t ratios.

5.4 A method to extract elastic moduli of films from nanoindentation measurements

Based on the above analysis, we now propose a method to extract the elastic moduli of films using conical nanoindentation of film/substrate systems for compliant films on stiff substrates. A flow chart for the method is shown in Fig.5.12. The method assumes there is no sink-in or pile-up, the effects of which will be considered in the next chapter. The required parameters are the film thickness and the elastic modulus of substrate. From nanoindentation tests, the stiffness, penetration depth and contact radius are obtained. The effective film thickness is calculated from the measured film thickness and penetration depth by Eq.(5.1). Finally, an approximate analytical solution for flat punch indentation is used to determine E_f with the known elastic modulus of the substrate, film thickness, contact radius and measured stiffness. It has been shown that the Xu-Pharr solution and the Bec-Loubet solution are the two best candidates for flat punch indentation of film/substrate systems. The applicability of these solutions in the new method are now tested using FEA results for conical indentation respectively.

First, the Xu-Pharr solution is examined. Fig.5.13 plots the errors in E_f against the depth of the hole normalized by the total film thickness. The errors are the difference between the actual E_f values input into the FEA and those computed from the Xu-Pharr solution. Two different film thicknesses (t_{eff} and t) are used. It is observed that the errors increase with increasing h/t. A large h/t ratio for conical indentation is equivalent to the case of conical indentation with a penetration depth large compared to the film thickness. Therefore, the deeper the conical indenter is driven into the film, the less accurate this method.

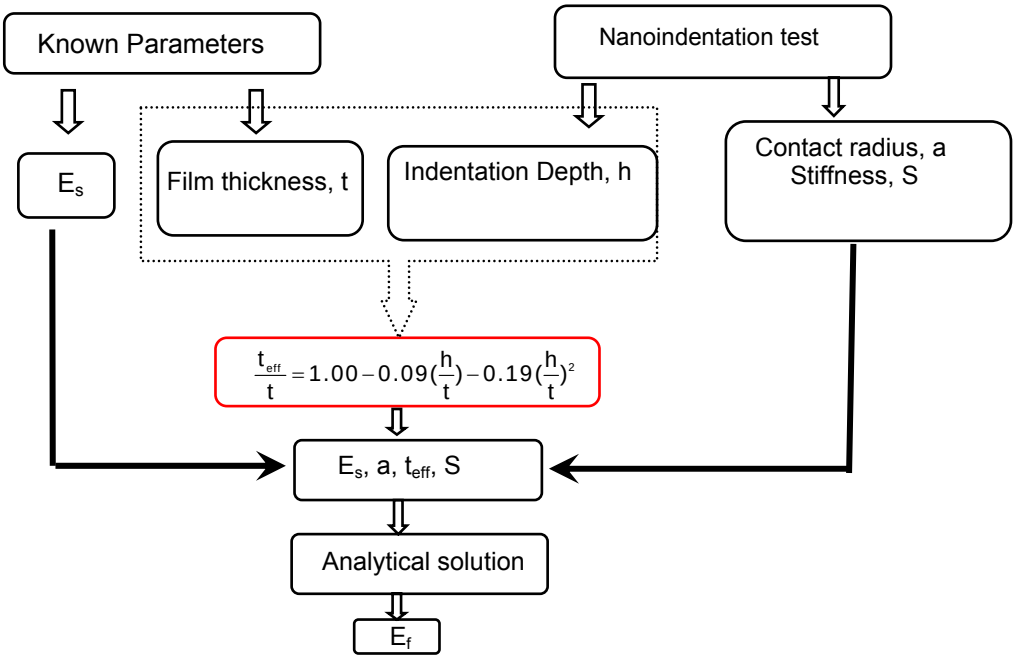

Figure 5.12 Flow chart showing how to extract film elastic moduli from nanoindentation tests using the effective film thickness and analytical solutions

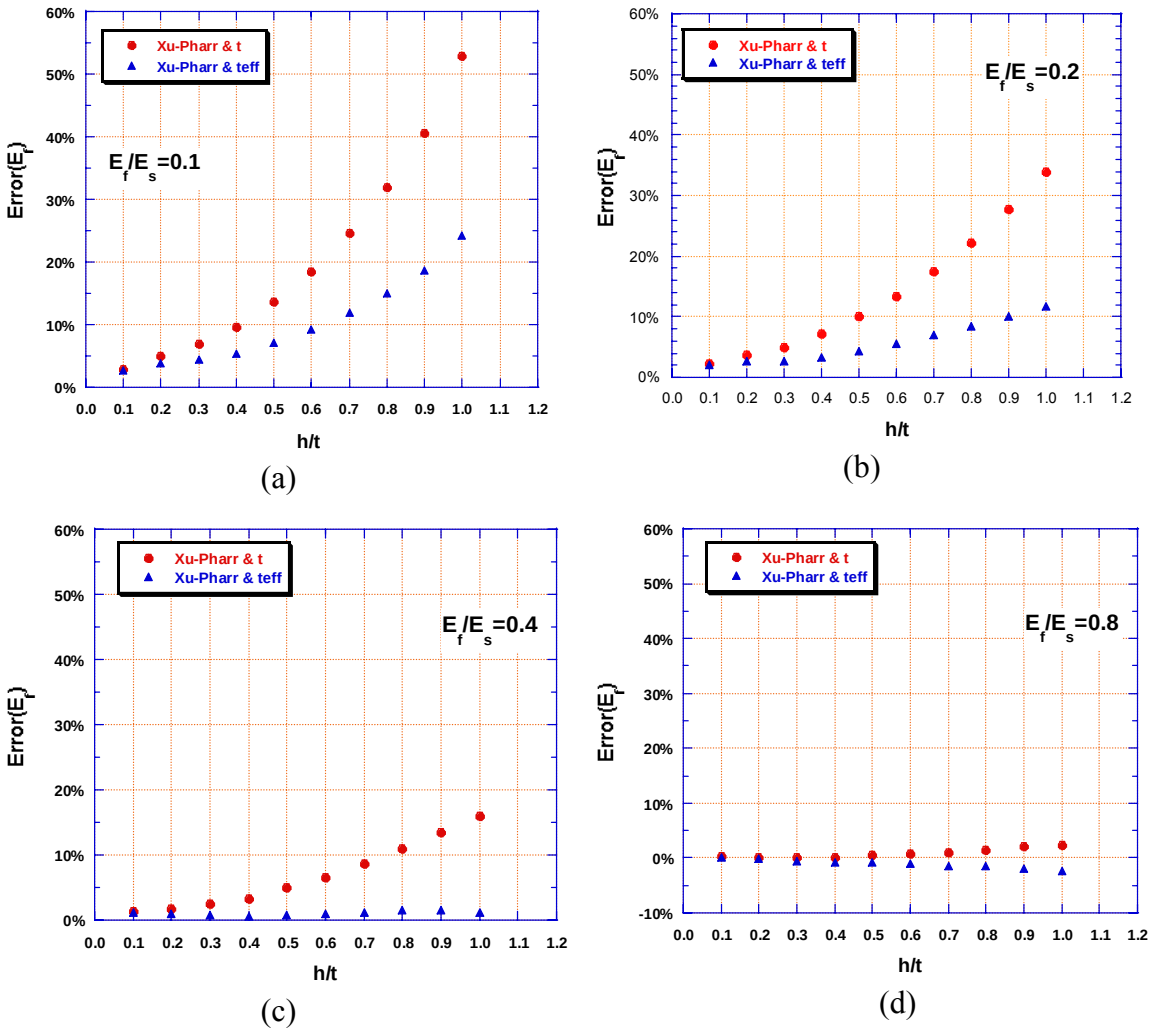

Figure 5.13 Comparison of errors in Ef from the Xu-Pharr solution using the effective film thickness teff and the total film thickness.

(a) E_f/E_s=0.1, (b) E_f/E_s=0.2, (c) E_f/E_s=0.4, (d) E_f/E_s=0.8.

As shown in Fig.5.13 (a), the Xu-Pharr solution based on the total film thickness yields a larger error than the solution with the effective film thickness for E_f/E_s=0.1. However, even when h (equivalent to the penetration depth) is as large as 70% of the film thickness, the solution with t_{eff} predicts E_f with an error less than 15%, while using the total film thickness gives an error of about 25%. For E_f/E_s =0.2 and 0.4, using the effective film thickness in the Xu-Pharr solution improves the accuracy significantly. The error is less than 10% and 5% for these two cases, even when h/t=0.8. For E_f/E_s =0.8, the Xu-Pharr solution works well with both film thicknesses. The absolute values of the error are less than 5%. Overall, it appears that we can measure E_f with an error less than 15% using the Xu-Pharr solution and the effective film thickness, even when the indentation depth is 70% of the film thickness for film/substrate systems with $0.1< E_f/E_s <1$. The smaller the mismatch between E_f and E_s, the more accurate the measured E_f.

Lastly we also assess the method using the Bec-Loubet solution. As shown in Fig.5.14, the Bec-Loubet solution with the total film thickness is more accurate than the one with the effective film thickness in predicting E_f when h/t varies from 0.1 to 0.5 for E_f/E_s=0.1. When h/t is larger than 0.5, the effective film thickness reduces the error significantly. In the cases of E_f/E_s=0.2, 0.4 and 0.8, the application of the effective thickness in Bec-Loubet solution does not improve the accuracy. This means the Bec-Loubet solution with the total film thickness can be used directly to give an error in E_f of less than 10% for all h/t ratios. It is noted that when h/t is in the small range from 0.1 to 0.3, the error has a maximum value about 10% when E_f/E_s =0.1, 0.2, and 0.4. The reason for this phenomenon is the same as that for flat punch indentation. Compared to the

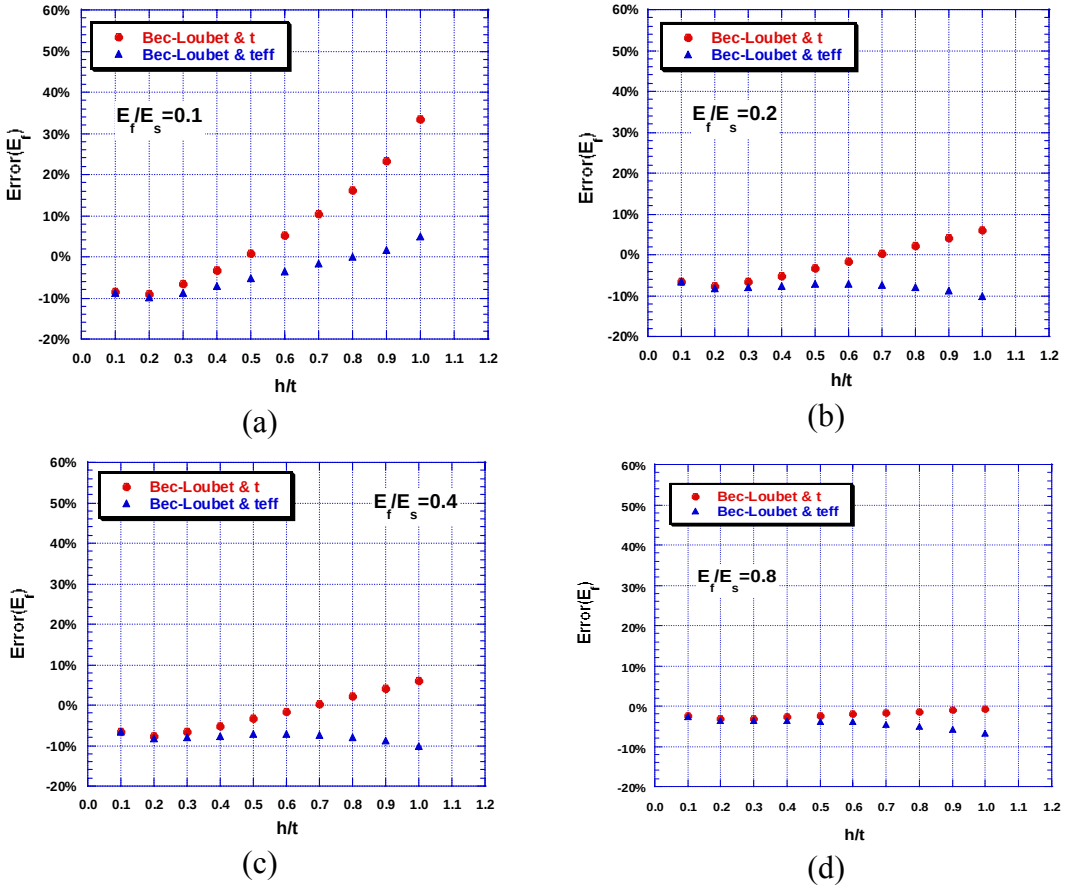

Figure 5.14 Comparison of the errors in Ef from the Bec-Loubet solution using the effective film thickness teff and the total film thickness:

(a) E_f/E_s=0.1, (b) E_f/E_s=0.2, (c) E_f/E_s=0.4, (d) E_f/E_s=0.8.

Xu-Pharr solution, the Bec-Loubet solution with the effective film thickness is more accurate when E_f/E_s =0.1. However, when E_f/E_s values are larger than 0.1, the Xu-Pharr solution with the effective thickness works better than the Bec-Loubet solution with the total film thickness.

5.5 Conclusions

Approximate analytical solutions for indentation of elastic film/substrate systems with flat cylindrical punch indenters were assessed by comparing to finite element simulations. To apply the solutions for flat punch indentation to conical indentation of elastic film/substrate systems, whether the effective film thickness or total film thickness should be used in conical indentation depends on the selected solution. Finite element simulations were performed to determine the effective film thickness. After the effective film thickness values were obtained for different h/t ratios, a new method to extract E_f from nanoindentation test was proposed, and the accuracies of the method were tested. Some important conclusions are as follows:

1. The Xu-Pharr and Bec-Loubet solutions describe well the effect of the substrate's elastic modulus on the measured stiffness for the case of flat cylindrical punch indentation of compliant films on stiff substrates with E_f/E_s in the range from 0.1 to 1.

2. The effective thickness values needed to apply the approximate analytical solutions of flat punch indentation to conical indentation were determined for different normalized film thickness ratios (h/t) using FEA. It was found that the effective thickness varies with h/t independent of E_f/E_s ratios, as shown by Eq.(5.1).

3. A new method which applies the effective thickness in the Xu-Pharr solution and the Bec-Loubet solution to extract the film elastic modulus from the measurements of conical indentation of film/substrate systems is suggested.

4. The effectiveness of using the effective film thickness in this new method depends on the approximate solution used. For the Xu-Pharr solution, the effective thickness improves the accuracy of predicting E_f for normalized indentation depths h/t up to 0.7. However, for the Bec-Loubet solution, the total film thickness works better than the effective film thickness. By comparison, the Xu-Pharr solution using the effective film thickness generally works better than the Bec-Loubet solution with the total film thickness.

6. Finite element simulation of indentation of elastic-perfectly plastic film/substrate systems by a rigid cone

In Chapter 5, we developed a new method to determine the elastic modulus of thin films on substrates based on finite element simulation of conical indentation into elastic holes. Although we showed the equivalence of conical indentation into a matching conical hole and elastic-plastic indentation for homogenous materials, it is not clear if the same applies to film/substrate systems during elastic-plastic deformation. The main objective of the chapter is to examine this and test if the Xu-Pharr solution with the effective film thickness works equally well for elastic-plastic film/substrate systems.

The indentation of a film/substrate system involving elastic-plastic deformation is very complex because the measurements are affected by both the elastic and plastic properties of the films and substrates. To separate the elastic modulus and hardness of films from measurements is only possible under limited circumstances. Thus, another objective of this chapter is to identify the situations in which we can measure the true properties of films. Numerous finite element simulations of indentation of elastic plastic film/substrate systems by a 70.3° cone are carried out.

6.1 Finite element analysis

Details of the model and boundary conditions are the same as in Chapter 3. The film thickness was fixed at 1μm, and the interface between the film and substrate was assumed to be perfectly bonded. The minimum element size under the indenter tip was varied from 5nm to 20nm depending on the indentation depth h and the material properties of the films and substrates. The mesh used in the region near the interface was

almost uniform to capture the stress continuity due to the variation of elastic and plastic properties. The indentation depth h was examined in the range from 0.1 to 1 times the film thickness t.

To simplify, only an elastic-perfectly-plastic material model was used, and Poisson's ratios for the film and substrate were fixed at 0.3. Different combinations of elastic moduli and yield stress were used. One consisted of an elastically homogeneous and plastically inhomogeneous film/substrate with E_f=E_s=100GPa and different σ_f/σ_s. To examine the materials over a broad range, the selected σ_f and σ_s values shown Table 6.1 were used. These materials cover very soft ones (σ=0.1GPa) such as aluminum and very hard ones (σ=10GPa) such as ceramics. In addition, soft films on hard substrates and hard films on soft substrates were modeled. Plastically homogenous materials with σ_f=σ_s were also included to verify the mesh and determine the hardness of the film materials.

Another set of calculations was performed for film/substrate systems that were elastically inhomogeneous but either plastically inhomogeneous or homogenous. Here, E_f was fixed at 100GPa and the E_s values are selected as 1000GPa and 10GPa to model compliant films on stiff substrates or vice versa. The σ_f and σ_s values are those in Table 6.1.

Table 6.1 The σf and σs values used in FEA of film/substrate systems

σ_f (GPa)	0.1			1			10		
σ_s (GPa)	0.1	1	10	0.1	1	10	0.1	1	10

6.2 Indentation of elastically homogenous and plastically inhomogeneous film/substrate systems

In this section, we discuss effects of film and substrate yield stress on the measured elastic moduli and hardness values.

6.2.1 Measurement of elastic moduli of films from FEA results and application of the Xu-Pharr method

Although we showed in chapter 3 that the stiffness equation works well for conical indentation of homogenous elastic-plastic materials, it is not clear if a difference between the plastic properties of film and the substrate affect the accuracy of the stiffness equation when applied to film/substrate systems. To examine this, FEA results of E_f=E_s=100GPa with different σ_f/σ_s were compared. Since the elastic properties are the same for film and substrate materials, the moduli measured directly from the stiffness equation should be close to 100GPa if the mismatch of plastic properties does not have a significant influence on the stiffness. We also expect that the method using the Xu-Pharr solution and the effective film thickness concept should work well for these cases. The main purpose of the comparison with FEA is thus to validate that the new method (which we will call the X-P method) for film/substrate systems with different plastic properties.

The Xu-Pharr solution can be written in a simple form in this instance since we use the same Poisson's ratios for films and substrates, specifically:

$$S/S_0 = 1/\left[(1 - I_0) + I_0 E_s/E_f\right] \qquad (6.1)$$

where S is the stiffness measured from the FEA results and S_0 is that calculated from the stiffness equation with the true contact area measured in simulation and the actual

substrate elastic modulus. The weighting parameter I_0 is a function of the ratio of true contact area to the film thickness, a/t, and Poisson's ratio.

First, we compare the elastic moduli determined from the stiffness equation using S and a measured from FEA results with the input E values for σ_f=0.1 and σ_s=0.1, 1 and 10GPa. Results are shown in Fig.6.1, where it is seen that all the measured elastic moduli are close to the actual value 100GPa but overestimate it by 4% to 8% depending on h/t. This agrees with our finding in Chapter 3 that β for homogenous materials is a little greater than 1, usually in the range 1.06-1.07. To get better accuracy, we should thus apply the correction factor β in the stiffness equation. For indentation of elastic-plastic materials with a 70.3° conical indenter, we suggested β=1.065, a value that averages the effects of pile-up and sink-in. After β is applied, the elastic moduli calculated from the stiffness equation are within 2% of the actual values. This illustrates that elastic modulus measurement using the stiffness equation depends primarily on the elastic properties of film and substrate and is not affected by the plastic properties if the true contact area is used. The same observations are found for the cases of σ_f=1GPa and 10GPa (the graphs are not shown).

To assess the applicability of the Xu-Pharr solution and the effective film thickness for conical indentation of elastic plastic films, the proper correction factor must be taken into account. Note that the Xu-Pharr solution is derived for flat punch indentation of elastic film/substrate systems, and since β=1 for flat punch indentation of elastic homogenous materials, there is no need to include β in the solution. However, for

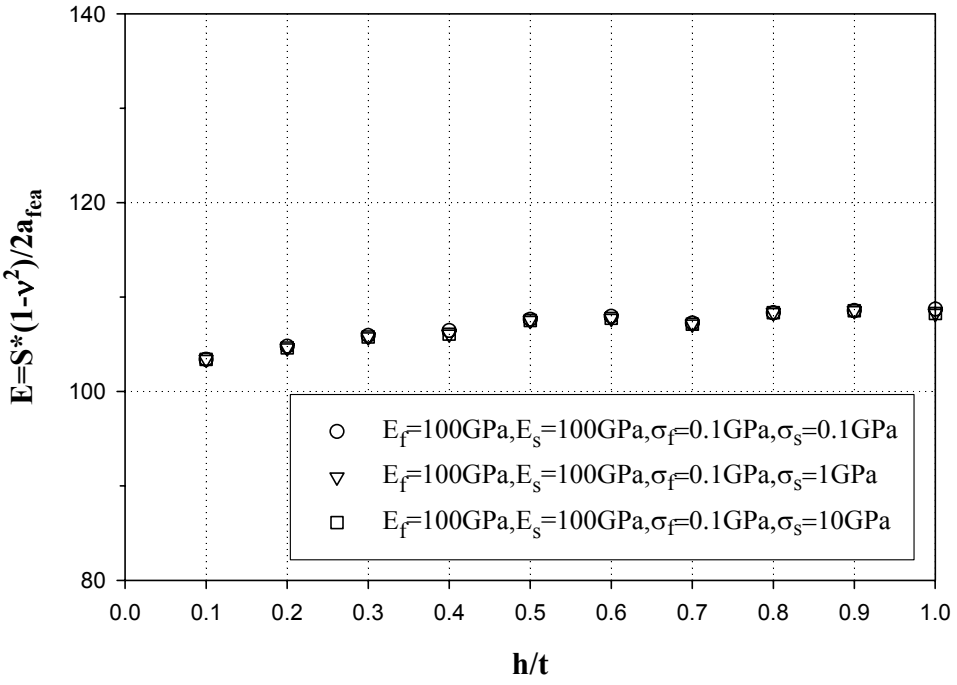

Figure 6.1 Effects of variation of σf/ σs on the elastic moduli measured from the stiffness equation and the true contact area for film/substrate systems with Ef=Es=100GPa and σf=1GPa

a conical indentation of an elastic-plastic material, β is 1.065 due to the effect of the permanent hardness impression. Therefore, the stiffness for a conical indenter, S, in the left term in Eq.(6.1) should be divided by β if S0 is calculated from the stiffness equation without including β.

Fig.6.2 shows the influence of assumed value of β and using the effective film thickness on E_f values predicted from the Xu-Pharr solution for σ_f=0.1. As shown in Fig.6.2 (a), without applying β and t_{eff}, the difference between the E_f estimated from the Xu-Pharr solution and the corrected value increases with increasing h/t up to 80%. After applying β, the Xu-Pharr solution gives errors less than 20% even for h/t =1. Fig.6. 2(b) shows that the predictions of the Xu-Pharr solution using t_{eff} gives errors less than 10% when h/t is less than 0.7. It is noted that β, instead of t_{eff} ,improves the accuracy of the Xu-Pharr solution in this case because the film and substrate have the same elastic properties. Fig.6.3 and Fig.6.4 show the comparison for σ_f=1 and 10GPa, respectively. The same conclusions are obtained.

6.2.2 Effects of yield stress difference on the hardness measurement from FEA

As pointed out by Johnson [27], the hardness of a homogenous material can be related to the yield stress by:

$$H = c\sigma_y . \tag{6.2}$$

where the constraint factor, c, can be calculated for an incompressible material from:

$$c = \frac{2}{3}\left\{1 + \ln\left(\frac{1}{3}\frac{E\tan\alpha}{\sigma_y}\right)\right\}. \tag{6.3}$$

Here, α is angle between the indenter and the indented surface, so α=π/2-θ. These

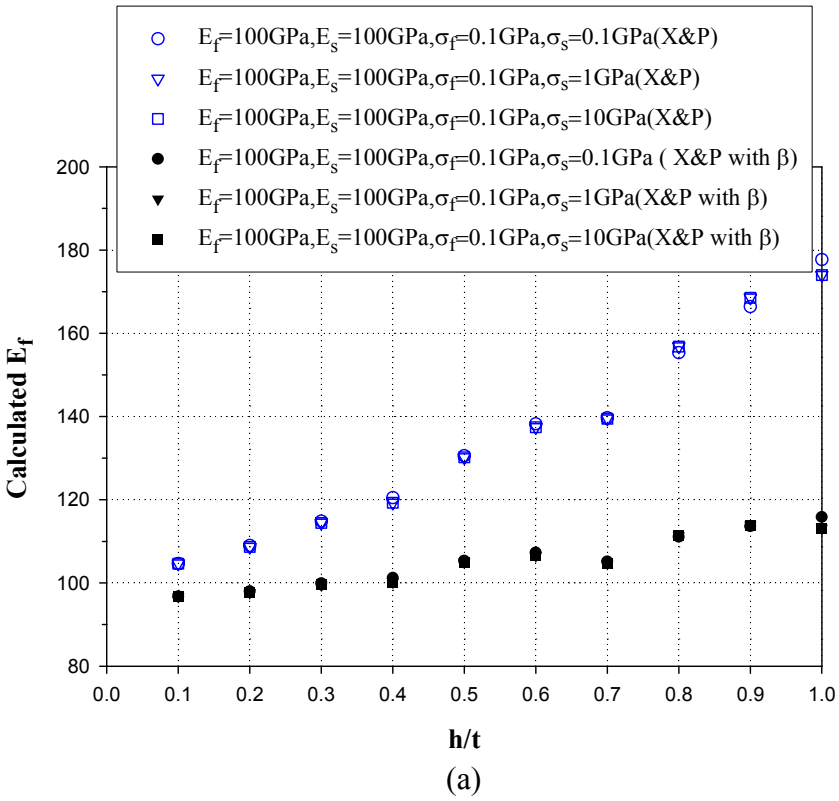

Figure 6.2 Measurement of elastic moduli of films using the Xu-Pharr solution. (a) β effects only (b) teff effects with/without β. Here, σf=0.1GPa and σs=0.1, 1 and 10GPa.

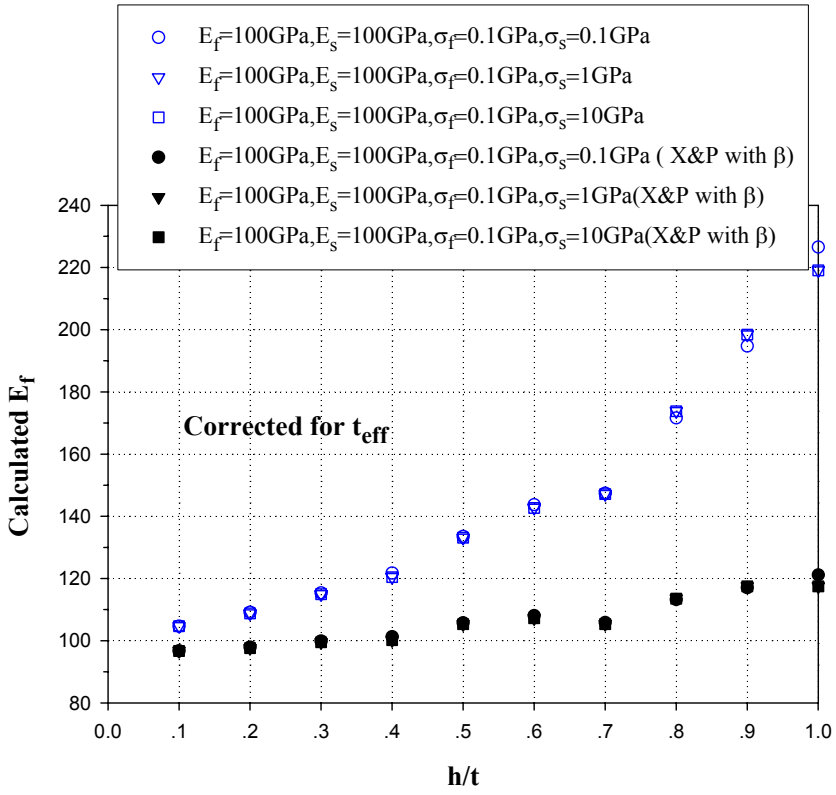
Ef=100GPa,Es=100GPa,σf=0.1GPa,σs=0.1GPa
Ef=100GPa,Es=100GPa,σf=0.1GPa,σs=1GPa
Ef=100GPa,Es=100GPa,σf=0.1GPa,σs=10GPa
Ef=100GPa,Es=100GPa,σf=0.1GPa,σs=0.1GPa (X&P with β)
Ef=100GPa,Es=100GPa,σf=0.1GPa,σs=1GPa(X&P with β)
Ef=100GPa,Es=100GPa,σf=0.1GPa,σs=10GPa(X&P with β)
Corrected for teff
Calculated Ef
h/t
240
220
200
180
160
140
120
100
80
0.0
.1
.2
.3
.4
.5
.6
.7
.8
.9
1.0

(b)

Fig. 6.2, cont.

Figure 6.3 Measurement of elastic moduli of films using the Xu-Pharr solution.
(a) β effects only (b) t_{eff} effects with/without β. Here, σ_f=1GPa and σ_s=0.1, 1 and 10GPa

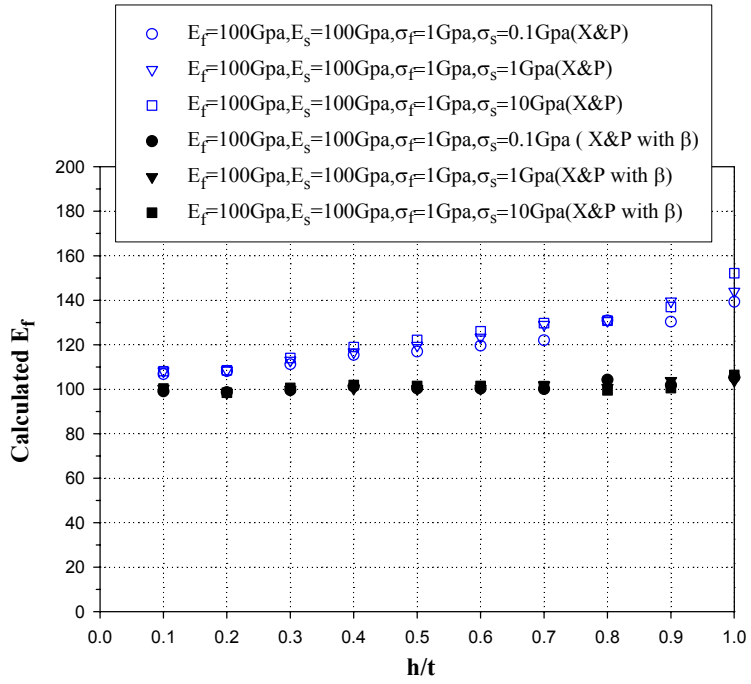
E_f=100Gpa,E_s=100Gpa,σ_f=1Gpa,σ_s=0.1Gpa(X&P)
E_f=100Gpa,E_s=100Gpa,σ_f=1Gpa,σ_s=1Gpa(X&P)
E_f=100Gpa,E_s=100Gpa,σ_f=1Gpa,σ_s=10Gpa(X&P)
E_f=100Gpa,E_s=100Gpa,σ_f=1Gpa,σ_s=0.1Gpa (X&P with β)
E_f=100Gpa,E_s=100Gpa,σ_f=1Gpa,σ_s=1Gpa(X&P with β)
E_f=100Gpa,E_s=100Gpa,σ_f=1Gpa,σ_s=10Gpa(X&P with β)
Calculated E_f
h/t
0
20
40
60
80
100
120
140
160
180
200
0.0
0.1
0.2
0.3
0.4
0.5
0.6
0.7
0.8
0.9
1.0

(a)

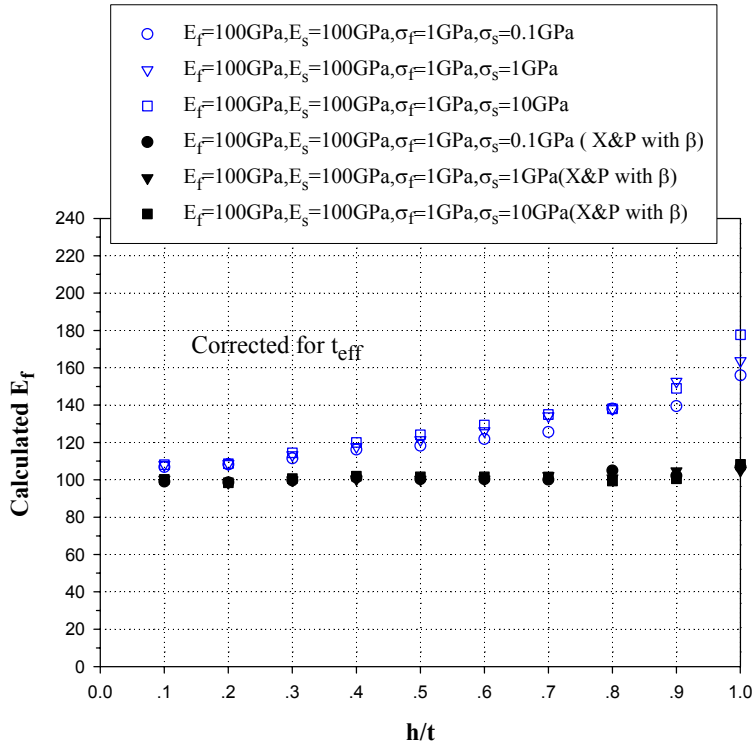
E_f=100GPa,E_s=100GPa,σ_f=1GPa,σ_s=0.1GPa
E_f=100GPa,E_s=100GPa,σ_f=1GPa,σ_s=1GPa
E_f=100GPa,E_s=100GPa,σ_f=1GPa,σ_s=10GPa
E_f=100GPa,E_s=100GPa,σ_f=1GPa,σ_s=0.1GPa (X&P with β)
E_f=100GPa,E_s=100GPa,σ_f=1GPa,σ_s=1GPa(X&P with β)
E_f=100GPa,E_s=100GPa,σ_f=1GPa,σ_s=10GPa(X&P with β)
Corrected for t_{eff}
Calculated E_f
h/t
0
20
40
60
80
100
120
140
160
180
200
220
240
0.0
.1
.2
.3
.4
.5
.6
.7
.8
.9
1.0

(b)

Figure 6.4 Measurement of elastic moduli of films using the Xu-Pharr solution.
(a) β effects only (b) t_{eff} effects with/without β. Here, σ_f=10GPa and σ_s=0.1, 1 and 10GPa.

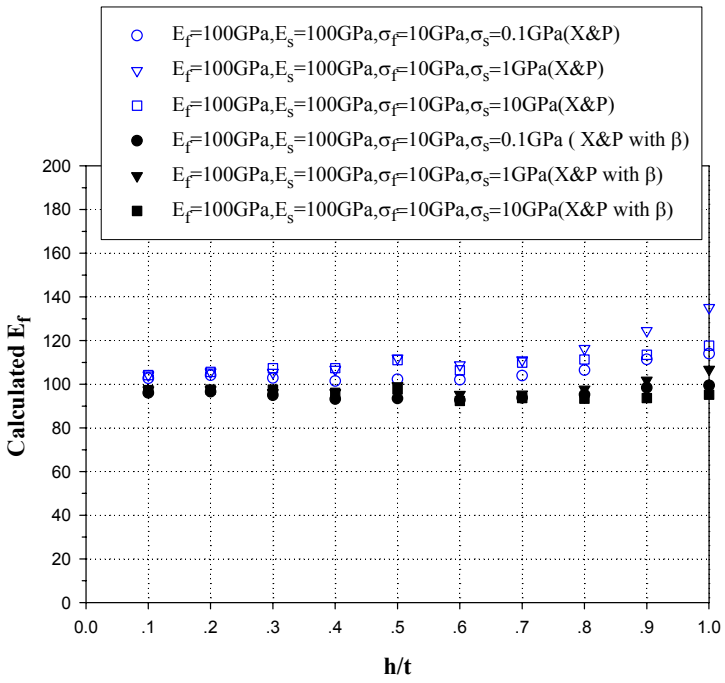
E_f=100GPa,E_s=100GPa,σ_f=10GPa,σ_s=0.1GPa(X&P)
E_f=100GPa,E_s=100GPa,σ_f=10GPa,σ_s=1GPa(X&P)
E_f=100GPa,E_s=100GPa,σ_f=10GPa,σ_s=10GPa(X&P)
E_f=100GPa,E_s=100GPa,σ_f=10GPa,σ_s=0.1GPa (X&P with β)
E_f=100GPa,E_s=100GPa,σ_f=10GPa,σ_s=1GPa(X&P with β)
E_f=100GPa,E_s=100GPa,σ_f=10GPa,σ_s=10GPa(X&P with β)
Calculated E_f
h/t

(a)

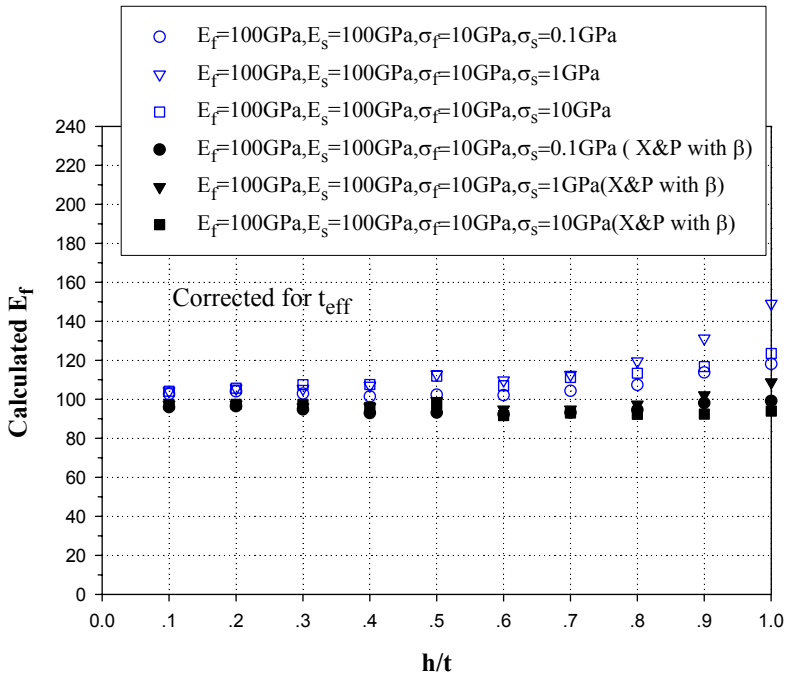
E_f=100GPa,E_s=100GPa,σ_f=10GPa,σ_s=0.1GPa
E_f=100GPa,E_s=100GPa,σ_f=10GPa,σ_s=1GPa
E_f=100GPa,E_s=100GPa,σ_f=10GPa,σ_s=10GPa
E_f=100GPa,E_s=100GPa,σ_f=10GPa,σ_s=0.1GPa (X&P with β)
E_f=100GPa,E_s=100GPa,σ_f=10GPa,σ_s=1GPa(X&P with β)
E_f=100GPa,E_s=100GPa,σ_f=10GPa,σ_s=10GPa(X&P with β)
Corrected for t_{eff}
Calculated E_f
h/t

(b)

equations show that the hardness is a function of non-dimensional variable $E\tan\alpha/\sigma_y$, which can be explained as the ratio of the plastic strain $\tan\alpha$ caused by the rigid indenter to the elastic strain limit of the material σ_y/E.

A figure describing the correlation between c and $E\tan\alpha/\sigma_y$ has been developed by Johnson [27], and the figure and Eq.(6.3) be used to approximate the hardness of the film for a given σ_f and E_f. For E_f=100GPa and σ_f =0.1 and 1GPa, c is about 3 since $E\tan\alpha/\sigma_y$ is larger than 30 and a limiting value is reached. The film hardness values should thus be 0.3 and 3GPa, respectively. For σ_f=10GPa and $E\tan\alpha/\sigma_y$= 3.5, c=1.6, and the film hardness is about 16 GPa.

Fig.6.5 presents finite element results for the hardnesses of several elastically homogenous film-substrate systems (E=100GPa) but with different yield strengths to demonstrate the effects of $E\tan\alpha/\sigma_y$ on the measured hardnesses. The hardnesses are plotted as a function of the depth of penetration h/t. As shown in Fig.6.5 (a), film/substrate systems with σ_f=0.1 and σ_s=1 or10GPa give the same hardness as the homogenous film materials (σ_f=σ_s=0.1 GPa) independent of h/t. In these cases, the substrates are harder than films. It is noted the hardness value of 0.25 is close to the film hardness estimated earlier about 0.3 GPa.

Fig.6.5 (b) shows the case for σf=1GPa. Here, it is found that the homogenous film material gives a hardness of 2.6GPa, again close to the prediction of Eq.(6.3). In addition, for the soft substrate (σs=0.1GPa) the hardness decreases when h/t > 0.3. The

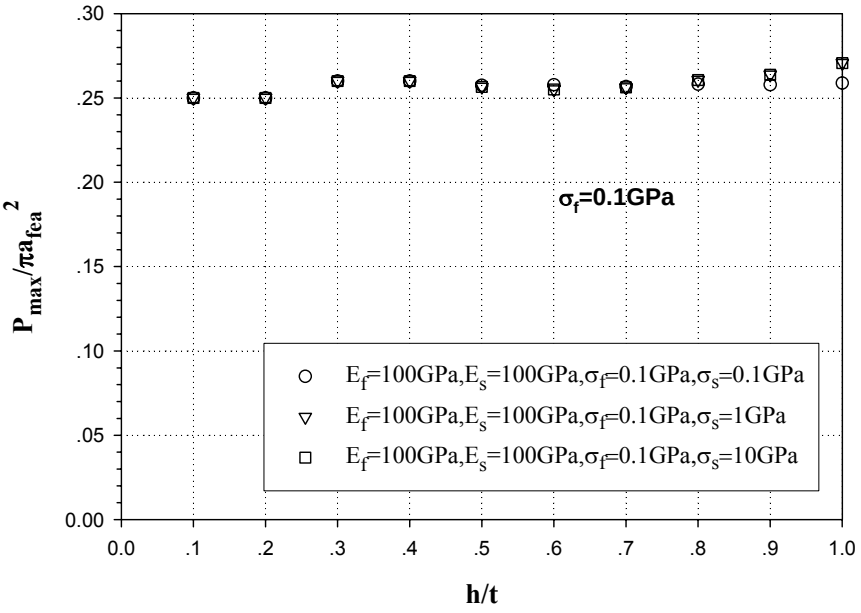

(a)

Figure 6.5 Measurements of hardness using the true contact radii from FEA for nanoindentation of elastically homogenous film/substrates systems with various yield strengths.

(a) σ_f=0.1GPa (b) σ_f=1GPa (c) σ_f=10GPa

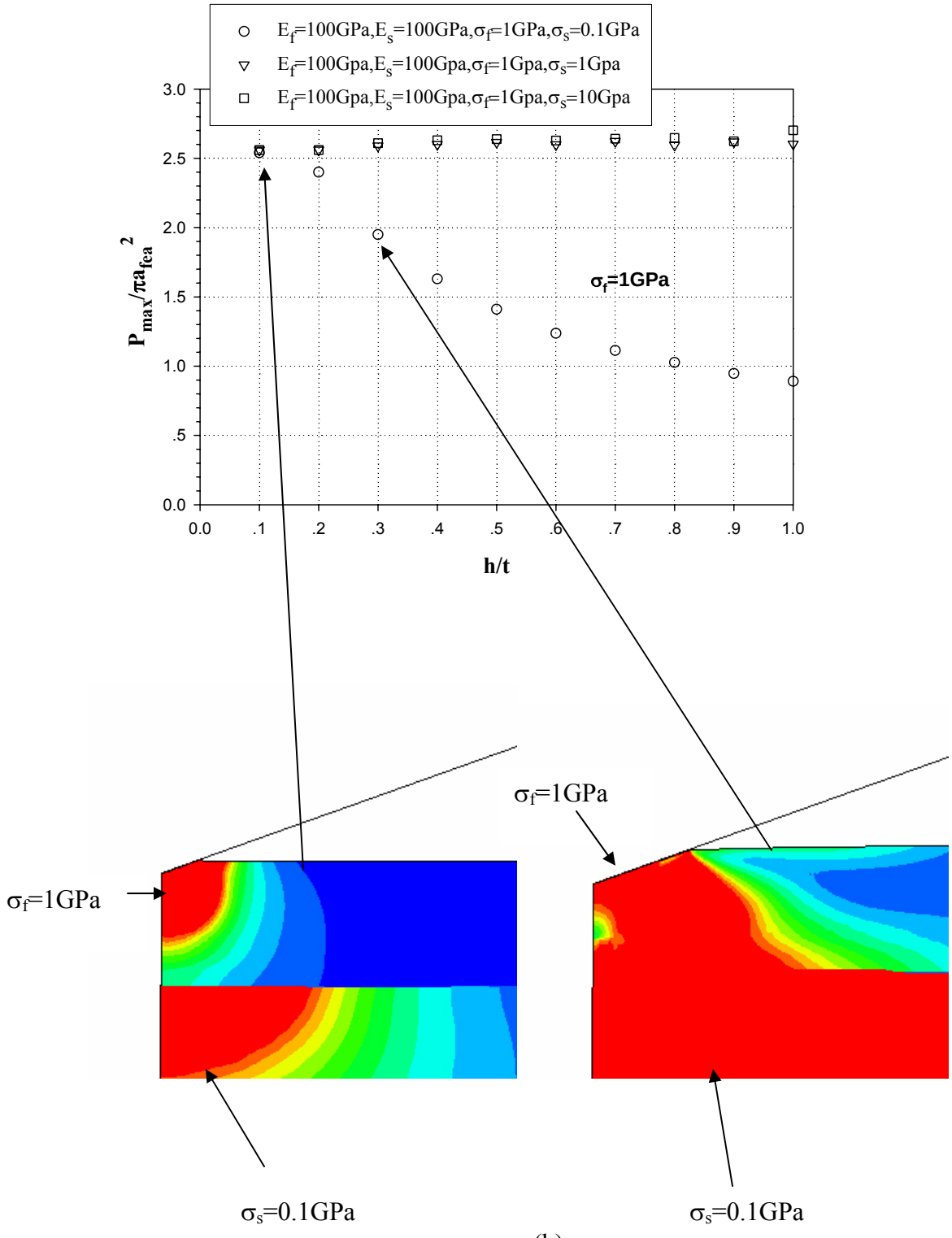

(b)

Figure 6.5, continued

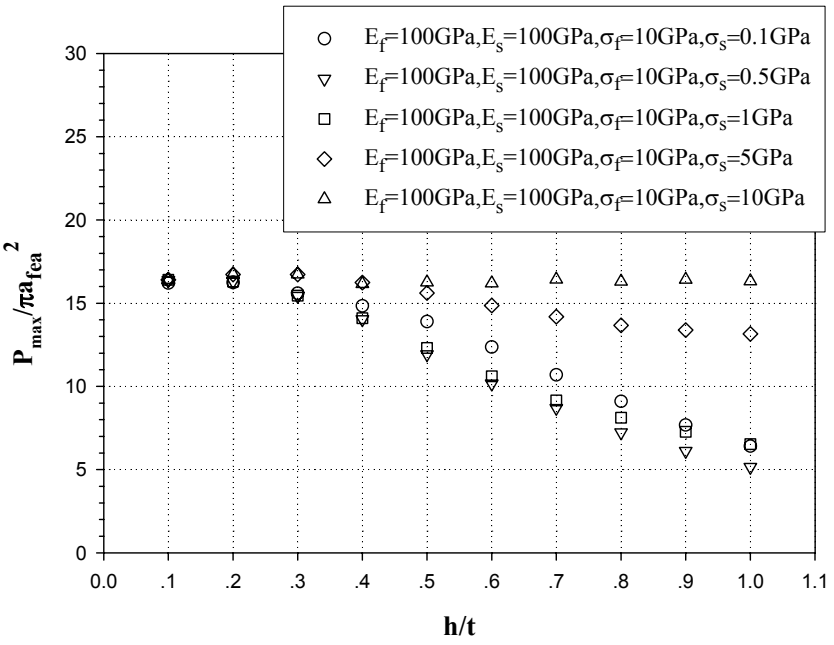
E_f=100GPa,E_s=100GPa,σ_f=10GPa,σ_s=0.1GPa
E_f=100GPa,E_s=100GPa,σ_f=10GPa,σ_s=0.5GPa
E_f=100GPa,E_s=100GPa,σ_f=10GPa,σ_s=1GPa
E_f=100GPa,E_s=100GPa,σ_f=10GPa,σ_s=5GPa
E_f=100GPa,E_s=100GPa,σ_f=10GPa,σ_s=10GPa
$P_{max}/\pi a_{fea}^2$
h/t
0
5
10
15
20
25
30
0.0
.1
.2
.3
.4
.5
.6
.7
.8
.9
1.0
1.1

(c)

Fig.6.5 (cont.)

plastic zones for σ_s=0.1GPa are also plotted for h/t=0.1 and 0.3. It is seen that the film and substrate yield for h/t=0.1 and 0.3, and the difference between these two cases is that the plastic zone in the film is not joined with the plastic zone in substrate for h/t=0.1, and the plastic zone of the film and the substrate are merged for h/t=0.3. In the latter case, the substrate effect is transmitted to the film region through the plastic zone, causing the drop of hardness. Thus, the soft substrate will have an influence on the hard film at the moment when the plastic zones of the film and substrate connect. For the hard substrate (σ_s=10GPa), there are no substrate effects on the measured hardness even when h/t is up to 1 because the plastic zones do not join.

Fig.6.5(c) compares the hardness values of film/substrate systems in which the substrates are softer than films. The film hardness predicted from Eq.(6.3) ,16GPa agrees well with the FEA results for indentation of the homogenous material. We also observe that decreasing the hardness of the substrate decreases the measured hardness correspondingly except for the case of σ_s=0.1GPa, which is believed to be caused by the bending of the film made possible by an extremely soft substrate [30]. We will use a comparison between the plastic zones for σ_s=0.1GPa and σ_s=1GPa at different penetration depths h/t to illustrate the reason for high hardness for σ_s=0.1GPa. As shown in Fig.6.6, the plastic zones of the film and substrate do not unite for σ_s=0.1GPa and σ_s=1GPa and both cases have the same hardness when h/t=0.3. Since the yield stress of the film is closer to the substrate in the case of σ_s=1GPa, the joining of the plastic zones occurs faster than for the case σ_s=0.1GPa. Thus, the hardness of σ_s=0.1GPa is larger than that of σ_s=1GPa for h/t=0.4. It is seen that the plastic zone in the film remains constant

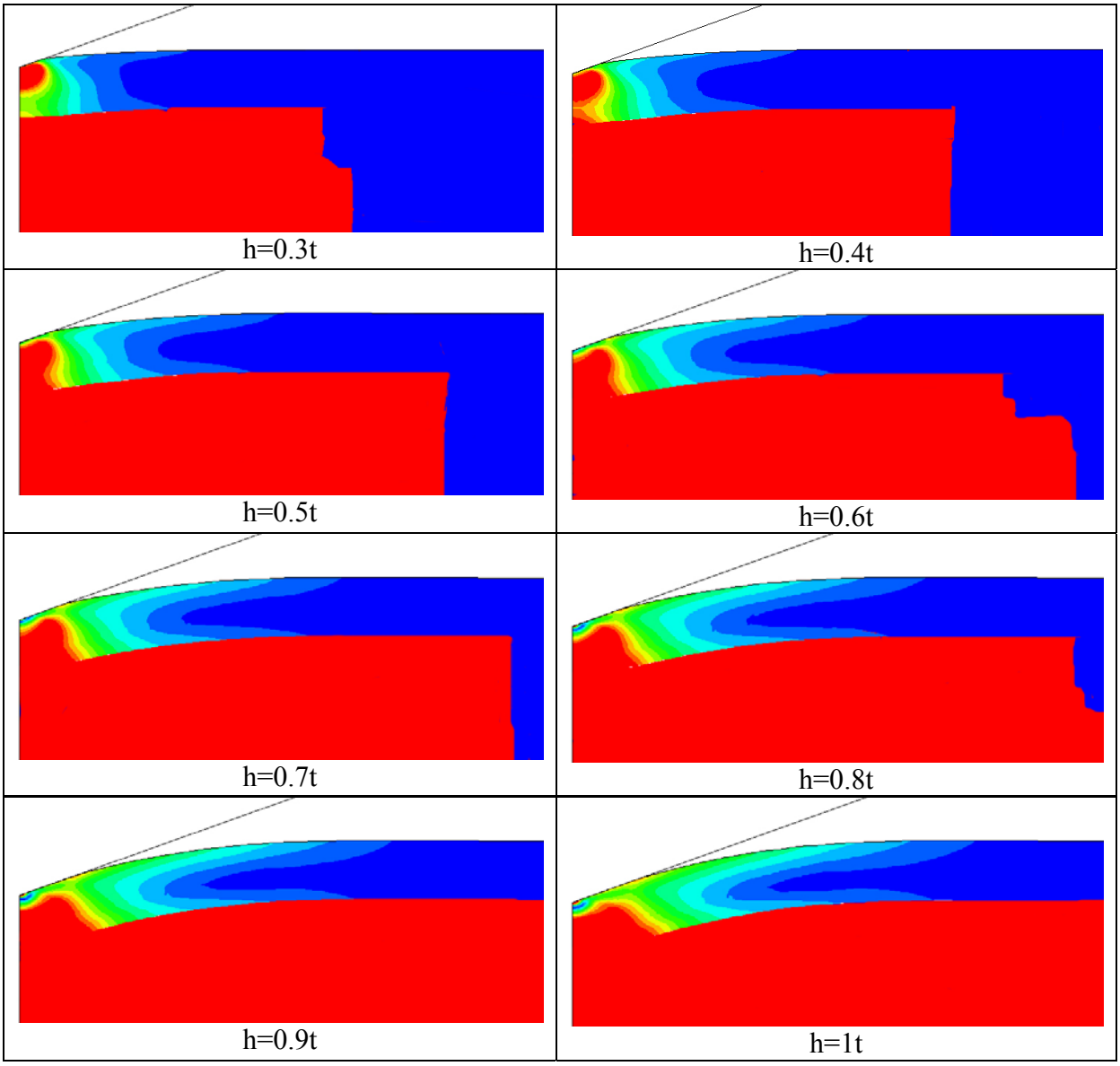

(a) E_f=E_s=100GPa, σ_f=10GPa, σ_s=0.1GPa

Figure 6.6 The plastic zones of films and substrates for indentation of hard films on soft substrates at different penetration depths. Color red represents plastic zones (a) σ_f=10GPa, σ_s=0.1GPa, (b) σ_f=10GPa, σ_s=1GPa

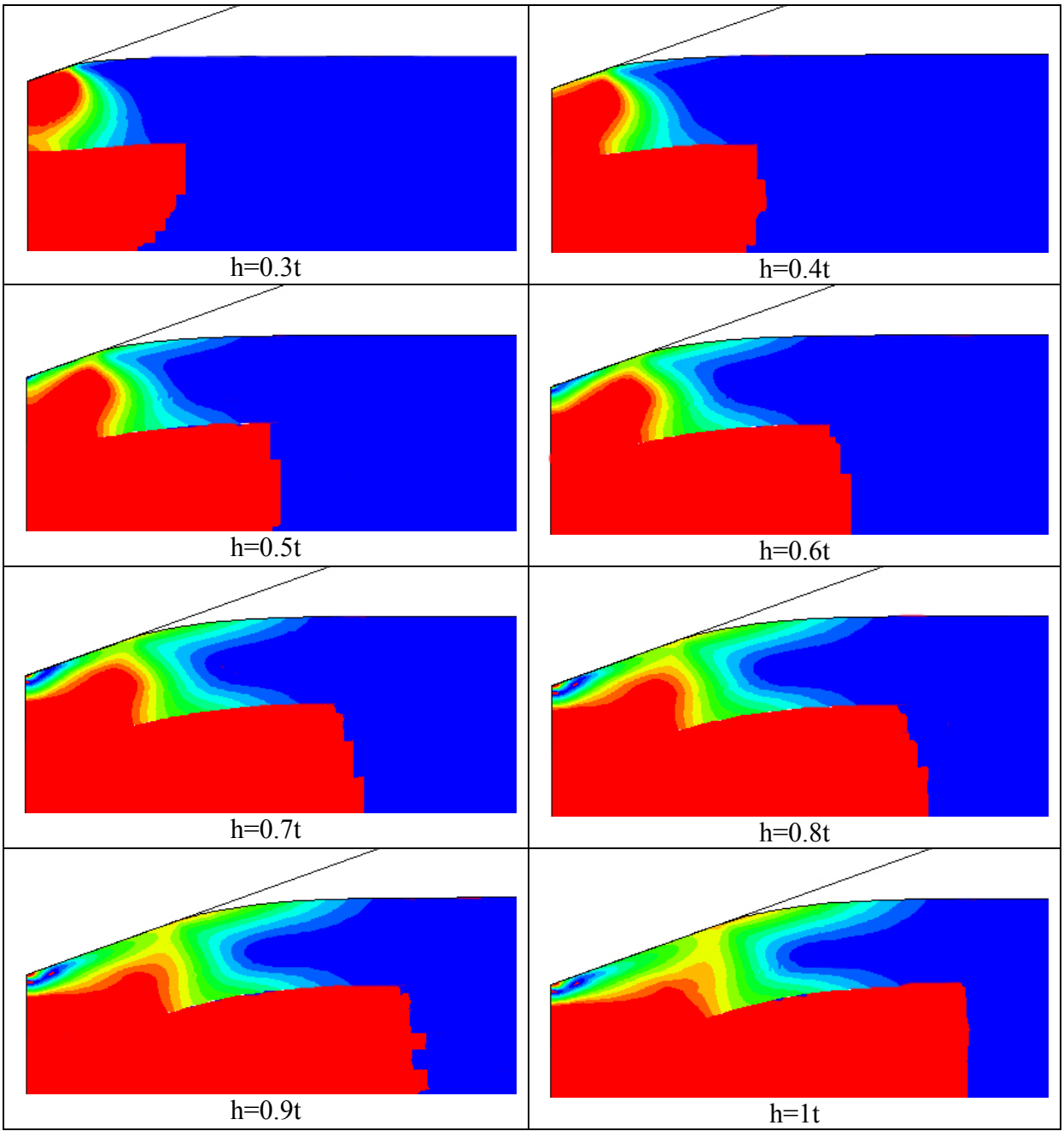

(b) E_f=E_s=100GPa, σ_f=10GPa, σ_s =1GPa
Figure 6.6, continued

for σs=1GPa while that for σs=0.lGPa increases with increasing h/t. In combination with the observation that the substrate is too soft to prevent the bending of the film for σs=0.1GPa, we conclude that indentation for an extremely soft substrate is accommodated by bending in the film and the hardness will be larger for a harder substrate which is still softer than film.

From these observations, we conclude that the measured hardness is the true film hardness for very soft films on hard substrates. However, for harder films, there is a significant substrate effect that depends on σ_f/σ_s and h/t.

6.3 Indentation of elastically inhomogeneous film/substrate systems

6.3.1 Measurement of elastic moduli of films from FEA results and application of the Xu-Pharr method

The Xu-Pharr method is now used to estimate the elastic moduli of thin films from the measured stiffness and the contact radius determined in the finite element analysis. First, Fig.6.7 shows the elastic moduli measured for film/substrate systems with E_s=1000GPa and E_s=10GPa without application of the Xu-Pharr method. We observe that both cases give the wrong film elastic moduli, even when h/t =0.1. The large errors are due to substrate influences on the modulus measurement.

Next, we use the Xu-Pharr solution to extract the film moduli from the FEA measurements. Since the Xu-Pharr solution only works well for compliant films on stiff substrates, we consider the case of E_s=1000GPa first. Fig.6.8 (a) shows the effects of including β in the Xu-Pharr solution on the prediction accuracy. Only a slight improvement is observed. The E_f values calculated from the Xu-Pharr solution including

Figure 6.7 Elastic moduli computed from the stiffness and contact radius determined in FEA as a function of penetration depth h/t: (a) Ef/Es=0.1; (b) E_f/E_s=10

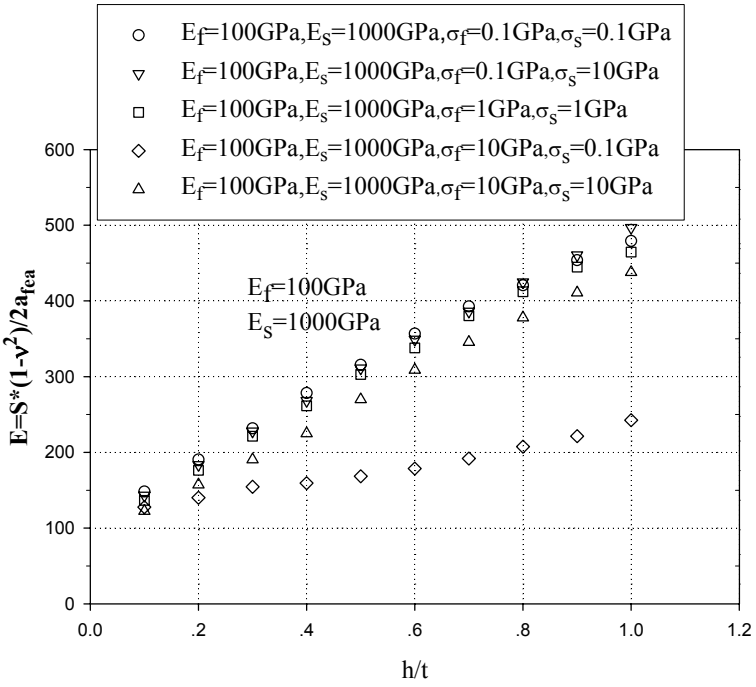
Ef=100GPa,Es=1000GPa,σf=0.1GPa,σs=0.1GPa
Ef=100GPa,Es=1000GPa,σf=0.1GPa,σs=10GPa
Ef=100GPa,Es=1000GPa,σf=1GPa,σs=1GPa
Ef=100GPa,Es=1000GPa,σf=10GPa,σs=0.1GPa
Ef=100GPa,Es=1000GPa,σf=10GPa,σs=10GPa
Ef=100GPa
Es=1000GPa
E=S*(1-ν²)/2afea
h/t
0
100
200
300
400
500
600
0.0
.2
.4
.6
.8
1.0
1.2

(a)

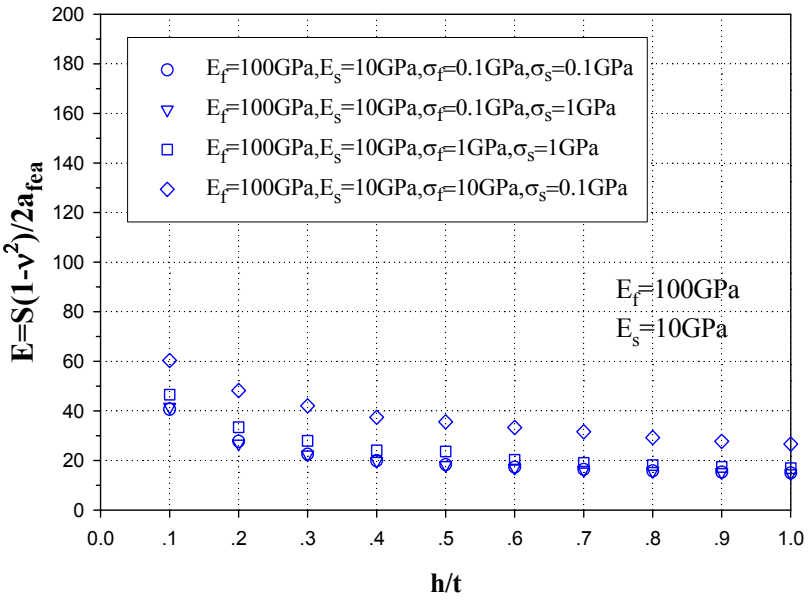
Ef=100GPa,Es=10GPa,σf=0.1GPa,σs=0.1GPa
Ef=100GPa,Es=10GPa,σf=0.1GPa,σs=1GPa
Ef=100GPa,Es=10GPa,σf=1GPa,σs=1GPa
Ef=100GPa,Es=10GPa,σf=10GPa,σs=0.1GPa
Ef=100GPa
Es=10GPa
E=S(1-ν²)/2afea
h/t
0
20
40
60
80
100
120
140
160
180
200
0.0
.1
.2
.3
.4
.5
.6
.7
.8
.9
1.0

(b)

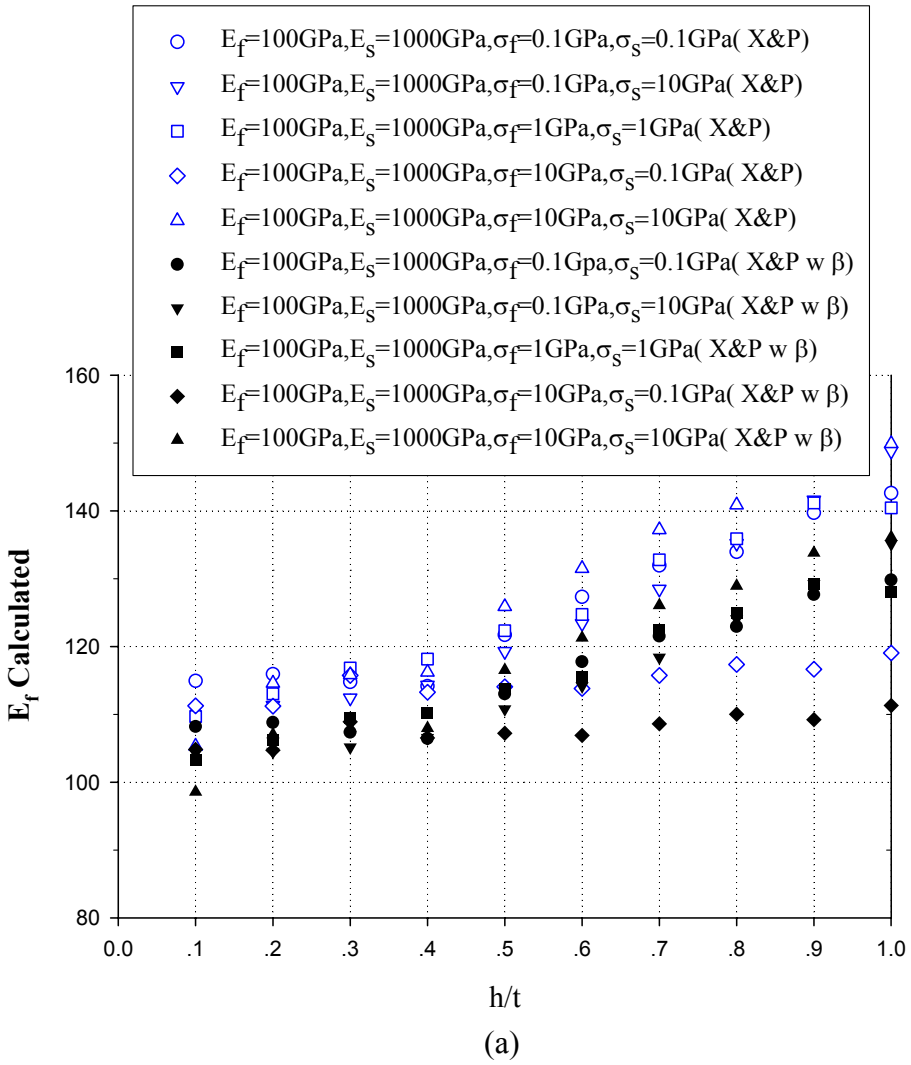

Figure 6.8 Measurement of film elastic moduli using the Xu-Pharr solution. (a) β effects (b) teff effects(with/without β).

Here E_f=100GPa, Es=1000GPa and different σ_f and σ_s are used.

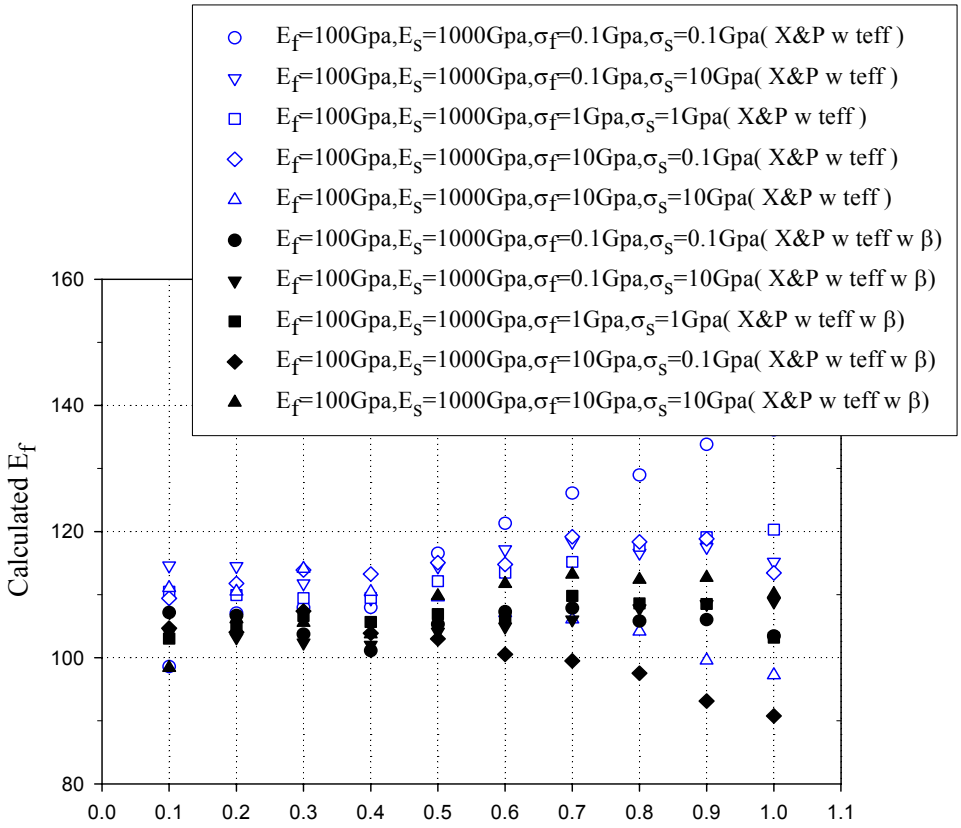
E_f=100Gpa,E_s=1000Gpa,σ_f=0.1Gpa,σ_s=0.1Gpa(X&P w teff)
E_f=100Gpa,E_s=1000Gpa,σ_f=0.1Gpa,σ_s=10Gpa(X&P w teff)
E_f=100Gpa,E_s=1000Gpa,σ_f=1Gpa,σ_s=1Gpa(X&P w teff)
E_f=100Gpa,E_s=1000Gpa,σ_f=10Gpa,σ_s=0.1Gpa(X&P w teff)
E_f=100Gpa,E_s=1000Gpa,σ_f=10Gpa,σ_s=10Gpa(X&P w teff)
E_f=100Gpa,E_s=1000Gpa,σ_f=0.1Gpa,σ_s=0.1Gpa(X&P w teff w β)
E_f=100Gpa,E_s=1000Gpa,σ_f=0.1Gpa,σ_s=10Gpa(X&P w teff w β)
E_f=100Gpa,E_s=1000Gpa,σ_f=1Gpa,σ_s=1Gpa(X&P w teff w β)
E_f=100Gpa,E_s=1000Gpa,σ_f=10Gpa,σ_s=0.1Gpa(X&P w teff w β)
E_f=100Gpa,E_s=1000Gpa,σ_f=10Gpa,σ_s=10Gpa(X&P w teff w β)
Calculated E_f
160
140
120
100
80
0.0
0.1
0.2
0.3
0.4
0.5
0.6
0.7
0.8
0.9
1.0
1.1

(b)

Fig.6.8(cont.)

β and t_{eff} are shown in Fig.6.8 (b), where much greater accuracy is achieved. It is also seen that the σ_f/σ_s ratio has only slight effects on the accuracy. The errors in predicting E_f are less than 20%, even for film/substrate systems in which the substrate is 10 times stiffer than the film.

Application of the Xu-Pharr solution to stiff films on compliant substrates is shown in Fig.6.9. As expected, the method does not give accurate predictions.

6.3.2 The effects of Ef/Es on the hardness measurement

Since we examined many combinations of E_f/E_s and σ_f/σ_s, a clear method is needed to present the data for the effects of E_f/E_s on hardness measurement. As shown in Section 6.1.2, the hardness depends on $E\tan\alpha/\sigma_y$,and the measured hardness is the true film hardness for soft films on hard substrates. Here,we use H_f approximated from Eq.(6.3) and the figure in Johnson's book to group the data.

First, results for H_f=0.3GPa (σ_f=0.1GPa) are shown in Fig.6.10. Even for large elastic mismatches such as E_f/E_s =0.1 or 10 and different σ_f/σ_s, the measured hardness is almost independent of h/t because all the substrates have hardness equal to or greater than the film.

Fig.6.11 shows the measured hardness for harder films, $H_f \rightarrow$3GPa (σ_f=1GPa). Both the film and substrate have the same yield stress 1GPa. Since c is 3 independent of $E\tan\alpha/\sigma_y$ for fully plastic indentation with $E\tan\alpha/\sigma_y \geq 30$, the substrate hardness will be the same as the film hardness if E_s is larger than 100GPa. In the case of E_s=10GPa, the

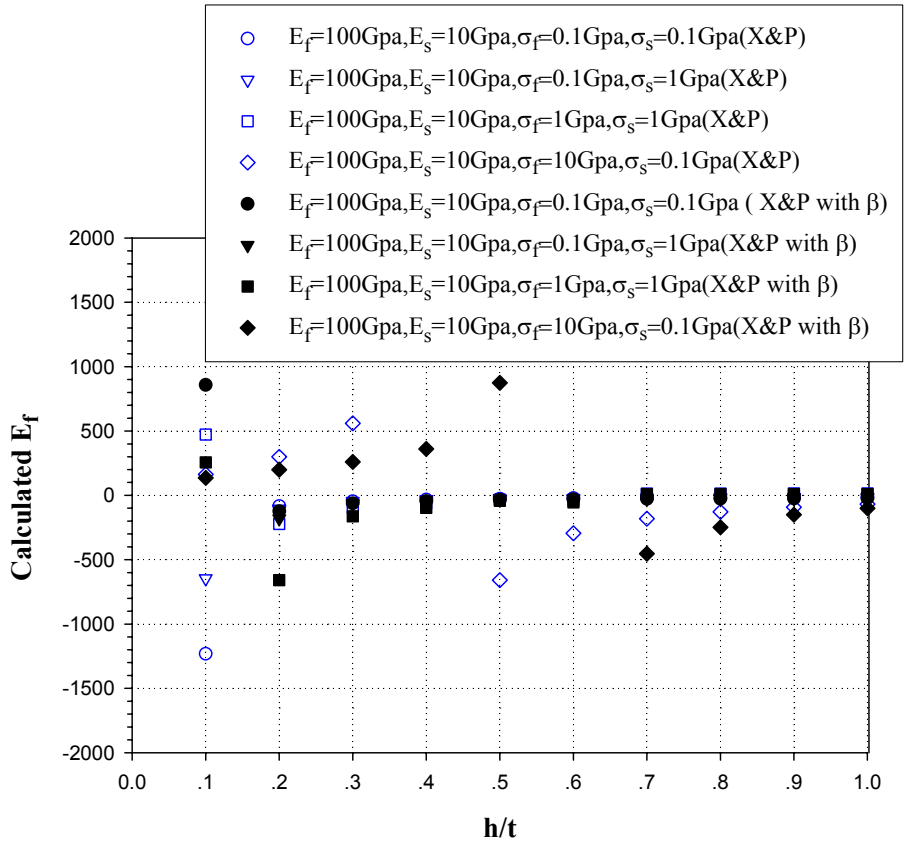

Figure 6.9 Measurement of elastic moduli of films using Xu-Pharr solution for stiff films on compliant substrates.

(a) β effects (b) t_{eff} effects(with/without β). Here E_f=100GPa, E_s=10GPa and different σ_f and σ_s are used

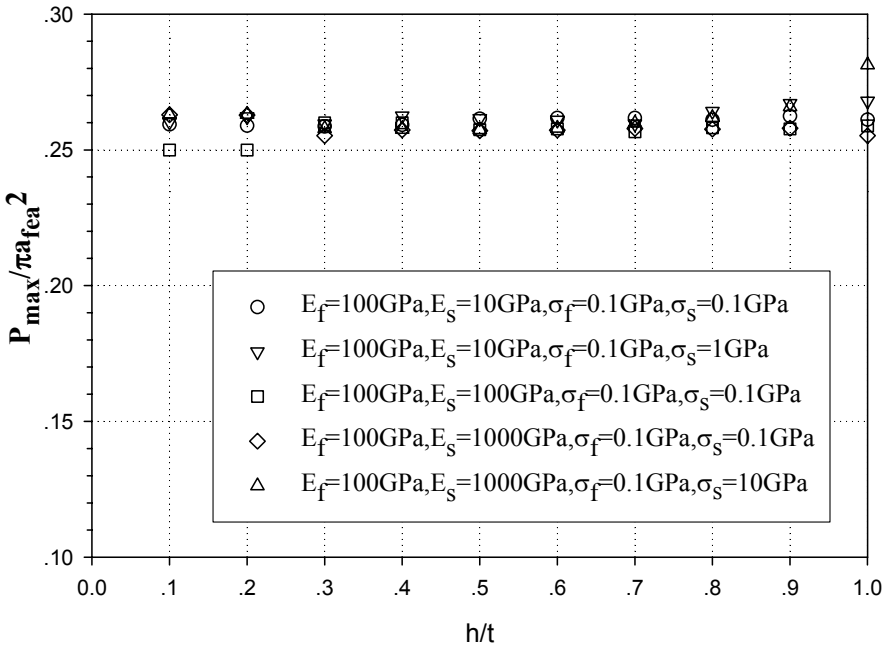

Figure 6.10 Measurements of hardness using true contact radii from FEA for nanoindentation of elastically inhomogeneous film/substrates systems (Hf=0.3GPa)

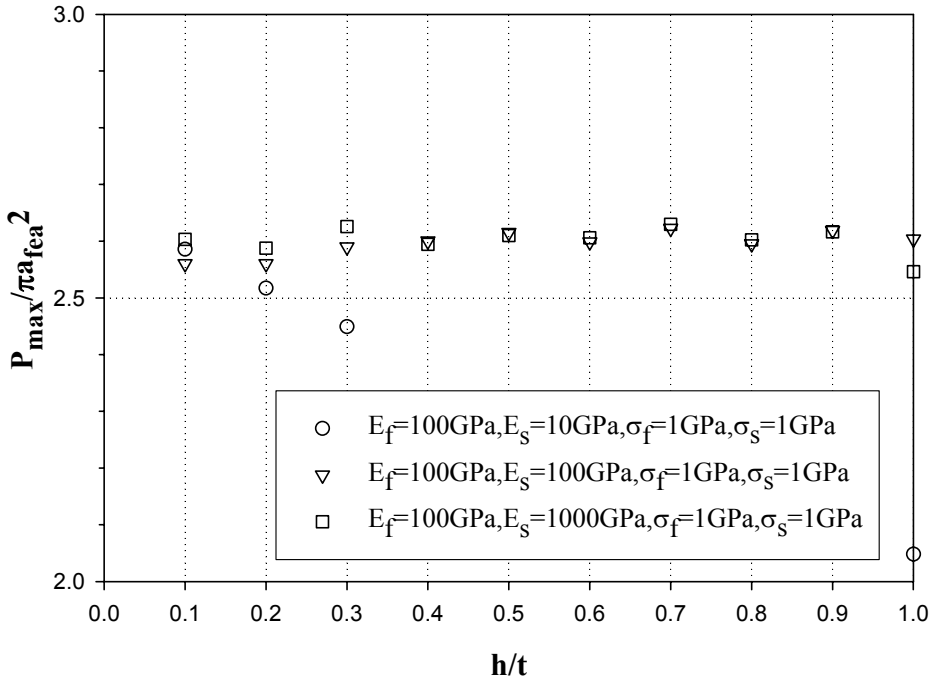

Figure 6.11 Measurements of hardness using true contact radii from FEA for nanoindentation of elastically inhomogeneous film/substrates systems (Hf=3GPa)

substrate hardness is 1.6 GPa, which is smaller than the film. With increasing h/t, the measured hardness decreases due to the substrate effect.

Lastly, we plot the measured hardness values against h/t for H_f=16GPa (σ_f=10GPa) in Fig.6.12. This comparison consists of soft films on hard substrates, homogenous film materials and hard films on soft substrates. It is seen that the soft substrate decreases the measured hardness, and the true film hardness can only be extracted when h/t is less than 0.3. One interesting phenomenon is that the measured hardness for soft films on hard substrates increases with increasing h/t. This is not consistent with our previous findings. One explanation is that fully plastic deformation occurs in the film materials when σ_f=0.1 and 1 GPa, and the indentation procedure is mainly accommodated by this deformation, while elastic-plastic deformation occurs in the film and substrate regions in the case of σ_f=10GPa.

6.4 Conclusions:

Based on finite element analysis of conical indentation of film/substrate systems with different elastic and plastic properties, we conclude the following:

1. The stiffness equation with β works well for film/substrate systems with similar elastic properties and different plastic properties, consistent with the notion that unloading is an elastic process.
2. The Xu-Pharr solution corrected for t_{eff} works well in extracting the true film moduli from stiffness measurements for compliant films on stiff substrates, but the

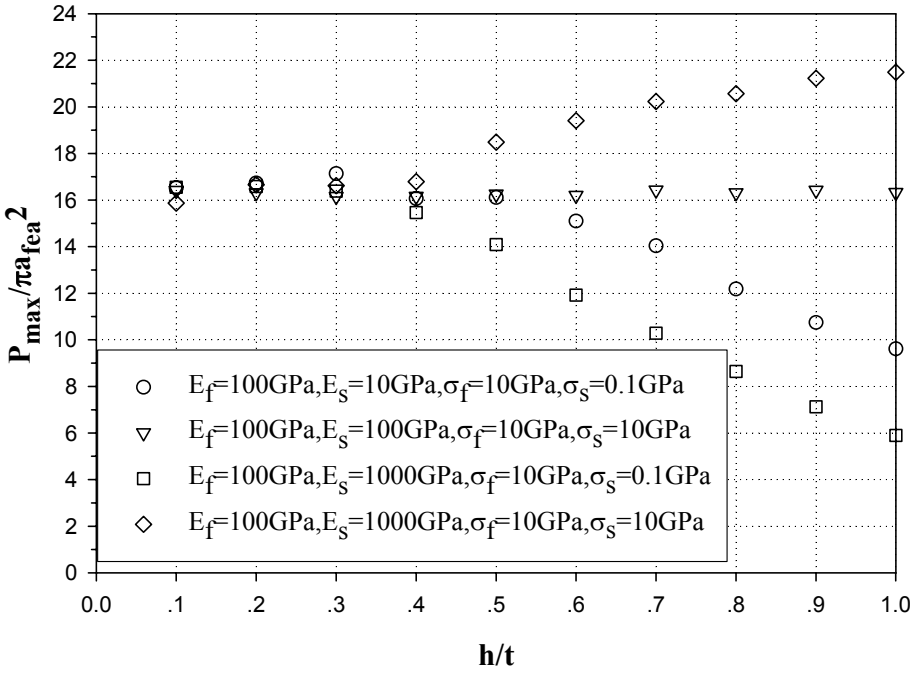

Figure 6.12 Measurements of hardness using true contact radii from FEA for nanoindentation of elastically inhomogeneous film/substrates systems (Hf=16GPa)

accuracy is improved greatly by including the effect of β. After employing the Xu-Pharr solution with t_{eff} and β, the errors in E_f are less than 20% for all h/t ratios up to 1. It is also noted that this new method works for plastically inhomogeneous systems.

3. To measure the film hardness, the general rule for film/substrate systems is that h/t should be less than 0.1. The results presented here show that for extremely soft films, the depth at which the substrate begins to affect the hardness is a function of σ_f / σ_s.

7. Comparison of the Han-Nix method and Xu-Pharr method for determining the hardness of films on substrates from nanoindentation tests

It was shown in the previous chapter that the hardness values measured from nanoindentation of film/substrate systems are a composite which depend on the mechanical properties of film and the substrate and also the normalized depth of penetration h/t. In order to measure the film hardness independent of the substrate, a rule of thumb is that the indentation depth should be less than 10% of the film thickness [31-32]. However, this one-tenth rule has been questioned as too strict for soft films on hard substrates [33] and is not restrictive enough for hard films on soft substrates [34]. Many researchers [30,35-39] have used finite element simulation of conical indentation of different film/substrate systems to show that the indention depth should be about 20%-50% of the film thickness for soft films on hard substrates or about 7%-20% for hard films on soft substrates, depending on the properties of films and substrates. In addition, Panich et al. [40] used FEA to show the critical h/t ratio to extract the film hardness depends on σ_f/σ_s and the indenter tip radius, and Zhu further pointed out that it is affected by E_f/E_s [41]. Lichinchi et al.[42] employed three dimensional FEA of indentation of a TiN film on a high speed steel substrate to show that h/t =0.15 can be used to obtain the film hardness without substrate effects. Nanoindentation experiments on soft films showed that h/t should be less than 20% for a gold film on a nickel substrate and 40% for an aluminum film on a glass substrate [43]. In the case of hard films, h/t =20% was found to be the limit for a carbon film on a M2 steel substrate and an alumina film on a nickel substrate [44]. While using an indentation depth less than the critical one

is feasible for thick films, this approach can not be used for very thin films due to limitations of the depth and load resolutions of the nanoindentation testing system. Other methods must thus be developed to determine the true film hardness of very thin films.

Great efforts have been put into developing the models which can relate the measured composite hardness to the film hardness and the substrate hardness. An early attempt by Buckle[31]defined the measured hardness as the sum of the substrate hardness and the difference between film hardness and substrate hardness weighted by a parameter. Since the success of this model depends on the choice of an empirically determined weighting parameter which was derived empirically, it proved impractical.

Jonsson and Hogmark [45] used a projected area "law of mixtures" to model the measured composite hardness, H_c as:

$$H_c = \frac{A_f}{A} H_f + \frac{A_s}{A} H_s \tag{7.1}$$

where A_f and A_s are the load supporting areas in the film and substrate, respectively. Based on geometric analysis of these relative sizes, they derived the following formula:

$$H_c = H_s + \left[2c\left(\frac{t}{d}\right) - c^2\left(\frac{t}{d}\right)^2 \right](H_f - H_s) \tag{7.2}$$

where d is the diagonal length of the Vickers indent and c is a constant that depends on the indenter geometry. This model was found to give a reasonable prediction of film hardness when the indentation depth is larger than the film thickness, but failed for a shallow indentation depth. This failure was due to the fact that the load dependence of hardness for small indentation depths [the indentation size effect (ISE)] was not considered. To extend the applicability of this model, the hardness was modified to

include the ISE [46] using:

$$H = H_0 + \frac{k}{d}. \tag{7.3}$$

where k is a constant and H_0 is the hardness at large indentation depths. As shown by [47] Korsunsky et al., the fit of the model is poor for film/substrate systems in which the composite hardness is mainly dominant by films or substrate.

A volume law-of-mixture hardness model which can be used in a broad range of circumstances originally proposed by Sargent has been extended by Bull, Burnett, Page and Rickerby [48-51]. In this model, the total deforming volume beneath the indenter (V) is assumed to be comprised of the volume deformed in the film (V_f) and the volume in the substrate (V_s). Therefore, the composite hardness can be obtained from:

$$H_c = \frac{V_f}{V} H_f + \frac{V_s}{V} \chi^3 H_s (H_f > H_s) \tag{7.4}$$

$$H_c = \frac{V_s}{V} H_s + \frac{V_f}{V} \chi^3 H_f (H_f < H_s) \tag{7.5}$$

where χ is a dimensionless parameter which allows for the modification of the deforming volume of the soft component in film/substrate systems. Both H_f and H_s include an indentation size effect:

$$H = H_1 d^{n-2} \tag{7.6}$$

where H_1 is the hardness measured at a standardized indentation size and n is the ISE index.The parameter χ is expected to depend on the difference between the plastic zone radii in the film and substrate predicted an the equation proposed by Lawn et al. [52] which has the form:

$$\chi = \left(\frac{E_f H_s}{E_s H_f} \right)^m . \tag{7.7}$$

Here m is a constant obtained by fitting the experimental data. It was shown that the volume mixture hardness model fits the experiment data very well except in the case of large indentation depths. However, the success of this model requires complex curve fitting to determine the various constants and good estimation of the deforming volume.

To simplify the curve fitting procedure with few empirical fitting parameters, a work-of-indentation model was developed for which the composite hardness is given by [53]:

$$H_c = H_s + \frac{(H_f - H_s)}{1 + k\beta^2} . \tag{7.8}$$

Here, k is a dimensionless parameter which is related to t for a cracked film and β is the indentation depth normalized by the film thickness t. This model agrees very well with experiment data.

Truck et al. [54] introduced two new parameters into the work-of-indentation model to further improve the quality of the curve fitting:

$$\frac{H - H_s}{H_f - H_s} = \frac{1}{1 + (\beta / \beta_0)^X} \tag{7.9}$$

Here, X is an exponent which allows for a transition from pure film hardness to pure substrate hardness, and β_0 is the h/t value at which the fractional hardness improvement is at 50% of the maximum. A better prediction of the real film hardness was observed using this modified model.

Although it is possible to employ the above models to predict the film hardness from the measured composite hardness, the estimation accuracy of these models is strongly determined by the curve fitting parameters and the quality of the experimental data. In general, models with fewer or no fitting parameters are needed.

Based on curve fitting of FEA data of indentation of different film/substrate systems, Nix et al. [35] developed two empirical equations which describe the variation of hardness with the indentation depth normalized by the film thickness. For soft films on hard substrates, the equation is of the form:

$$\frac{H}{H_s} = 1 + \left(\frac{H_f}{H_s} - 1\right)\exp\left[-\frac{(\sigma_f / \sigma_s)}{(E_f / E_s)}\left(\frac{h}{t}\right)^2\right]. \tag{7.10}$$

In the case of hard films on soft substrates, the equation can be expressed as:

$$\frac{H}{H_s} = 1 + \left(\frac{H_f}{H_s} - 1\right)\exp\left[-\frac{(H_f / H_s)}{(\sigma_f / \sigma_s)\sqrt{(E_f / E_s)}}\left(\frac{h}{t}\right)^2\right] \tag{7.11}$$

However, Xu et al. [41] showed that there is a large difference between FEA predictions and Eq.(7.10) for soft films on hard substrates and a good agreement for hard films on soft substrates(Eq.(7.11).

Saha and Nix [21] tested aluminum and tungsten films on four substrates including aluminum, glass, silicon and sapphire and found that the effect of substrate hardness can be neglected for soft films on hard substrates such as Al on glass, silicon and sapphire and W on sapphire, provided the true contact area was measured. However, using the commonly Oliver-Pharr method [1], which only works for materials that sink in but neglects pile-up, there is a significant “substrate effect” on the measured film

hardness due to the inaccuracy of measuring the contact area. To account for the pile up effects on the contact area and determine the true hardness, Saha and Nix adopted the method of Joslin and Oliver [55], in which the hardness can be related to measurements of P/S^2 through:

$$H = \frac{4}{\pi}\beta^2 E_r^2 \left(\frac{P}{S^2}\right) \tag{7.12}$$

This method accounts for the effect of pile-up on the contact area, provided the elastic modulus is known. To apply this method to the film/substrate problem, Saha and Nix made noted that the elastic properties of film and substrate should be similar. In their experiments, Al/glass and W/sapphire were considered as elastic homogenous. Therefore, the true film hardness can be calculated from Eq.(7.12) from measurements of S and P.

In the case of elastically inhomogeneous film/substrate systems, Saha and Nix modified King's model with the film thickness reduced by the indention depth to predict E_r from:

$$\frac{1}{E_r} = \frac{1-\nu_i^2}{E_i} + \frac{1-\nu_f^2}{E_f}\left(1-e^{-\frac{\alpha(t-h)}{a}}\right) + \frac{1-\nu_s^2}{E_s}\left(e^{-\frac{\alpha(t-h)}{a}}\right) \tag{7.13}$$

where E_i and ν_i are the elastic modulus and Poisson's ratio of the indenter, and α is a constant which is a function of a/t. This modified model gave the correct reduced modulus for small indentation depth. Han and Nix [56] used E_r from the modified model and Eq.(7.11) and observed a plateau of constant hardness at small indentation depths in the case of Ti-Al films on Si substrates. However, Eq.(7.11) with E_r predicted from Eq.(7.13) gave an unrealistic hardness when the indentation depth was greater than 50%

film thickness. They assumed that these errors were caused by using a model for flat punch rather than a cone.

Han et al.[23] proposed a new method to determine the film hardness which accounts for the conical geometry using the relation:

$$H = \frac{P}{A_c(h_c)} = \frac{P}{\pi[a(S)]^2} . \tag{7.14}$$

Here, A_c is the contact area which can be obtained from the relation between the contact radius, a, and the stiffness, S, which can be derived based on Yu's analytical solution for elastic indentation of layered structures.

In Yu's work, the axisymmetric mixed boundary problem of rigid conical indentation on an elastic film/substrate system was solved using a Fredholm integral equation of the second kind. The equation is:

$$H(\tau) - \frac{1}{\pi}\int_0^1 [K(y+\tau) + K(y-\tau)]H(y)dy = F_0(\tau) \tag{7.15}$$

where $F_0(\tau) = 1 - \gamma\tau$ for a conical indenter and γ is the ratio of the contact radius "a" for the film/substrate system to that for the pure film materials, a_h. The complex nestled function K(u) can be determined using a numerical quadrature method to integrate the equation:

$$K(u) = \frac{a}{h}\int_0^\infty g(w)\cos(\frac{auw}{h})dw . \tag{7.16}$$

Here, g(w) is a function of the shear moduli and Poisson's ratio for the film and substrate.

Using the El-Gendi method [57] to solve the Fredholm equation, a numerical

solution for H(τ) was found in the form of a Chebyshev series with order N=5. With the function H(τ) and the corresponding γ being solved, the normalized load P/P_h can be obtained from the equation:

$$\frac{P}{P_h} = 2\gamma \int_0^1 H(\tau) d\tau \tag{7.17}$$

where P_h is the load for conical indentation of the pure film material.

Han and Nix modified Yu's method to solve the Freholm equation to obtain the relationship between S and a with improved accuracy using a Chebvyshev series of order N=6, and they also included the stiffness of diamond indenter tip in the calculated S.

Although Yu's solution is derived strictly for the elastic layered systems, Han and Nix used it to determine the true film hardness for elastic-plastic film/substrate systems. To argue that the solution applies equally to elastic-plastic materials, they adopted an observation by Chen and Vlassak that the relationship between the stiffness and contact radius is the same for both purely elastic and elastic-plastic indentations of films/substrate. Chen and Vlassak suggested this based on the results of FEA calculations of conical indentation of elastic-plastic film/substrate systems [7].

Based on Chen and Vlassak's finding, Han and Nix used the S-a relationship derived from Yu's solution to successfully determine the true contact area of elastic-plastic film/substrate systems and extract the true hardness for systems with large elastic mismatches such as E_f/E_s=0.16 and 5.35.

In this chapter, Yu's solution and the X&P solution are compared with FEA results for indentation of elastic film/substrate systems with a conical indenter and flat

cylindrical punch. Then, the S-a relations derived from these solutions are compared with FEA results for elastic and elastic-plastic film/substrate systems indented by a 70.3° cone. Finally, we use these two solutions to predict the contact radii from the stiffness measured from FEA results of elastic plastic indentation and compare their accuracy.

7.1 Comparison to FEA results for indentation of elastic films/substrates systems by a 70.3° cone and a flat cylindrical punch

Since Yu's solution is derived for elastic film/substrate systems indented by a rigid cone, it is useful to compare the solution with our elastic FEA results. Fig.7.1 shows this comparison in terms of normalized load P/P_h vs. normalized film thickness t/a_h for film/substrate systems with E_f/E_s=0.5 and 2. Here, P_h represents the indentation load and a_h is the contact radius for a homogenous half space with elastic properties of the film material indented by a cone. We also include the prediction of Yu's solution and FEA results of Chen et al. It is observed that although there are slight differences among the FEA results, there is generally good agreement between the finite element calculations and Yu's solution.

We obtained and modified the Han-Nix numerical codes to determine the dependence of P/P_h on t/a_h for frictionless contact between a flat cylindrical punch and elastic film/substrates. As shown in Fig.7.2, the prediction of the modified Han-Nix solution for a flat punch matches the FEA results well. For comparison, the predictions of the X&P solution, which are computed by normalizing the stiffness in Eq.(4.8) with the stiffness from Eq.(1.1) at the same contact radius, are included. The X&P solution works as well as Yu's solution for compliant films on stiff substrates, but for stiff films on

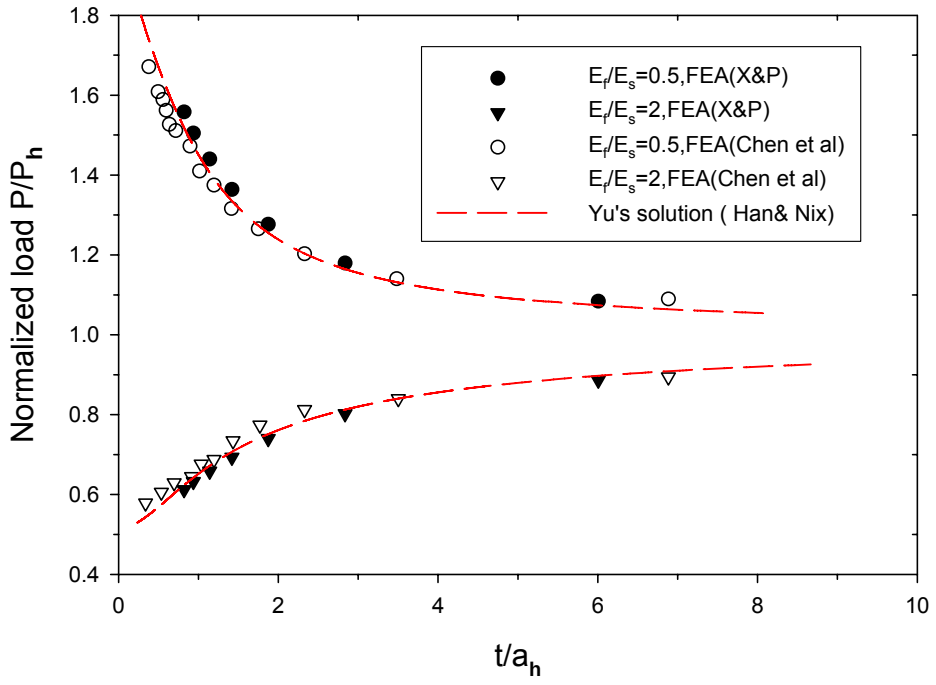

Figure 7.1 The variation of normalized P/Ph against t/ah; comparing FEA results and Yu's solution

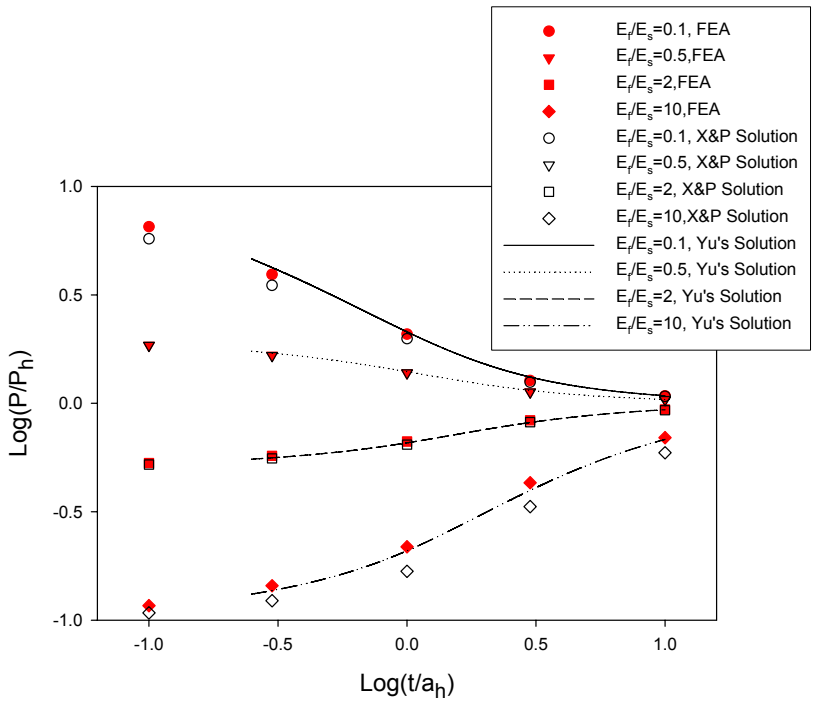

Figure 7.2 Log-Log plot of the normalized load P/Ph against t/ah for a frictionless flat-ended cylindrical punch

compliant substrates, especially with large elastic mismatches such as E_f/E_s=10, Yu's solution is better. This is consistent with the observation that X&P solution does not work well for stiff films on compliant substrates.

It is also useful to compare the S-a relation predicted from Yu's solution and the X&P solution with that obtained from FEA results for a conical indenter and a flat punch. To do so, E_f is fixed at 100GPa and the E_f values are selected as 1000 GPa, 200GPa, 50GPa, and 10GPa with Poisson's ratios fixed at $\nu_f=\nu_s=0.3$. Fig.7.3 shows the comparison for E_f/E_s = 0.5 and 2. In the case of E_f/E_s=0.5, both Yu's solution and the X&P solution for a conical indenter agree well with the FEA results for the flat punch. This shows that Yu's solution gives the same stiffness for a flat punch and conical indenter at the same a/t. However, our FEA results show that the stiffness of conical indention is larger than of the flat punch at the same contact radius. This implies that the stiffness equation for conical indentation of elastic materials should be modified with the correction factor β=1.06 (Chapter 3) while β=1 for the flat punch (Chapter 2). Therefore, Yu's solution and the X&P solution need to be modified with β for rigid conical indenters. As shown in Fig.7.3 (a), the corrected Yu's solution and X&P solution agree well with FEA predictions.

Fig.7.3 (b) shows the case of E_f/E_s=2. It is noted that the X&P solution does not work as well for stiff films on compliant substrates. Thus, Yu's solution is closer to the punch results than the X&P solution. Again, the correction factor β=1.06 must be applied to set good agreement for the conical indentation.

To explore how well Yu's solution and the X&P solution work when the difference between E_f and E_s is large, cases where E_f/E_s=0.1 and E_f/E_s =10 are considered

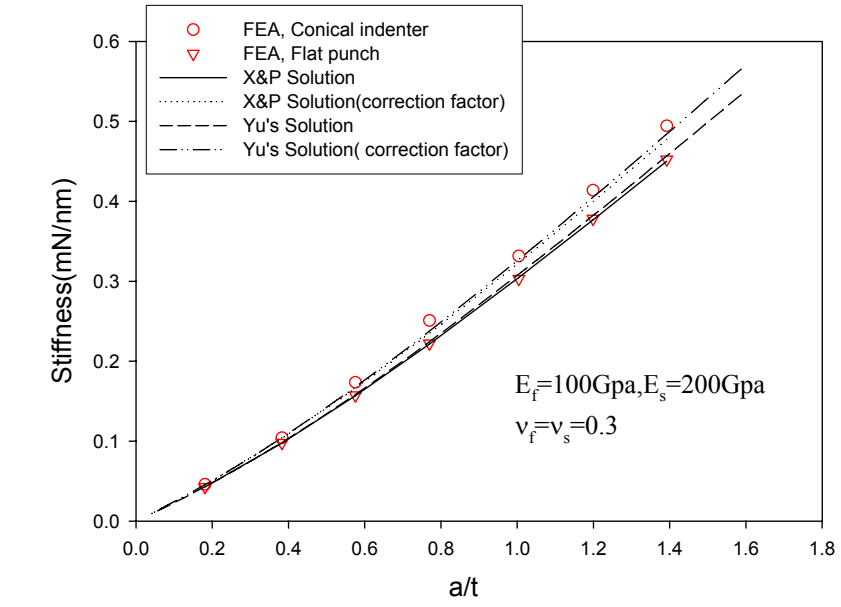

(a)

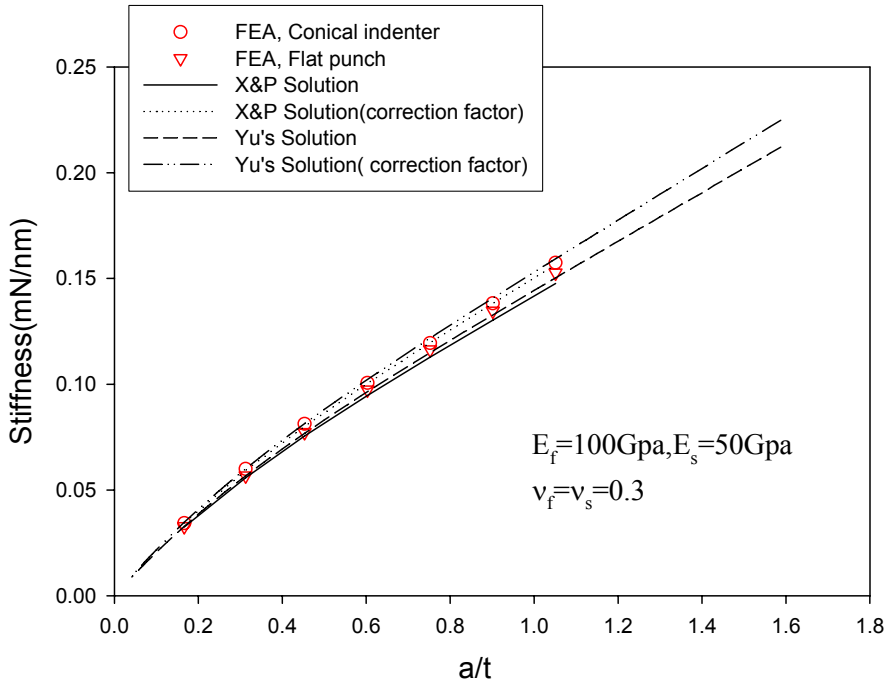

Figure 7.3 The variation of the stiffness with a/t for small elastic mismatch between films and substrates. (a) Ef/Es=0.5 (b) Ef/Es=2

in Fig.7.4. For E_f/E_s =0.1, the corrected Yu's solution works better than the X&P solution when compared to the FEA results (Fig.7.4 (a)). For E_f/E_s =10 (Fig.7.4 (b)), the X&P solution is significantly incorrect, and Yu's solution gives a much better prediction of the S-a relationship. It is found that the corrected Yu's solution is closer to the conical FEA results than the uncorrected one.

We also examined Yu's solution for conical indentation and flat punch indentation for film/substrate systems with E_f/E_s=0.5. The results are shown in Fig.7.5. The relationship between S and a is the same for both cases, demonstrating that the important parameter in determining the stiffness is the contact radius, not the geometry. However, for conical indentation, Yu's solution must be modified with β to give the correct stiffness.

7.2 Comparison to FEA results for conical indentation of elastic-plastic film/substrate systems

To determine the true contact area from indentation of elastic-plastic film/substrate systems including the effects of pile up or sink in, Han and Nix relied on Chen and Valassk's statement that the stiffness should be nearly the same for elastic indentation and elastic-plastic indentation of film/substrates with the same elastic properties at a given contact area. In this section, we compare elastic indentation and elastic-plastic indentation to verify whether this statement holds for very soft films or very hard films.

Fig.7.6 shows the comparison for a complaint film on a stiff substrate with E_f/E_s=0.1. Different combinations of σ_f/σ_s are included to cover the extreme cases of

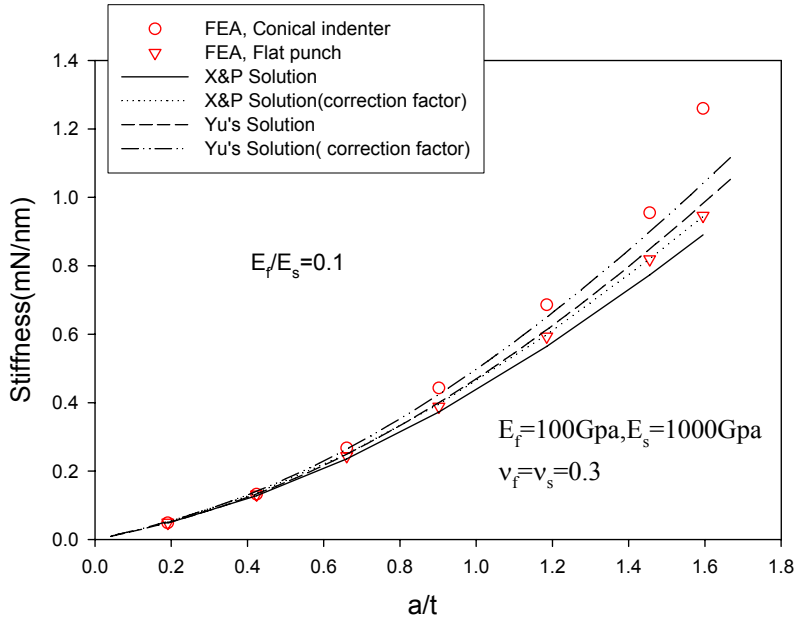

(a)

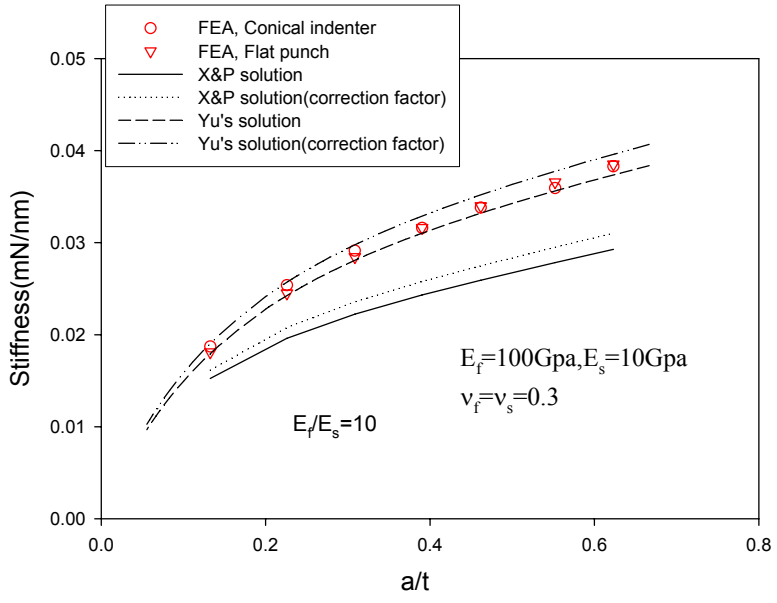

(b)

Figure 7.4 The variation of the stiffness with a/t for large elastic mismatch between films and substrates (a) Ef/Es=0.1 (b) Ef/Es=10

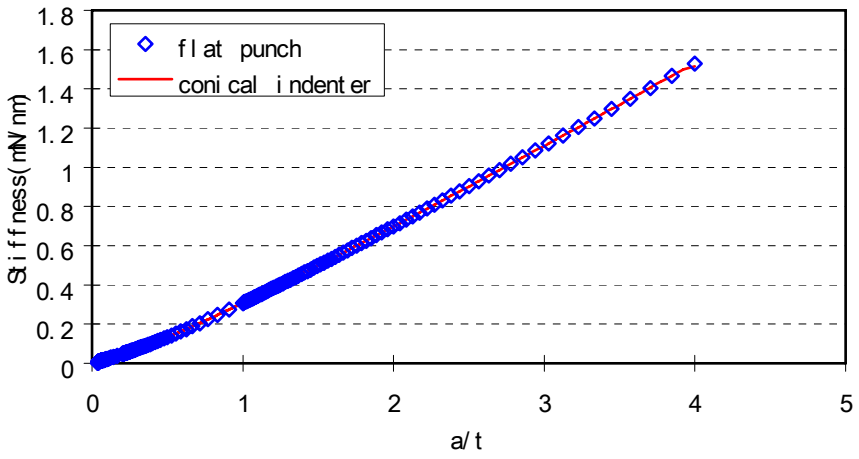

Figure 7.5 Comparison between Yu's solution for flat punch and conical indenters for Ef/Es=0.5(νf=νs=0.3).

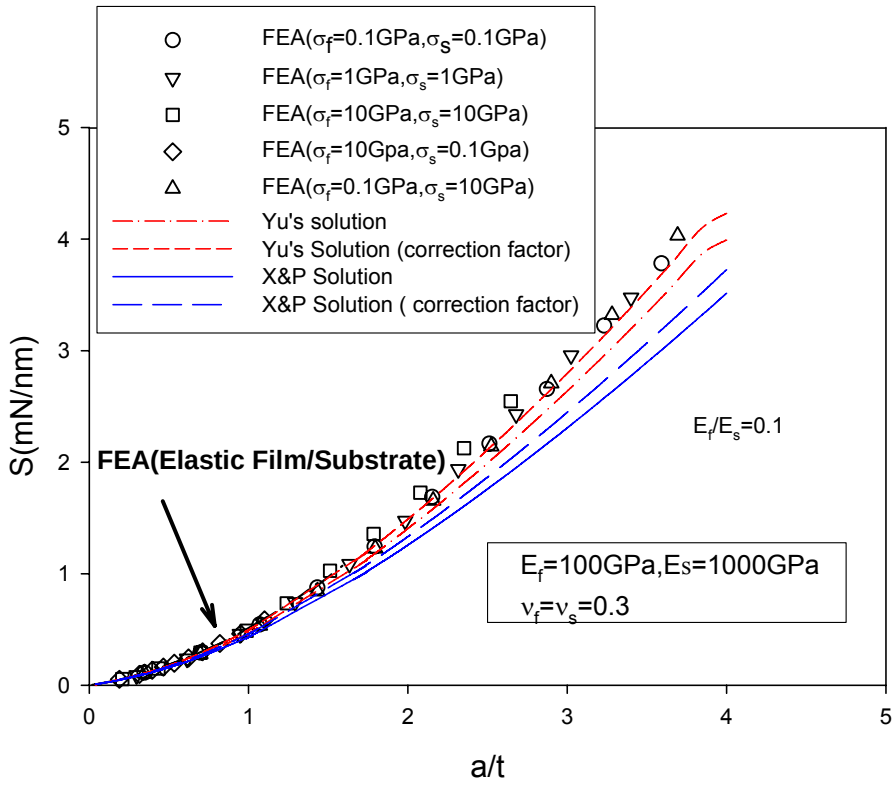

Figure 7.6 A comparison of the S-a relationship from FEA of elastic indentation, elastic-plastic indentation, Yu's solution, and the X&P solution for compliant films on stiff substrates (Ef/Es=0.1)

plasticity. We see that the FEA calculations for elastic-plastic indentation fall near the solid curve showing the results of elastic FEA, indicating that the relationship between S and a should be the same or at least similar for elastic and elastic-plastic indentation of complaint films on stiff substrates. We also see that Yu's solution corrected with β matches the FEA results well for the entire range of a, but the X&P solution only works for small a values.

Fig.7.7 examines stiff films on compliant substrates. Once again, the FEA results for elastic-plastic indentation can be predicted by those for elastic indentation and are bounded by Yu's solution and the corrected one. On the other hand, there is significant deviation between FEA results and the predictions from X&P with/without β.

From the above observations, it can be concluded that the stiffnesses are almost same for elastic indentation and elastic-plastic of film/substrate systems with the same E_f/E_s at a given contact radius. Yu's solution works better than the X&P solution especially for stiff films on compliant substrates. In all cases, the solutions must be corrected by β to obtain good results for conical indentation. It is noted that the maximum contact radii in the elastic-plastic indentation simulation represent the case of h/t=1 for a 70.3° cone. This means that Yu's solution corrected with β works well even for the case in which the conical indenter is driven to a depth comparable to the film thickness.

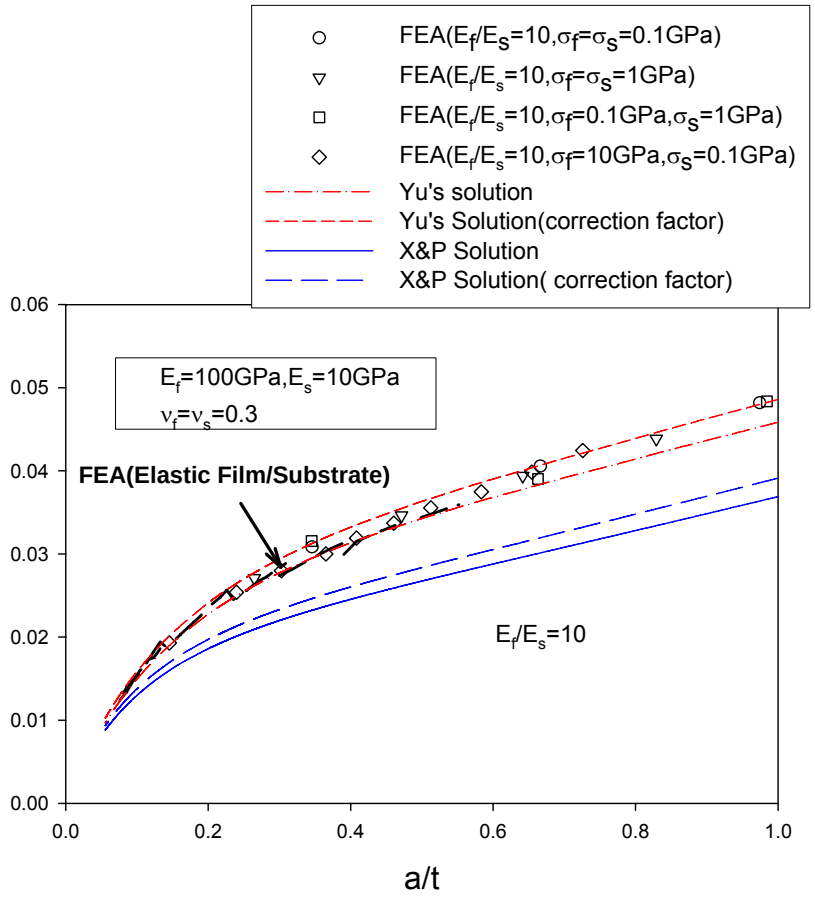

Figure 7.7 A comparison of the S-a relationship from FEA of elastic indentation, elastic-plastic indentation, Yu's solution, and the X&P solution for stiff films on compliant substrates (Ef/Es=10).

7.3 An assessment of the accuracy of determining the true contact radii using the Han-Nix method and the X&P method

Since the relationship between S and a is unique for elastic indentation and elastic-plastic indentation with a rigid cone for the same film/substrate systems, we can use this relation to determine the true contact radius from the measured stiffness. As shown in 7.2, Yu's solution works better than the X&P solution, but the X&P solution still offers some advantages in that it can be written in simple closed form. We now explore the maximum possible errors when those solutions are used to determine the contact radii.

Using the stiffness values measured from FEA of conical indentation of elastic-plastic film/substrate systems, we calculate the predicted contact radii for indentation by a 70.3° cone and compare them with the real contact radii measured from FEA. Three types of film/substrate systems are considered: elastically homogenous and plastically inhomogeneous, elastically inhomogeneous and plastically homogenous, and elastically and plastically inhomogeneous.

Let us first consider the elastically homogenous and plastically inhomogeneous film/substrate systems. In this case, we choose $E_f=E_s=100$GPa, and σ_f and σ_s are selected as 0.1, 1 and 10 GPa, respectively. As shown in Fig.7.8 (a), using $\beta=1.06$ improves the accuracy of predicting the contact radii using Yu's solution for $\sigma_f=0.1$ GPa and different σ_s. The differences between the β-corrected Yu's solution and the FEA results are less than 3%, which would give a calculated hardness with error less than 9%. The X&P solution also works well, and including β

Figure 7.8 The difference between the contact radii predicted from FEA and the analytical solutions for elastically homogenous systems (Ef=Es) and □f=0.1GPa. (a) Yu's solution (b) the X&P solution

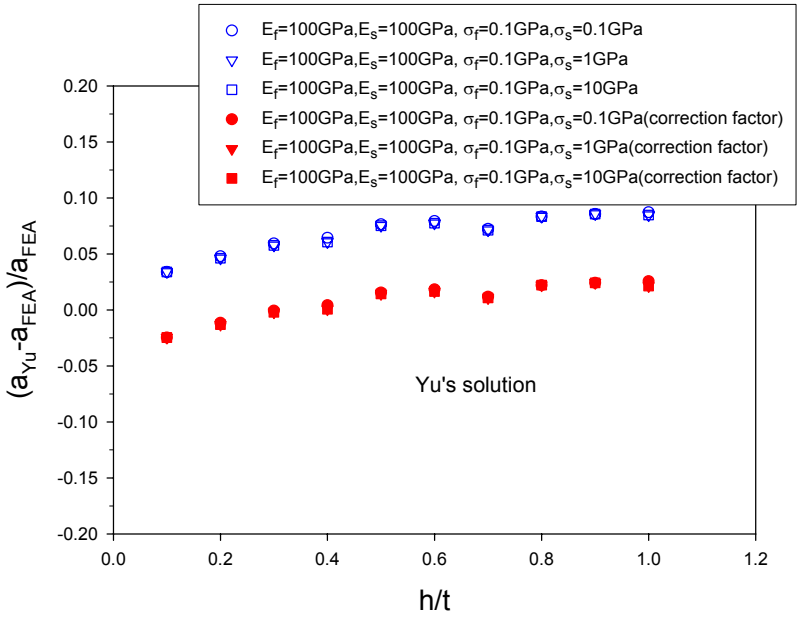
Ef=100GPa,Es=100GPa, σf=0.1GPa,σs=0.1GPa
Ef=100GPa,Es=100GPa, σf=0.1GPa,σs=1GPa
Ef=100GPa,Es=100GPa, σf=0.1GPa,σs=10GPa
Ef=100GPa,Es=100GPa, σf=0.1GPa,σs=0.1GPa(correction factor)
Ef=100GPa,Es=100GPa, σf=0.1GPa,σs=1GPa(correction factor)
Ef=100GPa,Es=100GPa, σf=0.1GPa,σs=10GPa(correction factor)
Yu's solution
(aYu-aFEA)/aFEA
h/t

(a)

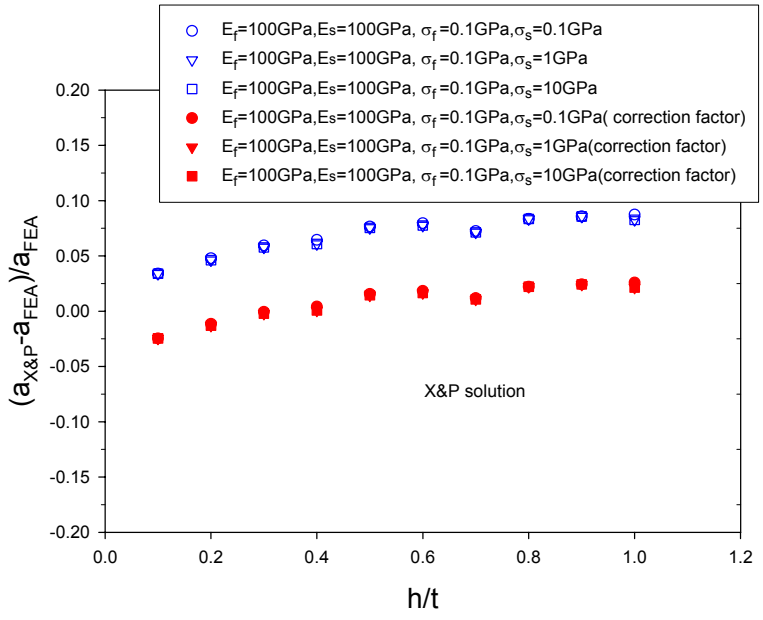
Ef=100GPa,Es=100GPa, σf=0.1GPa,σs=0.1GPa
Ef=100GPa,Es=100GPa, σf=0.1GPa,σs=1GPa
Ef=100GPa,Es=100GPa, σf=0.1GPa,σs=10GPa
Ef=100GPa,Es=100GPa, σf=0.1GPa,σs=0.1GPa(correction factor)
Ef=100GPa,Es=100GPa, σf=0.1GPa,σs=1GPa(correction factor)
Ef=100GPa,Es=100GPa, σf=0.1GPa,σs=10GPa(correction factor)
X&P solution
(aX&P-aFEA)/aFEA
h/t

(b)

is also important to determine the contact radii accurately with error less than 3%. The same conclusions can be reached for the other cases with σ_f=1GPa and 10GPa (shown in Fig.7.9 and Fig.7.10).

For elastically mismatched film/substrate systems with the same yield stress, we need to consider the results separately according to the ratio of E_f/E_s. Fig.7.11 (a) shows the effects of β on Yu's solution when E_f/E_s =0.1. After applying β, Yu's solution reduces the maximum errors of estimated contact radii less than 7% even when h/t =1. Fig.7.11 (b) also shows that using X&P solution with β correction still gives errors that are larger than 10% when h/t is greater than 0.5. It is noted that the error increases with increasing h/t. In Chapter 5, we showed that the effective film thickness will improve the accuracy of the X&P solution for compliant films on stiff substrates. After applying the effective film thickness and applying β to X&P solution, all the errors are reduced to less than 8 %(Fig .7.12).

For stiff films on compliant substrates (Fig.7.13), the β-correction slightly improves the accuracy of the contact radii predicted from Yu's solution, giving errors less than 10% (Fig.7.13 (a)). Even though it was shown in the previous chapters that X&P solution does not work for this case, we still include it here for comparison. We observe large errors even for small h/t ratios (Fig.7.13 (b)). It is recommended that Yu's solution should be used in this situation.

In the case of both elastically and plastically inhomogeneous films and substrates, we consider only compliant films on stiff substrates. As shown in Fig.7.14 (a), correction for β reduces the prediction error of Yu's solution form 8% to 4%. correction for t_{eff} and

Figure 7.9 The difference between the contact radii predicted from FEA and the analytical solutions for elastically homogenous systems (Ef=Es) and σf=1GPa.

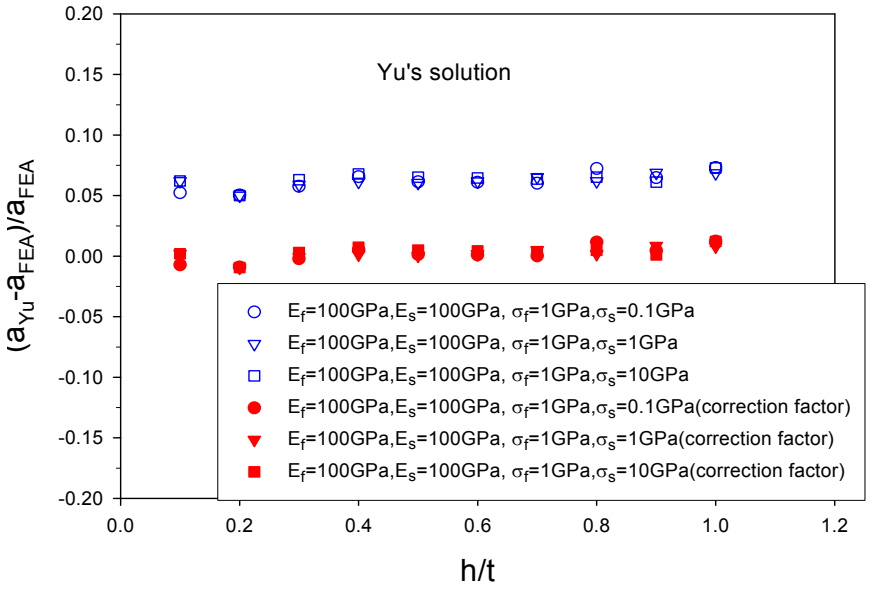
Yu's solution
$(a_{Yu}-a_{FEA})/a_{FEA}$
h/t
E_f=100GPa,E_s=100GPa, σ_f=1GPa,σ_s=0.1GPa
E_f=100GPa,E_s=100GPa, σ_f=1GPa,σ_s=1GPa
E_f=100GPa,E_s=100GPa, σ_f=1GPa,σ_s=10GPa
E_f=100GPa,E_s=100GPa, σ_f=1GPa,σ_s=0.1GPa(correction factor)
E_f=100GPa,E_s=100GPa, σ_f=1GPa,σ_s=1GPa(correction factor)
E_f=100GPa,E_s=100GPa, σ_f=1GPa,σ_s=10GPa(correction factor)

(a)

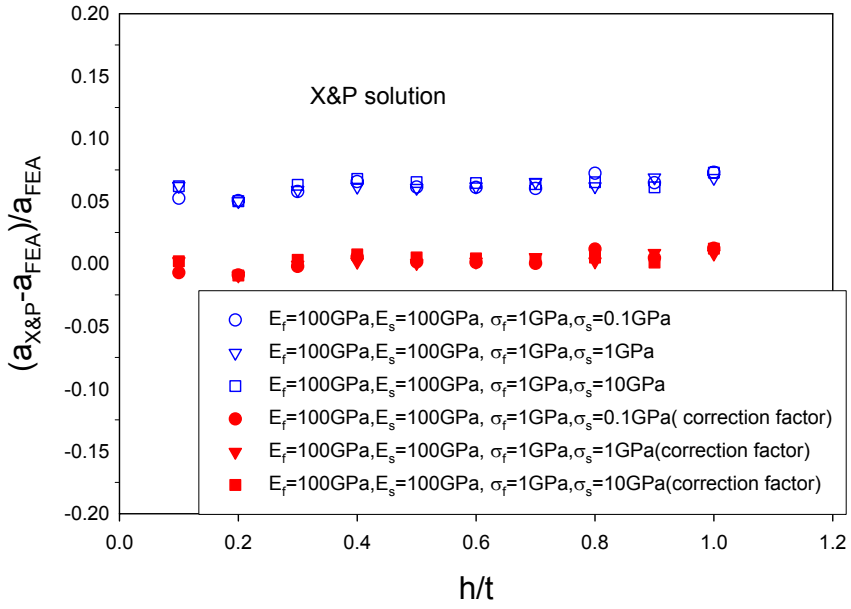
X&P solution
$(a_{X\&P}-a_{FEA})/a_{FEA}$
h/t
E_f=100GPa,E_s=100GPa, σ_f=1GPa,σ_s=0.1GPa
E_f=100GPa,E_s=100GPa, σ_f=1GPa,σ_s=1GPa
E_f=100GPa,E_s=100GPa, σ_f=1GPa,σ_s=10GPa
E_f=100GPa,E_s=100GPa, σ_f=1GPa,σ_s=0.1GPa(correction factor)
E_f=100GPa,E_s=100GPa, σ_f=1GPa,σ_s=1GPa(correction factor)
E_f=100GPa,E_s=100GPa, σ_f=1GPa,σ_s=10GPa(correction factor)

(b)

Figure 7.10 The difference between the contact radii predicted from FEA and the analytical solutions for elastically homogenous systems (Ef=Es) and σf=10GPa (a) Yu's solution (b) X&P solution

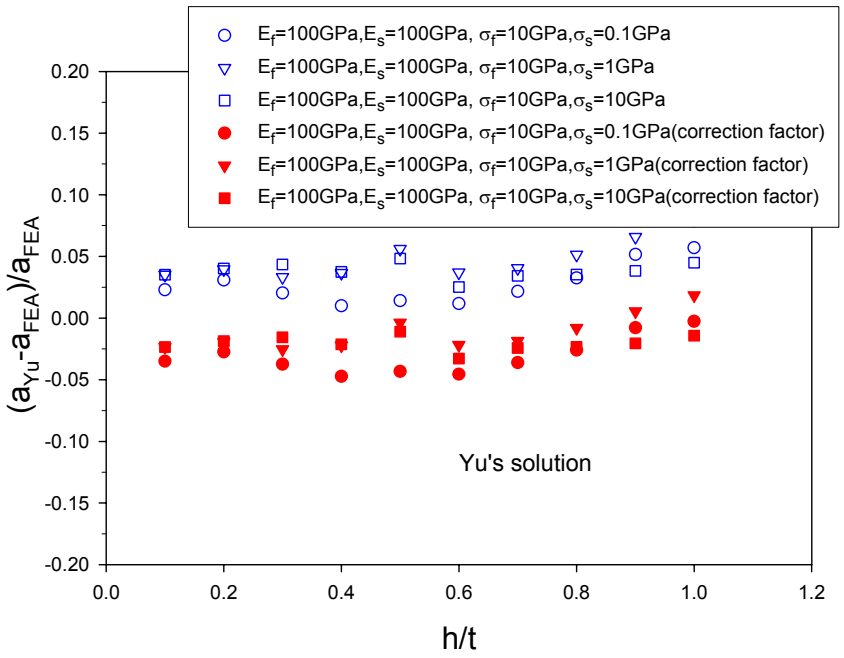
Ef=100GPa,Es=100GPa, σf=10GPa,σs=0.1GPa
Ef=100GPa,Es=100GPa, σf=10GPa,σs=1GPa
Ef=100GPa,Es=100GPa, σf=10GPa,σs=10GPa
Ef=100GPa,Es=100GPa, σf=10GPa,σs=0.1GPa(correction factor)
Ef=100GPa,Es=100GPa, σf=10GPa,σs=1GPa(correction factor)
Ef=100GPa,Es=100GPa, σf=10GPa,σs=10GPa(correction factor)
(aYu-aFEA)/aFEA
Yu's solution
h/t
0.20
0.15
0.10
0.05
0.00
-0.05
-0.10
-0.15
-0.20
0.0
0.2
0.4
0.6
0.8
1.0
1.2

(a)

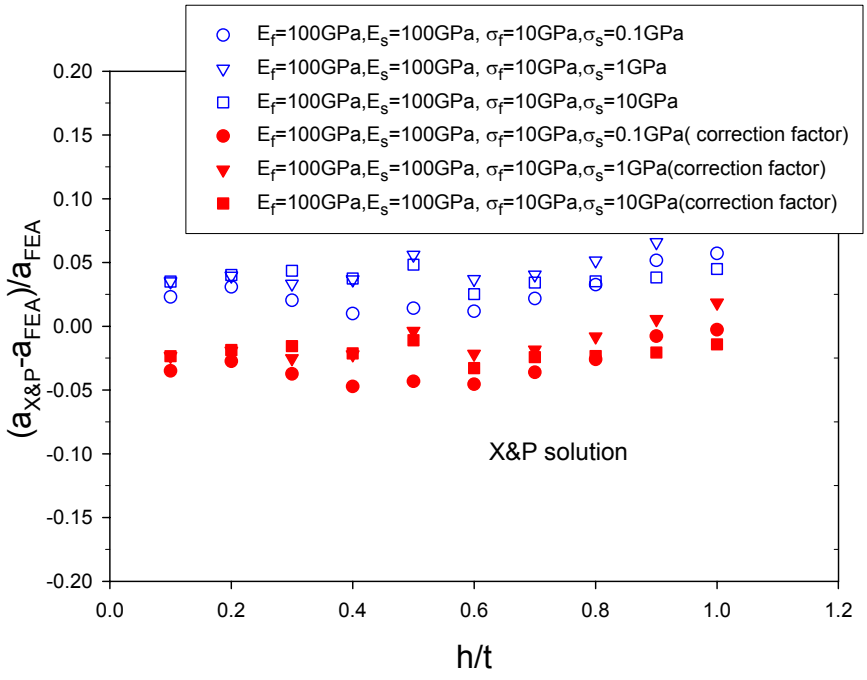
Ef=100GPa,Es=100GPa, σf=10GPa,σs=0.1GPa
Ef=100GPa,Es=100GPa, σf=10GPa,σs=1GPa
Ef=100GPa,Es=100GPa, σf=10GPa,σs=10GPa
Ef=100GPa,Es=100GPa, σf=10GPa,σs=0.1GPa(correction factor)
Ef=100GPa,Es=100GPa, σf=10GPa,σs=1GPa(correction factor)
Ef=100GPa,Es=100GPa, σf=10GPa,σs=10GPa(correction factor)
(aX&P-aFEA)/aFEA
X&P solution
h/t
0.20
0.15
0.10
0.05
0.00
-0.05
-0.10
-0.15
-0.20
0.0
0.2
0.4
0.6
0.8
1.0
1.2

(b)

Figure 7.11 The difference between the contact radii predicted from FEA and the analytical solutions for elastically inhomogeneous systems (Ef/Es=0.1) and $\sigma_f=\sigma_s$. (a) Yu's solution (b) X&P solution

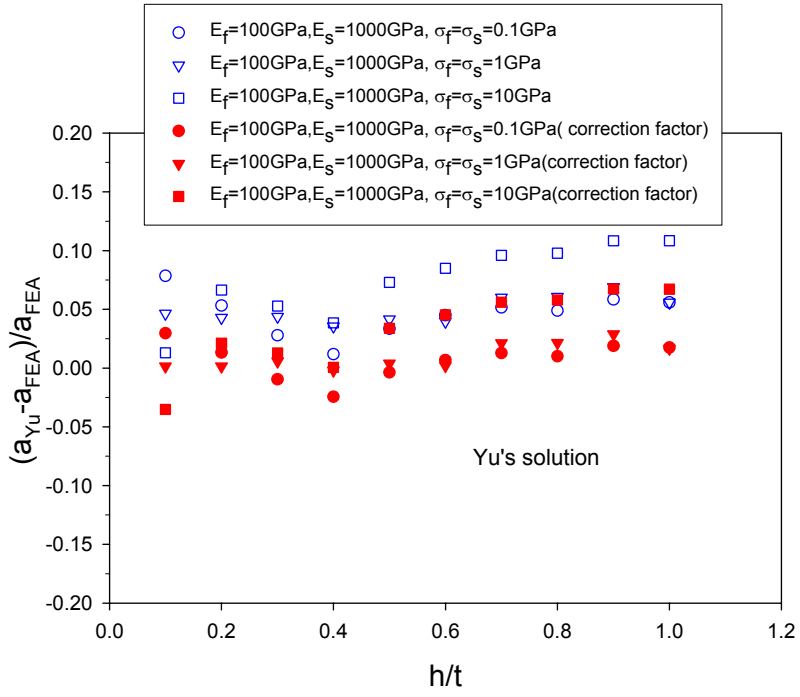
E_f=100GPa,E_s=1000GPa, σ_f=σ_s=0.1GPa
E_f=100GPa,E_s=1000GPa, σ_f=σ_s=1GPa
E_f=100GPa,E_s=1000GPa, σ_f=σ_s=10GPa
E_f=100GPa,E_s=1000GPa, σ_f=σ_s=0.1GPa(correction factor)
E_f=100GPa,E_s=1000GPa, σ_f=σ_s=1GPa(correction factor)
E_f=100GPa,E_s=1000GPa, σ_f=σ_s=10GPa(correction factor)
$(a_{Yu}-a_{FEA})/a_{FEA}$
Yu's solution
h/t

(a)

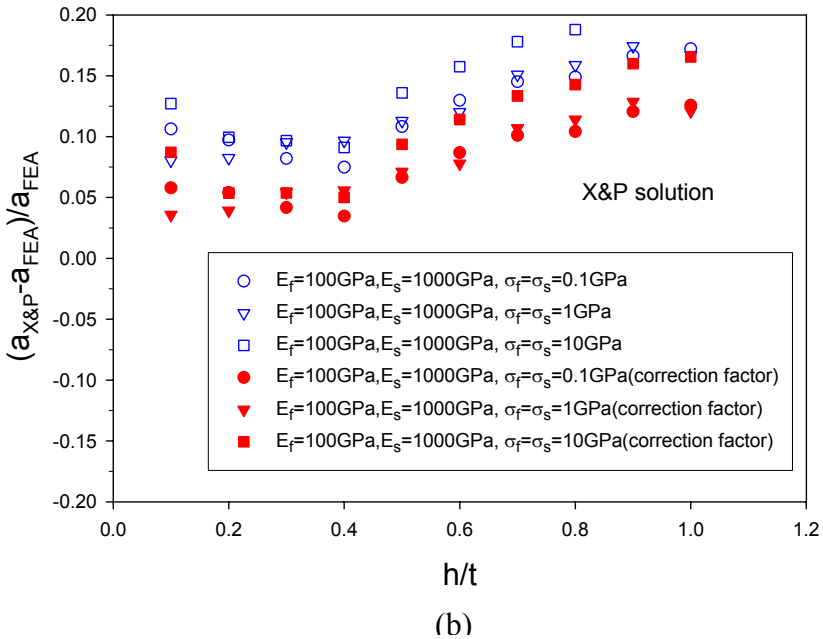
$(a_{X\&P}-a_{FEA})/a_{FEA}$
X&P solution
E_f=100GPa,E_s=1000GPa, σ_f=σ_s=0.1GPa
E_f=100GPa,E_s=1000GPa, σ_f=σ_s=1GPa
E_f=100GPa,E_s=1000GPa, σ_f=σ_s=10GPa
E_f=100GPa,E_s=1000GPa, σ_f=σ_s=0.1GPa(correction factor)
E_f=100GPa,E_s=1000GPa, σ_f=σ_s=1GPa(correction factor)
E_f=100GPa,E_s=1000GPa, σ_f=σ_s=10GPa(correction factor)
h/t

(b)

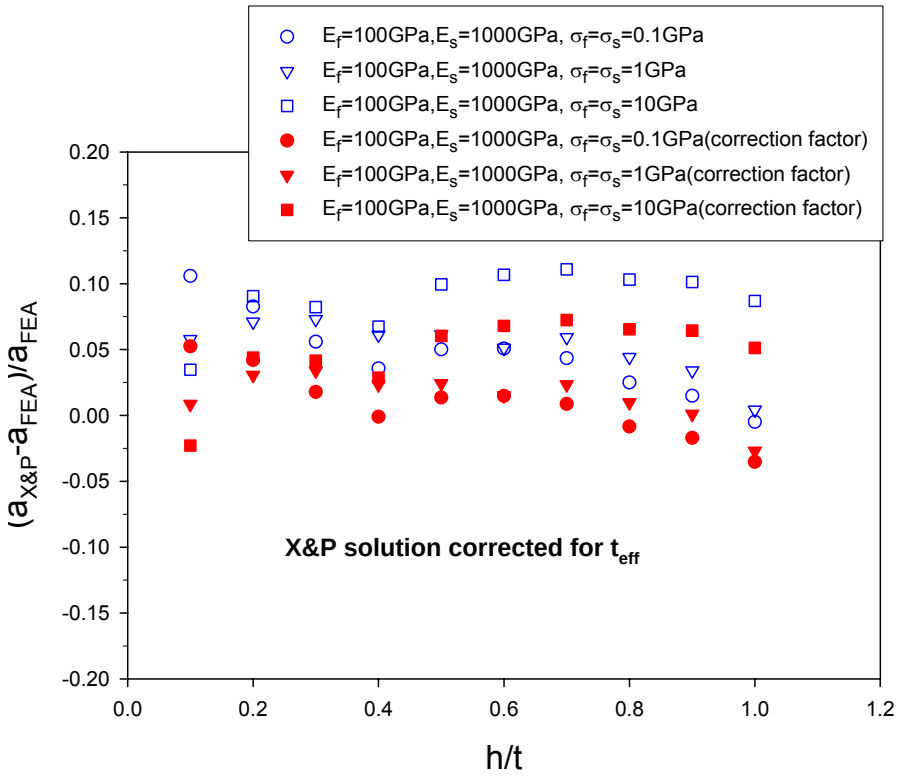

Figure 7.12 The difference between the contact radii predicted from FEA and the X&P solution for elastically inhomogenous systems (Ef/Es=0.1) and σf=σ.

Figure 7.13 The difference between the contact radii predicted from FEA and the analytical solutions for elastically inhomogeneous systems (Ef/Es=10) and $\sigma_f=\sigma_s$. (a) Yu's solution (b) X&P solution

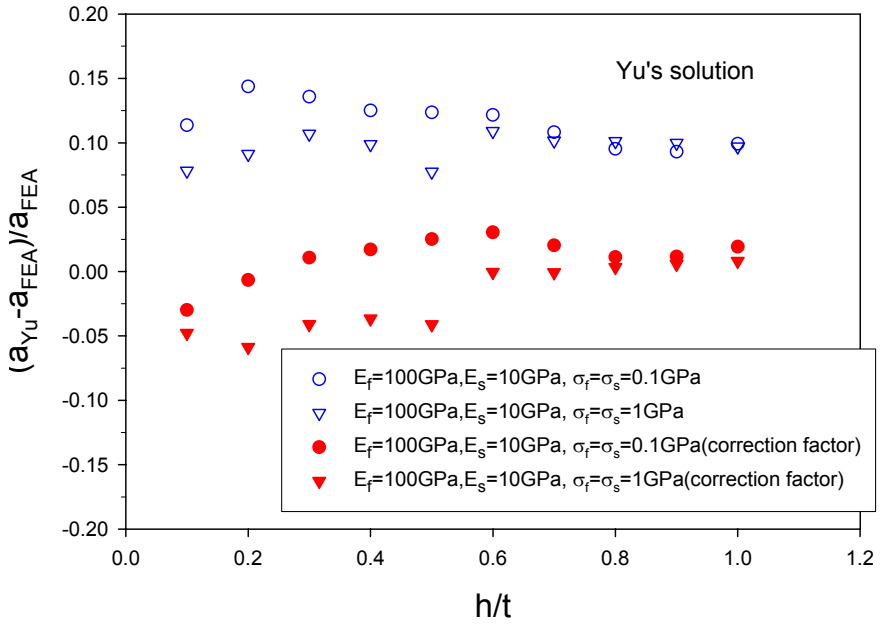
Yu's solution
E_f=100GPa,E_s=10GPa, σ_f=σ_s=0.1GPa
E_f=100GPa,E_s=10GPa, σ_f=σ_s=1GPa
E_f=100GPa,E_s=10GPa, σ_f=σ_s=0.1GPa(correction factor)
E_f=100GPa,E_s=10GPa, σ_f=σ_s=1GPa(correction factor)
$(a_{Yu}-a_{FEA})/a_{FEA}$
h/t

(a)

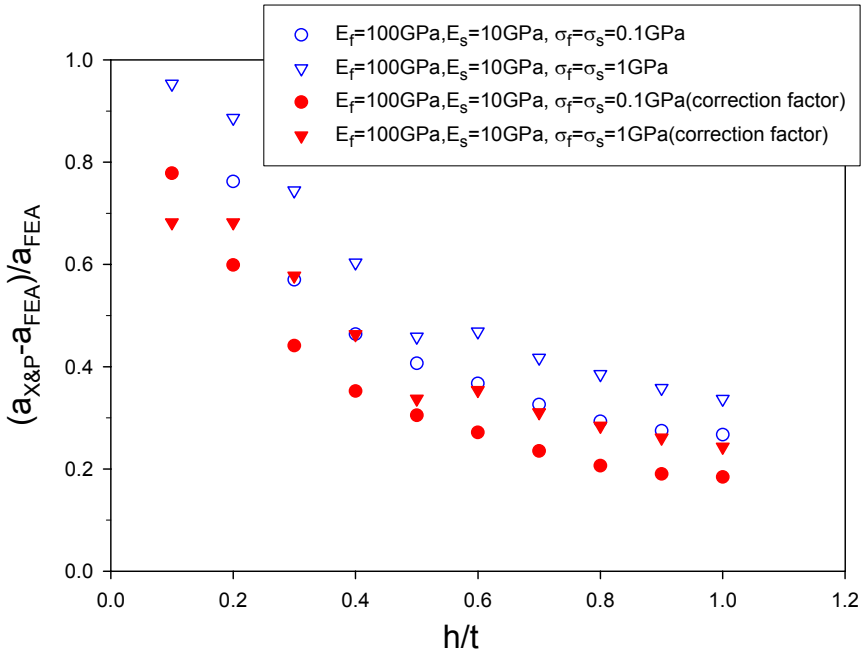
E_f=100GPa,E_s=10GPa, σ_f=σ_s=0.1GPa
E_f=100GPa,E_s=10GPa, σ_f=σ_s=1GPa
E_f=100GPa,E_s=10GPa, σ_f=σ_s=0.1GPa(correction factor)
E_f=100GPa,E_s=10GPa, σ_f=σ_s=1GPa(correction factor)
$(a_{X\&P}-a_{FEA})/a_{FEA}$
h/t

(b)

Figure 7.14 The difference between the contact radii predicted from FEA and the analytical solutions for elastically and plastically inhomogeneous systems (Ef/Es=0.1 and $\sigma_f \neq \sigma_s$). (a) Yu's solution (b) X&P solution

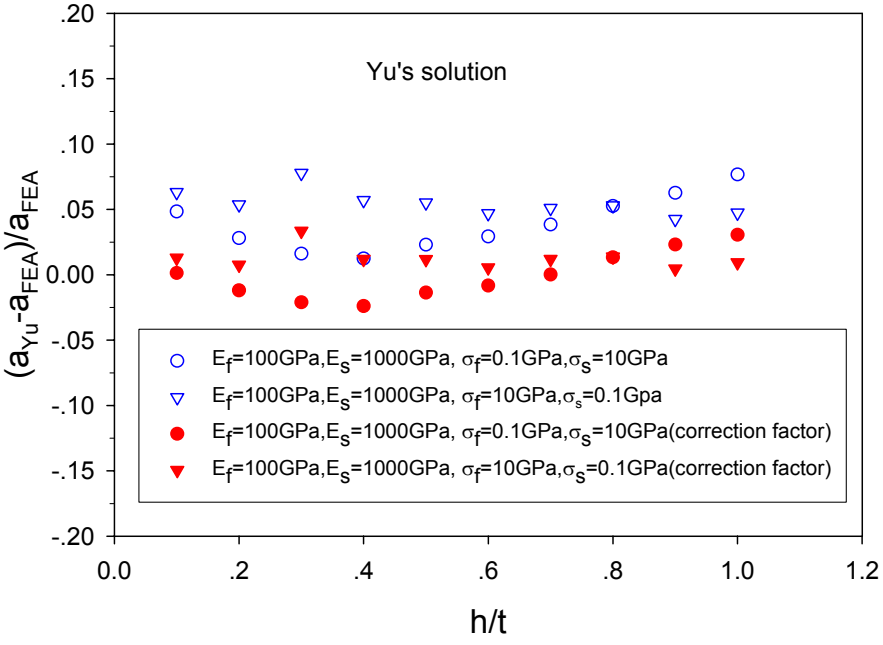
Yu's solution
$(a_{Yu}-a_{FEA})/a_{FEA}$
h/t
E_f=100GPa,E_s=1000GPa, σ_f=0.1GPa,σ_s=10GPa
E_f=100GPa,E_s=1000GPa, σ_f=10GPa,σ_s=0.1Gpa
E_f=100GPa,E_s=1000GPa, σ_f=0.1GPa,σ_s=10GPa(correction factor)
E_f=100GPa,E_s=1000GPa, σ_f=10GPa,σ_s=0.1GPa(correction factor)

(a)

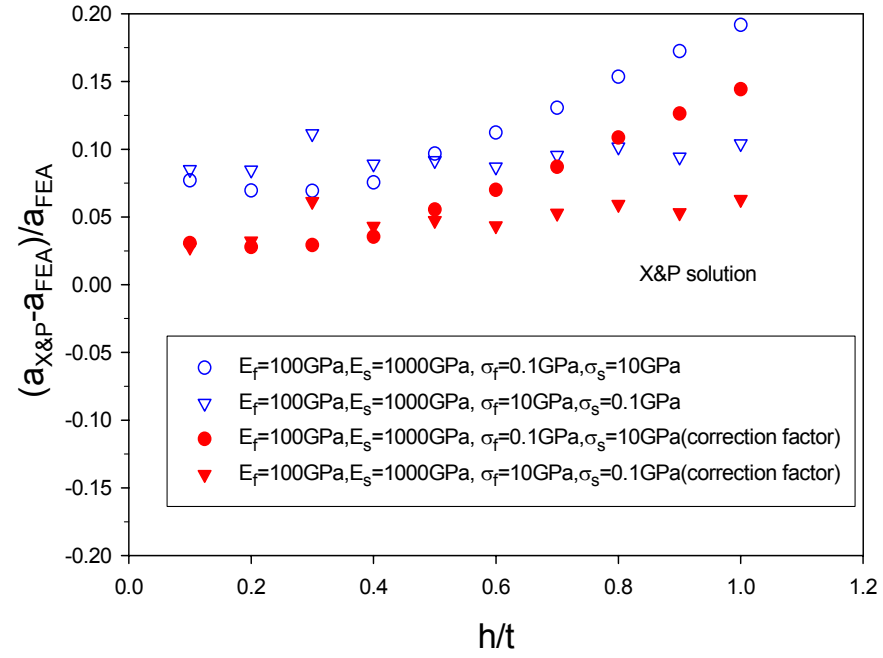
X&P solution
$(a_{X\&P}-a_{FEA})/a_{FEA}$
h/t
E_f=100GPa,E_s=1000GPa, σ_f=0.1GPa,σ_s=10GPa
E_f=100GPa,E_s=1000GPa, σ_f=10GPa,σ_s=0.1GPa
E_f=100GPa,E_s=1000GPa, σ_f=0.1GPa,σ_s=10GPa(correction factor)
E_f=100GPa,E_s=1000GPa, σ_f=10GPa,σ_s=0.1GPa(correction factor)

(b)

β decreases the maximum error of the contact radius using X&P solution from 20% to 7 % (Fig.7.14 (b) and Fig 15).

From these observations, it is clear that Yu's solution works well for a broad range of film/substrate systems, and the X&P solution applies only to compliant films. β corrections should be included in both solutions for accuracy. To use the X&P solution to determine the contact radii accurately, t_{eff} corrections must also be included in the solution.

7.4 Conclusions

By comparing FEA results of elastic indentation of film/substrate systems by a 70.3° conical indenter and flat cylindrical punch with Yu's solution and the X&P solution, it was shown that a correction for β must be included to predict the S-a relation accurately. The used β values are 1 and 1.06 for the flat punch and the conical indenter, respectively.

The statement that the stiffness is the same for an elastic indentation and an elastic-plastic indentation of the same film/substrate systems if both cases have the same contact radii was validated by FEA of elastic/elastic-plastic indentation. In addition, Yu's solution corrected for β works well for conical indentation for both compliant and stiff films with h/t up to 1 while the X&P solution works only for compliant films.

The prediction of the contact radii from Yu's solution and the X&P solution were compared with the true contact radii measured from FEA for different combinations of

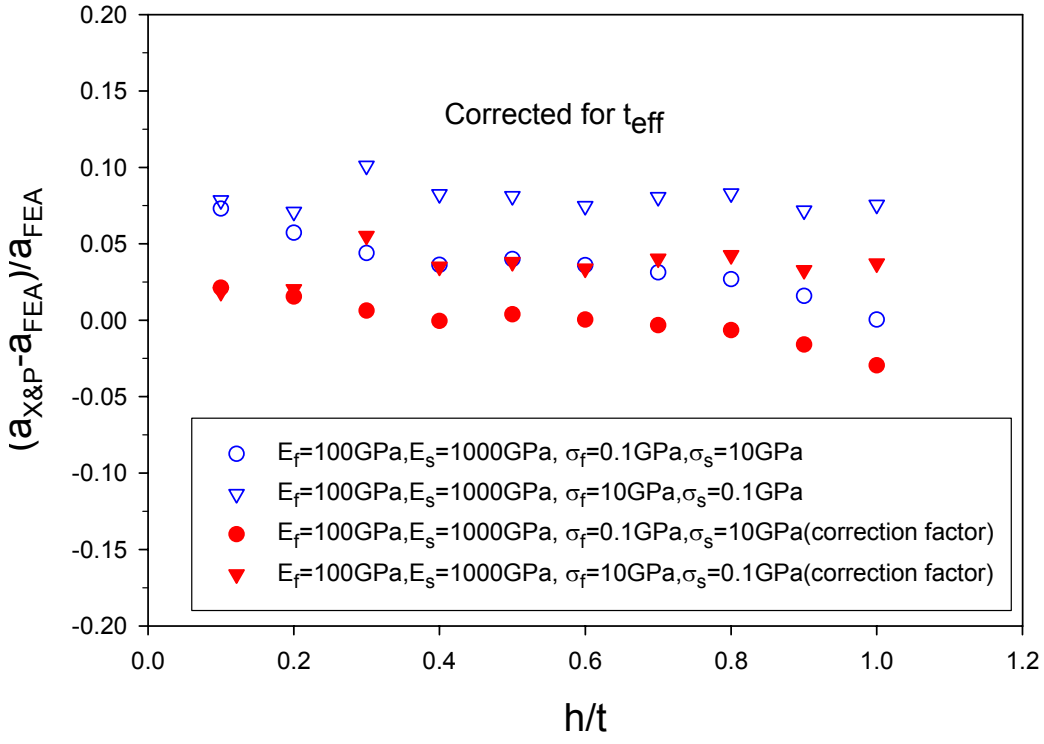

Figure 7.15 The difference between the contact radii predicted from FEA and the X&P solution with/without the effective film thickness for elastically and plastically inhomogeneous systems (Ef/Es=0.1 and □f≠□s)

elastic and plastic properties. It was found that Yu's solution corrected for β can estimate the contact radii accurately for all film/substrate systems while the X&P solution with β and t_{eff} only works for compliant films. It is noted that
β must be included in Yu's solution and β and t_{eff} must be used in the X&P solution to predict contact radii with errors less than 10%.

Although Yu's solution has advantages over the X&P solution in its accuracy and broad applicability, it has limitations, in particular, the solution can be evaluated only by numerical methods and is therefore not convenient to use. Compared with Yu's solution, the X&P solution has a simple form and can be used to predict the elastic moduli without numerical analysis. Therefore, the X&P solution provides some advantages for the case of compliant films on stiff substrates.

8. Summary and future work

In this chapter, we summarize important results in this dissertation and give some possible future research directions.

As described in Chapter 2, the correction factor in the stiffness equation depends on friction coefficient, Poisson's ratio and indenter angle for elastically homogenous materials. For a flat punch, β=1 for frictionless contact and $\beta = (1-\nu)/(1-2\nu)\ln(3-4\nu)$ for infinite friction. For a finite friction, β can be determined from Fig.2.4 provided ν is known. In the case of conical indentation of flat elastic materials, β can be obtained from Fig.2.7 from known μ,ν and θ. In addition, β can be approximated from Eq. (1.3) for any friction for θ in the range from 50° to 70°. For conical indentation of matching conical holes, which can be used to approximate the hardness impression caused by the plasticity, β can be determined from Fig.2.12. For a cone with θ= 70°, β can also be predicted from Eq. (1.3) for any friction coefficients and Poisson's ratios. Although the dependence of β on Poisson's ratios and the friction condition for a flat punch is understood physically, we propose some possible physical explanations for the relationships among β, ν, θ and μ for conical indentation of elastic flat materials and holes.

In Chapter 3, the correction factors for elastic-plastic indentation by a 70.3° cone were investigated by using FEA. We found that the stiffness equation works for elastic-plastic materials, including both soft and hard materials, but needs to be modified to correct for β. Sink-in and pile-up affect β only slightly provided the true contact radius is used. One important observation is that the effect of working hardening on β can be neglected. It should be noted that all of these conclusions are based on the assumption

that true contact radii are available to be used in the stiffness equation.

The equivalence of the stiffness between conical indentation of elastic holes and flat elastic-plastic materials at the same contact radii is shown by comparison to FEA results. This implies that it is reasonable to use elastic holes to approximate the hardness impression. It is also found the correction factor for elastic holes is close to the average value for elastic-plastic indentation of extreme soft and hard materials. This indicates that we can use the correction factor for indenting elastic holes to approximate that for elastic-plastic flat indentation. For a 70.3° cone, we suggest that $\beta=1.065$ should be used as the correction factor for elastic-plastic indentation (equivalent to real experiments). In addition, the equivalence of β for elastic holes and elastic-plastic materials at the same contact radii is shown for other cones with $\theta\geq50°$. Fig.2.12 is also a useful reference for β in conical elastic-plastic indentation with $\theta\geq50°$. It is found that the correction factor for elastic holes (equivalent to the unloading of elastic plastic indentation) is caused by the hole geometry only for $\nu=0.5$. For other Poisson's ratios, the radial displacement mechanism is involved and both must be included.

In chapter 4, we provided a new relationship between the effective compliance and the elastic properties of films and substrates based on Gao's model. It is shown by using FEA that the new relation works better than Gao's solution especially when the film is more compliant than the substrate. However, neither solutions work well for stiff films on compliant substrates when $E_f/E_s\geq2$.

Chapter 5 introduced a new method to apply the approximate analytical solution for flat punch indentation to conical indentation of film/substrate systems. The effective

film thickness must be used instead of the total film thickness to account for the hole, which is equivalent to the hardness impression. A simple equation between t_{eff} and the indentation depth is given.

In Chapter 6, we employed FEA of conical indentation of elastic plastic film/substrates to show that the stiffness equation modified with β works for elastic homogenous film/substrate systems, and the Xu-Pharr solution with β and t_{eff} corrections can be used to determine E_f with error less than 20%, even when h/t is up to 1 for compliant films on stiff substrates. In addition, it is shown that the depth below which the true hardness of the film can be obtained depends on E_f/E_s and σ_f/σ_s in a complex way.

Yu's solution is compared with the Xu-Pharr solution and FEA of elastic and elastic-plastic film/substrate systems with conical indenters and flat cylindrical punches in Chapter 7. Both Yu's solution and the Xu-Pharr solution can predict the S-a relation accurately for a flat punch, but need to be modified with β for a 70.3° cone in the case of compliant films on stiff substrates. It is noted that the Xu-Pharr solution must be corrected by t_{eff}. Yu's solution works better than the Xu-Pharr solution for large h/t. For stiff films on compliant substrates, Yu's solution still works but the Xu-Pharr solution does not.

One possible future research topic is that we need to understand better the physical origin of the dependence of β on μ,ν and θ for conical indentation of elastic flat materials and elastic holes. This will help us to use the stiffness equation corrected with β to measure elastic properties more accurately.

It is also suggested that the effects of friction on β for conical indentation of

elastic-plastic materials be investigated. These effects have not been considered here but could be important.

For film/substrate systems, a good, closed form (approximate) analytical solution is needed to describe the relation between the effective compliance (the stiffness) and the elastic properties of film and substrate materials for a stiff film on a compliant substrate. A good, closed form model to determine the true film hardness from the composite hardness is also needed.

REFERENCES

1. W.C.Oliver and G.M.Pharr,J.Mater.Res.7,1564(1992).
2. A.E.H.Love, Quart.J.Math.10, 161 (1939).
3. A.E.H.Love, Philos. Trans. A 228,377 (1929).
4. I.N.Sneddon,Int.J.Eng.Sci. 3,47 (1965).
5. I.N.Sneddon,Fourier Transforms (McGraw-Hill Book Company, Inc., New York,1951),pp.450-467.
6. G.M.Pharr, W.C.Oliver and F.R.Brotzen, J.Mater.Res. 7,613 (1992)
7. R.B.King, Int.J.Solids Struct.23, 1657 (1987).
8. J.J.Vlassak and W.D. Nix, J. Mech.Phys. Solids, 42, 1223(1994).
9. A.Bolshakov, G.M.Pharr, J.Mater.Res.13, 1049(1998).
10. Y-T.Cheng and C-M. Cheng, J.App.Phys.84, 1284(1998).
11. Y-T. Cheng and C-M. Cheng, Int. J. Solids Structures 36, 1231 (1999).
12. M. Dao, N. Chollacoop, K. J. Van Vliet, T. A. Venkatesh and S. Suresh, Acta Materialla 49,3899(2001).
13. M.Martin, and M, Troyon, J.Mater.Res. 17, 2227(2002).
14. Jeremy H. Strader, Sanghoon Shim, Hongbin Bei, W.C. Oliver, and G.M. Pharr, Philosophical Magazine 86, 5285-5298 (2006).
15. J.C.Hay, A.Bolshakov, and G.M.Pharr, J.Mater.Res.14, 2296(1999).
16. Nix WD. Metall.Trans. 2217(1989).
17. Pharr GM and Oliver WC. MRS Bulletin 28(1992).
18. Doerner,M.F. and Nix,W.D, J.Mater.Res.4,601-609(1986).
19. H.Y.Yu,S.C. Sanday and B.B.Rath,J.Mech.Phys.Solids 38, 745(1990).

20. Huajian Gao,Cheng-Hsin Chiu and Jin Lee, Int.J.Solids Structures 29,2471(1992).
21. S.Bec,A.Tonck,J.M.Georges,E.Georges and J.L Loubet,Phil.Mag. A., 74, 1061(1996).
22. R. Saha and Nix,W.D,Acta Materialia,50,23(2002).
23. SM. Han, R. Saha and Nix,W.D, Acta Materialia,54,1571(2006).
24. J.mencik,D. Munz,E.Quandt, and E.R.Weppelmann,J.Mater.Res.,12,2475(1997).
25. D.A.Spence, J. of Elasticity. 5, 297, (1975).
26. B. Storakers and D. Elaguine, J.Mechacis and Physics of solids. 53, 1422(2005).
27. K.L. Johnson, Contact Mechanics, Cambridge University Press, Cambridge, UK (1985).
28. Shield,R.T. and Anderson, C.A., Z.angew.Math.Phys.17,663-676 (1966).
29. A.F.Bower,N.A. Fleck,A. Needleman, N.Ogbonna,Proc.R.Soc. Lond. A 441, 97(1993).
30. X.Chen, J.J. Vlassak, J. Mater.Res. 16, 2974(2001).
31. H.Buckle, in J.W.Westbrook and H.Conrad, The Science of Hardness Testing and Its Research Applications, American Society for Metals, Metals Park,OH, 453(1973).
32. E.A.Almond, Vaccum, 35835(1984).
33. D.Lebouvier, P.Gilormini,E.Felder, J.Phys. D: Appl. Phys.18, 199(1985).
34. D.Lebouvier, P.Gilormini,E.Felder, Thin Solid films 172, 227(1989).
35. A.K. Bhattacharya, W.D.Nix, Int.J.Solids Struct. 24, 1287(1988).
36. H.Wang, H. Bargert, Mater.Res.Soc.Symp.Proc.308,183(1993).

37. M. Lichinchi, C.Lenardi, J. Haugt,K.Vitali, Thin Solid Films 312, 240(1998).

38. Y.Sun, T.Bell, S.Zhang, Thin Solid Films 258,198(1995).

39. X.Cai, H.Barget, Thin Solid Films 264, 59(1995).

40. N.Panich, Y.Sun, Sufr.Coat. Technol. 182,342(2004).

41. Z.-H. Xu, D.Rowcliffe, Thin. Solid. Films. 447-448,399 (2004).

42. M. Lichinchi, C.Lenardi, J. Haugt,K.Vitali, Thin Solid Films 333,278(1998).

43. Z.-H. Xu, D. Rowcliffe, Surf.Coat. Technol. 157,231(2002).

44. Z.-H. Xu, D. Rowcliffe, Surf.Coat. Technol. 161,44(2002).

45. B.Jonsson and S. Hogmark, Thin Solid Films,114,257(1984).

46. O.Vingsbo, S. Hogmark, B. Jonsson, A. Ingemarsson, in: P.J. Blau, B.R. Lawn, Microindentation Techniques in Materials Science and Engineering, ASTM, Philadlphia, PA, 257(1986).

47. P.M.Sargetn, PhD thesis, University of Cambridge, 1979.

48. P.J. Burnett, T.F. Page, J.Mater.Sci. 19,845(1984).

49. P.J. Burnett, D.S.Rickerby, Thin Solid Films 148,41(1987).

50. P.J. Burnett, D.S.Rickerby, Thin Solid Films 148,51(1987).

51. S.J.Bull, D.S.Rickerby, Surf.Coat.Technol. 42,149(1990).

52. B.R. Lawn, A.G. Evans,D.B. Marshall, J.Am.Ceram.Soc. 63,574(1980).

53. A.M. Korsunsky, M.R. McGurk, S.J. Bull, T.F. Page, Surf.Coat.Technol. 99,171 (1998).

54. J.R. Tuck, A.M.Korsunsky, D.G.Bhat, S.J.Bull, Surf.Coat.Technol. 39, 74(2001).

55. D.L. Joslin and W.C. Oliver, J. Mater. Res. **5,** 123(1990).

56. S.M. Han, R. Shah, R. Banerjee, G.B. Viswanathan, B.M. Clemens and W.D. Nix, Acta. Mater. **53** 2059 (2005).

57. El-Gendi,S.E. Comput.J.12,282(1969).

VITA

Haitao Xu was born in China in 1979. After graduated from Lujiang No.1 High School, Anhui province, in 1996, he attended Jilin University, Changchun, and completed his undergraduate study in the Department of Materials Science and Engineering in 2000. He worked as a project engineer for two years before coming to the University of Tennessee, Knoxville to pursue a doctorate in materials science and engineering in 2002. He received a Ph.D degree under the guidance of Professor George Pharr in 2007.